Modeling and Control of Electrolysis Based Hydrogen Production System

Abdulrahman M. Abomazid

A THESIS SUBMITTED IN PARTIAL FULFILLMENT OF
THE REQUIREMENTS FOR THE DEGREE OF

MASTER OF APPLIED SCIENCE

Graduate Program in Electrical Engineering and Computer Science

YORK UNIVERSITY

TORONTO, ONTARIO

November 2021

Abstract

Currently, hydrogen fuel is essential for mitigating the effects of climate change and for solving energy sector challenges. There are significant challenges associated with producing hydrogen through water electrolysis as a results of the lack of an accurate electrolyzer model and the high costs associated with hydrogen production. Therefore, this thesis intends to (1) model and characterize the electrolyzer system accurately and (2) develop an energy management system (EMS) in order to minimize the cost of hydrogen (CoH) production.

In general, the literature on electrolyzers modeling assumes a linear model and omits nonlinear behavior. This may lead to an inefficient hydrogen production approaches. As a result, the first part of this thesis studies the modeling and characterization problem of electrolyzer systems in terms of the parameter estimation of a detailed model which is designed to capture all electrochemical phenomena that may occur during electrolysis in a timely manner.

Moreover, most existing EMSs ignore variations in electrolyzer efficiency. Therefore, in the second part of this thesis, an EMS is developed for minimizing CoH production by accounting for electrolyzer conversion efficiency variation. Furthermore, historical electricity prices have been incorporated into EMS in order to enable the seasonal storage of hydrogen energy.

Acknowledgements

The completion of this thesis would not have been possible without the generous assistance and constant support of my supervisor, colleagues, collaborators, friends, and family members. I would like to express my deepest gratitude to each of them. Firstly, I would like to thank my supervisor Professor Hany Farag for his constant guidance, support, and patience throughout my MASc program. I have had the pleasure of working with him at the York University's Smart Grid Research Lab. I could not have asked for more from him. In addition, I wish to thank Dr. Afshin Razaei Zara and Dr. Usman T Khan for being members of my committee and for their encouragement and advice throughout the process.

It is with great gratitude that I acknowledge my dear colleague at York University working on the same project with me: Dr. Nader El-Taweel who contributed to the publications of the proposed work. In addition, I would like to thank other people from York University with whom I have spent a lot of time: Abdullah Sawas, Abdullah Al-Obaidi, Mohammed Zaki, Gouri Barai, Shivam Saxena. I am honored to work with all these brilliant minds. Finally, I wish to express my gratitude to my entire family, including my parents, grandparents, uncles, aunts, and cousins, whose unconditional love and support have meant the world to me throughout the years.

Table of Contents

List of Tables

List of Figures

Nomenclature

Abbreviations

J-V	Current density-voltage.
APE	Absolute percentage error.
BESS	Battery energy storage system.
BoP	Balance of plant components.
Cmp	Compressor.
CoH	Cost-of-hydrogen.
DER	Distributed energy resource.
Elz	Electrolyzer.
EMS	Energy management system.
Grd	Power grid.
Ld	Electrical load.
LSE	Least square error.
MAPE	Mean absolute percentage error.
NN	Neural network.
PEM	Proton exchange membrane.
PSO	Particle swarm optimization.
PtG	Power-to-gas.
PV	Photovoltaic.
RMSE	Root mean square error.

SAPE Standard deviation absolute percentage error.

SoC State of charge.

SOEC Solid oxide electrolysis cell.

SoH State of hydrogen.

Constants

α Charge transfer coefficient.

α^{a}_{max} Maximum anode charge transfer coefficient.

α^{a}_{min} Minimum anode charge transfer coefficient.

α^{c}_{max} Maximum cathode charge transfer coefficient.

α^{c}_{min} Minimum cathode charge transfer coefficient.

α^{a} Anode charge transfer coefficient.

α^{c} Cathode charge transfer coefficient.

ΔG Change in Gibbs free energy (kJ).

$\eta^{BESS,Chg}$ BESS charging efficiency (%).

$\eta^{BESS,Dhg}$ BESS discharging efficiency (%).

η^{Cmp} Compressor efficiency (%).

$\eta^{PV,M}$ Maximum power point tracking efficiency (%).

$\eta^{PV,r}$ PV rated system efficiency (%).

$\gamma^{BESS,Dsp}$ BESS dissipation factor (%).

$\gamma^{HS,Dsp}$ HS dissipation factor (%).

λ^{PV} Penalty cost of PV power curtailment.

π^{H_2O} Water pressures (bar).

π^{H_2} Electrolyzer hydrogen pressure (bar).

Π^{HS}_{max} HS maximum pressure (bar).

Π_{min}^{HS} HS minimum pressure (bar).

π^{O_2} Oxygen pressures (bar).

σ^m Membrane conductivity parameter ($1/\Omega$cm).

σ_{max}^m Maximum membrane conductivity ($1/\Omega$cm).

σ_{min}^m Minimum membrane conductivity ($1/\Omega$cm).

A^{PV} PV module area (m^2).

C^s CapEx (\$/MW) of unit s.

D^{Elz} Electrolyzer stack replacement cost (\$/MWh).

F Faraday constant (C/mol).

HHV Higher heating value of hydrogen gas (J/kg).

$J^{0,a}$ Anode exchange current density (A/cm^2).

$J_{max}^{0,a}$ Maximum anode exchange current density (A/cm^2).

$J_{min}^{0,a}$ Minimum anode exchange current density (A/cm^2).

$J^{0,c}$ Cathode exchange current density (A/cm^2).

$J_{max}^{0,c}$ Maximum cathode exchange current density (A/cm^2).

$J_{min}^{0,c}$ Minimum cathode exchange current density (A/cm^2).

J^0 Exchange current density (A/cm^2).

J^{Lim} Limiting current density (A/cm^2).

J_{min}^{Lim} Minimum limiting current density (A/cm^2).

k Polytropic Coefficient.

M_{max}^{Elz} Electrolyzer maximum production rate (kg/hr).

m_{H_2} Hydrogen molar mass (kg/mol).

N Total number of measurements.

$N^{Elz,c}$ Electrolyzer number of cells.

N^{PV} PV module number.

O^s OpEx ($/MWh) of unit s.

P^s_{max} Maximum power of unit s (MW).

P^s_{min} Minimum power of unit s (MW).

Q^{BESS} BESS capacity (MWh).

Q^{HS} HS capacity (kg).

R Ideal gas constant (J/mol·K).

r Interest rate (%).

R^{Elz} Electrolyzer resistance (Ω).

RS^{BESS} BESS residual value ($).

S^N Solar radiation at NCOT (W/m^2).

SoC_{max} BESS maximum state-of-charge (%).

SoC_{min} BESS minimum state-of-charge (%).

SoH_{max} HS maximum state-of-hydrogen (%).

SoH_{min} HS minimum state-of-hydrogen (%).

t^m Thickness of the electrolyzer's membrane (cm).

T^{Elz} Electrolyzer temperature (K).

T^{HS} HS temperature (K).

T^N Normal cell operating temperature (NCOT) (°C).

$T^{PV,a,N}$ Ambient temperature at NCOT (°C)

$T^{PV,r}$ PV rated temperature (°C).

TC System total CapEx ($/hr).

$V^{Elz,c}_{max}$ Maximum electrolyzer cell voltage.

$V^{Elz,oc}$ Electrolyzer open-circuit cell voltage (V).

$V_{max}^{Elz,oc}$ Maximum open-circuit voltage of electrolyzer cell (V).

y^s unit s's lifetime (yr).

z Hydrogen compressibility factor.

Indices and Sets

Δt Time interval of the optimization problem (h).

$\mathcal{N}, n$ Set of collected measurement data points of J-V of the PEM electrolyzer cell, indexed by n.

$\mathcal{S}, s$ Set of hydrogen facility integrated units, indexed by $s \in \{Elz, Cmp, PV, BESS\}$.

$\mathcal{T}, t$ Set of optimization time steps, indexed by t.

Variables

β_t^{PV} Temperature coefficient of efficiency (1/°C).

η_t^{Elz} Electrolyzer efficiency (%).

η_t^{F} Faraday's conversion efficiency (%).

η_t^{PV} PV system conversion efficiency (%).

π_t^{HS} HS pressure (bar).

ACC_t Achievable cycle count.

CoH_t Cost of hydrogen ($/kg).

D_t^{BESS} BESS Degradation cost ($/MW).

DoD_t BESS depth of discharge (%).

E_t^{Grd} Electricity bill cost ($/hr).

e_t^{Pr} Electricity purchasing price ($/MWh).

j_t^{Elz},J^{Elz} Electrolyzer current density (A/cm^2).

M_t^{Elz} Electrolyzer hydrogen production rate (kg/hr).

M_t^{Ld} Hydrogen demand (kg/hr).

$p_t^{BESS,Chg}$ BESS charging power (MW).

$p_t^{BESS,Dhg}$ BESS discharging power (MW).

p_t^{Cmp} Compressor input power (MW).

p_t^{Grd} Grid purchasing power (MW).

p_t^{Ld} Electrical demand (MW).

$p_t^{PV,Crt}$ PV curtailment power (MW).

$p_t^{PV,M}$ PV maximum power (MW).

S_t Solar radiation (W/m^2).

SC_t Total system cost ($/hr).

SoC_t BESS state of charge (%).

SoH_t HS state-of-hydrogen (%).

$T_t^{PV,a}$ PV ambient temperature (^{o}C).

T_t^{PV} PV system temperature (^{o}C).

TD_t Total degradation cost ($/hr).

TO_t Total operation cost ($/hr).

$v_t^{Elz,\Omega}$ Electrolyzer cell ohmic overvoltage (V).

$v_t^{Elz,act}$ Electrolyzer cell activation overvoltage (V).

$v_t^{Elz,c,est}$ Estimated value of electrolyzer cell voltage (V).

$v_t^{Elz,con}$ Electrolyzer cell concentration overvoltage (V).

$v_t^{Elz,c}$ Electrolyzer cell voltage (V).

p_t^{Elz} Electrolyzer input power (MW).

TC_t^{BESS} Total BESS costs ($/hr).

$TC_t^{H_2}$ Total hydrogen system costs ($/hr).

TC_t^{PV} Total PV system costs ($/hr).

$v_t^{Elz,s}$ Electrolyzer stack voltage (V).

Publications

JOURNAL PAPERS

A. M. Abomazid, N. A. El-Taweel and H. E. Farag, "Novel Analytical Approach for Parameters Identification of PEM Electrolyzer", in *IEEE Transactions on Industrial Informatics*.

A. M. Abomazid, N. A. El-Taweel and H. E. Farag, "Optimal Energy Management of Hydrogen Energy Facility Using Integrated Battery Energy Storage and Solar Photovoltaic Systems". [Submitted]

CONFERENCE PAPERS

A. M. Abomazid, N. A. El-Taweel and H. E. Farag, "Electrochemical Optimization Model for Parameters Identification of PEM Electrolyzer," *2020 IEEE Electric Power and Energy Conference (EPEC)*, 2020, pp. 1-5, doi: 10.1109/EPEC48502.2020.9320048.

A. M. Abomazid, N. A. El-Taweel and H. E. Farag, "Energy Management System for Minimizing Hydrogen Production Cost Using Integrated Battery Energy Storage and Photovoltaic Systems," *2021 IEEE Power Energy Society Innovative Smart Grid Technologies Conference (ISGT)*, 2021, pp. 1-5, doi: 10.1109/ISGT49243.2021.9372279.

Chapter 1

Introduction

This chapter introduces the research background and summarizes the contributions of this thesis.

1.1 Research Backgrounds

In this section, the background of the research in this thesis is introduced, including hydrogen production, mathematical modeling of electrolyzers, and EMS.

1.1.1 Hydrogen Production

Hydrogen is the most abundant and simplest element on Earth. Hydrogen energy has been gaining interest due to its properties and potential to transform the world's energy systems in order to overcome current environmental challenges [9, 10]. Hydrogen fuel is widely used for various industrial, commercial, and domestic applications [10, 11]. Thus, hydrogen demand has been increasing continuously, reaching 70 million tons in 2018 and expected to reach 545 million tons per year by 2050 [12]. Hydrogen is produced from fossil fuel, biomass, and water electrolysis [10, 11, 13]. Water electrolysis uses electricity to produce hydrogen by separating hydrogen from water molecules. In contrast to steam-methane reforming, which produces hydrogen along with carbon monoxide and carbon dioxide, water electrolysis only produces hydrogen and oxygen, with zero greenhouse gas emissions [11]. While hydrogen has numerous benefits, its excessive flammability poses significant health and safety hazards when used on a large scale. Therefore, risks and safety considerations should be well managed, otherwise, the deployment of hydrogen could be slowed down or even prevented.

Furthermore, hydrogen produced by water electrolysis is of considerable interest to both industrial and residential consumers. This interest is motivated by the continuous declines in renewable electricity costs, especially from solar and wind power, and the modularity of electrolysis to build power-to-gas (PtG) units on a large megawatt scale [10, 14]. The PtG

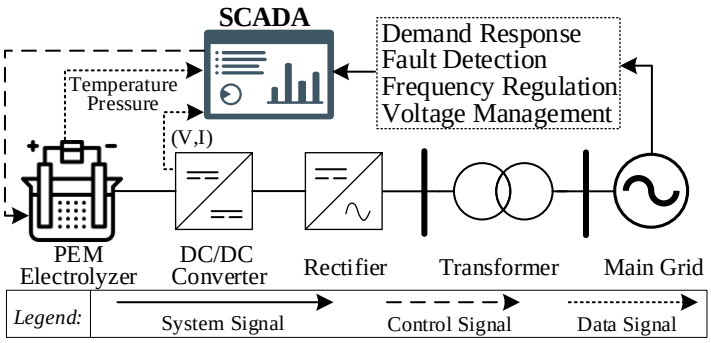

Figure 1.1: Smart grid application of PEM electrolyzer.

technology allows the use of hydrogen as an energy storage medium, where the hydrogen can be converted back to electricity using a fuel cell when needed. In addition, PtG technology can be utilized by the power sector for grid balancing services, since water electrolyzers are renowned for their fast response times [2, 15]. Therefore, techno-economical models to produce hydrogen from water electrolysis are experiencing substantial interest with a steadily increasing number of projects around the world [12, 16].

There are three main different technology options of electrolysis: alkaline technology, solid oxide electrolysis cells (SOECs), and proton exchange membrane (PEM) electrolysis [2, 17]. The PEM electrolysis technology was first brought out by General Electric in the 1960s to overcome the operational limitations of alkaline technology such as low pressure operations and limited ranges of operation [17]. Furthermore, the PEM electrolyzer is distinguished by having a quick response time and having a simple device structure [17]. Even though SOECs have a high conversion efficiency and low material costs, the technology is still under development and has not yet been commercialized [17]. The PEM electrolyzer is therefore an attractive option and is widely used by several hydrogen companies including Cummins in Canada, AREVA H2 Gen in France and ITM Power in the United Kingdom [18].

1.1.1.1 A Review of Modeling Methods for PEM Electrolyzer Cells

The grid-connected PEM electrolyzer shown in Fig.1.1 allows grid operators to properly control and schedule hydrogen production in addition

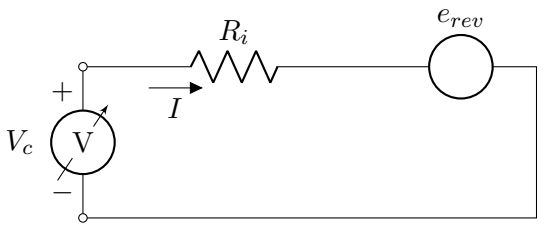

Figure 1.2: Equivalent circuit model for a single PEM electrolzyer cell [6]

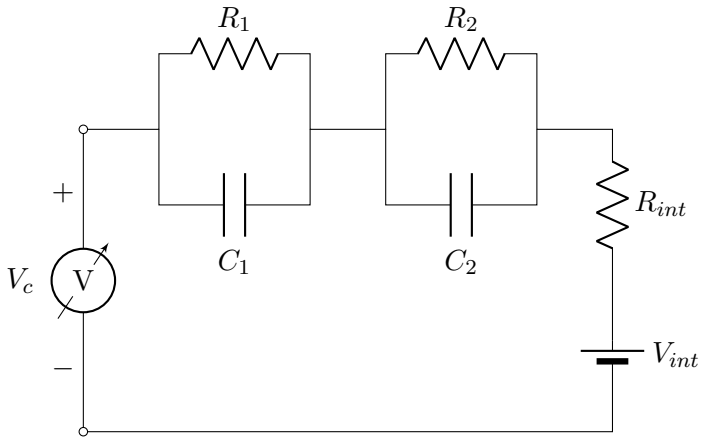

Figure 1.3: Equivalent circuit model for a single PEM electrolzyer cell [7]

to the provision of several ancillary services to the grid. In this regard, accurate mathematical modeling of the PEM electrolyzer is vital to address and analyze its design, optimization, evaluation, and control under different operating conditions. Therefore, several electrical and electrochemical models have been developed and tested to describe the characteristics of PEM electrolyzers.

Electrical Models

The electrical modeling of an electrolyzer is based directly on the relationship between voltage and current. Atlam and Kolhe [6] developed an equivalent electrical model for the PEM electrolyzer as shown in Fig. 1.2, and its mathematical model describes the current density-voltage (J-V) as a function of operating pressure and temperature. In [7], an equivalent dynamic electrical model for a PEM electrolyzer is presented as shown in

Fig.1.3. The model is approximated as a voltage source and the characteristics of the overvoltage are analyzed by determining the resistance and capacitance during sudden changes in the supply current. Although the linear and nonlinear models proposed in [6, 7] are accurate and easy to construct, they do not take into consideration the effect of the physical and chemical characteristics such as water content and rate of electrolysis on the J-V characteristic curve.

Electrochemical Models

In current research on PEM electrolyzer, the electrochemical model is widely used because it takes into consideration physical parameters such as cell area, membrane type, and chemical parameters such as water content and electrolysis rate. The electrochemical electrolyzer model is ideally realized by a voltage source, which uses the minimum energy necessary to initiate electrolysis [19]. However, in real-life electrolysis cells, there are losses associated with a series resistance connected to a voltage source [20]. In order to accurately model the PEM electrolyzer cells, electrochemical phenomena present in the electrolyzing process must also be considered. In [14, 21], the activation overvoltage considered to address the non-idealities associated with electrochemical reactions. In [22], a detailed PEM electrolyzer model is presented that accounts for the previous voltages as well as concentration phenomena. Reference [23] presents two electrochemical models of alkaline electrolyzer cell: an empirical model and a semi-empirical model that depends on the electrolyzer's temperature. These models are also used to model PEM electrolyzers as reported in [24]. Reference [25] has improved the accuracy of the detailed model proposed in [23] by considering both the effect of temperature and pressure on the J-V characteristic curve. Yet, the proposed models in [23–25] are derived from empirical and semi-empirical current and voltage relationships. The shortcoming of the proposed simplified model in [23] is clearly recognized by ignoring the influence of temperature and pressure on the empirical parameters, whereas the detailed models in [23–25] require estimating up to eight empirical fitting parameters. Further, by utilizing the empirical parameters defined in [23–25], the chemical properties of the electrolysis process are not fully characterized.

1.1.2 Mathematical modeling of PEM Electrolyzer System

Fig. 1.4 illustrates the basic concept of a PEM electrolyzer operation. The electrolysis process involves an electric current being applied to a liquid water to decompose it into hydrogen and oxygen gasses. Oxygen gas is produced as a result of the oxidation reaction occurring on the anode electrode,

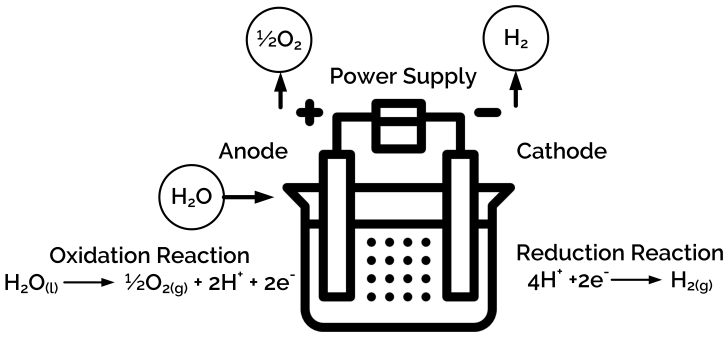

Figure 1.4: Operation concept of PEM electrolyzer.

while hydrogen is produced from the reduction reaction occurring on the cathode electrode. Combining these two electrochemical reactions gives the following result [26]:

$$\mathrm{H_2O} \xrightarrow{\text{Electricity+Heat}} \mathrm{H_2} + \frac{1}{2}\,\mathrm{O_2} \tag{1.1}$$

The hydrogen production rate of the electrolyzer is proportional to the applied current. It is governed by the following relationship [27, 28]:

$$M_t^{Elz} = \frac{\eta_t^F \cdot N^{Elz,c} \cdot i_t^{Elz}}{2F} \quad \forall\, t \in \mathcal{T}. \tag{1.2}$$

The energy conversion efficiency of the electrolyzer system is described as [29]:

$$\eta_t^{Elz} = M_t^{Elz} \cdot \frac{HHV}{p_t^{Elz}} \quad \forall t \in \mathcal{T}, \tag{1.3}$$

where Faraday's efficiency is computed using [30]:

$$\eta_t^F = (c_1 \pi^{H_2} + c_2) \cdot (j_t^{Elz})^d + f \quad \forall\, t \in \mathcal{T}. \tag{1.4}$$

It is noteworthy that the HHV is utilized in (1.3) since hydrogen is assumed to be directly used in the gas industry. However, the lower heating value (LHV) should be used for computing electrolyzer efficiency in instances where hydrogen is converted into another form of energy, such as mechanical, electrical, or thermal.

The circuit model for the PEM electrolyzer cell can be shown in Fig. 1.5 [2, 8]. The PEM electrolyzer circuit model is made up of open-circuit

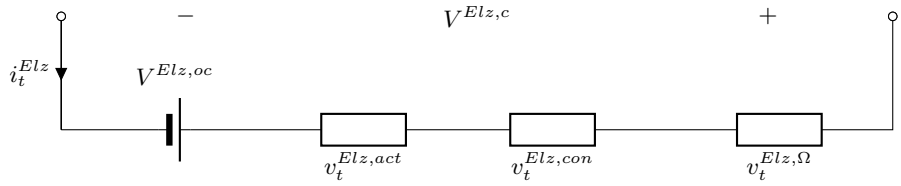

Figure 1.5: Electrolyzer cell equivalent electrical circuit [2, 8]

voltage and three different types of overvoltages as depicted in Fig. 1.5. These overvoltages are ohmic, activation, and concentration overvoltage. The mathematical representation of the characteristics of the non-linear J-V relationship of an electrolyzer cell can be expressed as [21]:

$$v_t^{Elz,c} = V^{Elz,oc} + v_t^{Elz,\Omega} + v_t^{Elz,act} + v_t^{Elz,con} \quad \forall\, t \in \mathcal{T}. \tag{1.5}$$

Ideally, one can consider the PEM electrolyzer cell as an open-circuit voltage source. This voltage simulates the minimum amount of energy necessary to initiate the electrolysis process, splitting water molecules into hydrogen and oxygen. It is described by using the Nernst equation, which defines the electrochemical cell voltage in non-standard conditions as a function of cell operating temperature, pressure, and change in Gibbs free energy as [3]:

$$V^{Elz,oc} = \frac{\Delta G}{2F} + \frac{RT^{Elz}}{2F} \ln\Big(\frac{\pi^{H_2}\sqrt{\pi^{O_2}}}{\pi^{H_2O}}\Big). \tag{1.6}$$

The change in Gibbs free energy (ΔG) is the minimal amount of free energy required to form one mole of a substance from its inert component. The value of that change is dependent on the initial and final substance states in addition to the temperature at which the chemical reaction takes place. The computation of the change in Gibbs free energy requires an understanding of the thermodynamics of the electrolysis process, which can be challenging under various temperatures and pressures [31].

Practical PEM electrolyzer cells, however, have an internal resistance which mimics that of electrode, membrane, electrolyte, and bipolar plates, as well as contact resistance. Changes in temperature and water content can greatly affect the equivalent resistance of a PEM electrolyzer. According to Ohm's law, the voltage due to internal resistance is calculated as [14]:

$$v_t^{Elz,\Omega} = j_t^{Elz} \cdot R^{Elz} \quad \forall\, t \in \mathcal{T}, \tag{1.7}$$

Several studies have dealt only with overvolatge caused by the internal resistance of the membrane, and it has been described as [14]:

$$v_t^{Elz,\Omega} = j_t^{Elz} \cdot \frac{t^m}{\sigma^m} \quad \forall\, t \in \mathcal{T}. \tag{1.8}$$

Another type of electrochemical overvoltage is raised when a current is applied to the anode and cathode electrodes of the PEM electrolyzer cell. This overvoltage is created as a result of the movement of protons and electrons between the cathode and anode in the electrochemical reaction [32]. Using Butler-Volmer's equation as the basis of calculation, the activation overvoltage is obtained as [33]:

$$v_t^{Elz,act} = \frac{RT^{Elz}}{2F\alpha^a} \operatorname{arcsinh}(\frac{j_t^{Elz}}{2J^{0,a}}) + \frac{RT^{Elz}}{2F\alpha^c} \operatorname{arcsinh}(\frac{j_t^{Elz}}{2J^{0,c}}) \quad \forall\, t \in \mathcal{T}, \tag{1.9}$$

Several studies in the literature have combined the activation overvoltage of the cathode and anode. The combined activation over voltage is represented as [32]:

$$v_t^{Elz,act} = \frac{RT^{Elz}}{2F\alpha} \operatorname{arcsinh}\big(\frac{j_t^{Elz}}{2J^0}\big) \quad \forall\, t \in \mathcal{T}. \tag{1.10}$$

The charge transfer coefficient (α) is a key parameter in determining the performance of a PEM electrolyzer. It represents the fraction of the electrostatic potential energy that is needed to limit the electrokinetic process in the electrolyzer. It greatly contributes to the polarization characteristic curve of the electrolyzer [34]. Moreover, it is affected by changes in temperature and not by changes in pressure. [35]. On the other hand, the exchange current density parameter (J^0) refers to the current flowing at the surface of electrodes at equilibrium. It depends on the electrode's operating conditions, the operating temperature, and the catalyst's structure [36].

Under high current densities, a difference in the concentration of hydrogen and oxygen is observed between the anode and cathode electrodes. In Fig. 1.5, similar to the activation phenomenon, an overvoltage is raised to represent the concentration phenomenon. The concentration overvoltage is given as [22]:

$$v_t^{Elz,con} = \frac{RT^{Elz}}{2F} \ln\Big(\frac{J^{Lim}}{J^{Lim} - j_t^{Elz}}\Big) \quad \forall\, t \in \mathcal{T}, \tag{1.11}$$

where the limiting current density (J^{Lim}) is the maximum allowable current density for water electrolysis.

The electrolyzer stack is a series of electrolyzer cells that are connected in series in order to produce a certain amount of hydrogen. The voltage across the electrolyzer stack model is given as the sum of all voltages across the electrolyzer cells:

$$v_t^{Elz,s} = \sum_{i=1}^{N^{Elz,c}} v_{t,i}^{Elz,c} \quad \forall\, t \in \mathcal{T}. \tag{1.12}$$

The power consumed by an electrolyzer stack can be calculated by using the following equation:

$$p_t^{Elz} = i_t^{Elz} \cdot v_t^{Elz,s} \quad \forall\, t \in \mathcal{T}. \tag{1.13}$$

1.1.3 Energy Management System

With the rapid development of the hydrogen industry, having an efficient, economical, and clean hydrogen production facility has become a major concern. Therefore, increasing research efforts to solve such techno-economical concern are being a prompted interest. In this regard, the incorporation of renewable energy sources (i.e., solar and wind) with electrolyzer systems in microgrids is considered to be a viable solution to mitigate the hydrogen production techno-economical concern. Microgrids make hydrogen production more accessible to consumers by being an affordable, scalable, and environmentally sustainable solution. Microgrids are low-voltage distribution systems that integrate distributed energy resources (DERs), such as solar photovoltaic (PV) systems and battery energy storage systems (BESSs), as well as controllable loads such as hydrogen production systems and electric vehicles. Microgrids can operate either independently by using their DERs to supply loads, in the islanded mode, or by being connected to the grid, in the grid-connected mode. The development of microgrids faces several economical and operational challenges due to the high capital costs of renewable energy resources, in addition to the uncertainty associated with intermittent renewable energy sources and demand. It is possible to overcome these challenges by using EMS. A microgrids' EMS is tasked with managing supply and demand for the purpose of achieving several economic, sustainable, and operational objectives, including a stable, safe, and adequate flow of electricity. Many efforts have been made on the development of economical and reliable microgrid's EMS strategies [37–39]. These strategies focus on scheduling either DERs or loads, or both at the same time. Different control approaches are used for optimum performance of

microgrid operation. In general, control strategies can be divided into two main categories: rule-based and optimization-based, and all subcategories can be categorized by the two main categories.

1.1.3.1 Rule-Based Control Approach

Rule-based control approaches are fundamental control schemes that depends on the mode of operation [40–43]. They can be easily integrated into the microgrid EMS. Typically, the rules are derived from human intelligence, heuristics, or mathematical models that require prior knowledge of the system's behavior. Accordingly, the operating points of the dispatchable DERs and adjustable loads are determined using lookup tables or flowcharts that meet the requirements of operator and customers. Generally, the main objective of rule-based control approaches is to maintain operational efficiency and performance.

1.1.3.2 Optimization-Based Control Approach

Contrary to the rule-based control approaches, optimization-based control approaches primarily aim to minimize/maximize a defined objective function [44–46]. Furthermore, the optimization-based control approaches differ from rule-based control approaches in that the optimal solution is based on the mathematical modeling of the system. This model can be numerical or analytical. Optimization-based control strategies are classified into mathematical optimization and metaheuristic optimization methods. Mathematical optimization consists of combinatorial optimization, dynamic optimization, numerical techniques, linear programming, mixed integer linear programming, and dynamic programming. On the other hand, the metaheuristic optimization methods include particle swarm optimization (PSO) methods and genetic algorithms [1].

1.1.3.3 Comparison between EMS Approaches

Rule-based control approach are easy to implement with low computational complexity, however, its solution might not lead to the best results due to its dependence on human intelligence. On the other hand, optimization-based control approaches ensure optimal operation of the microgrid, and they are capable of solving complicated and nonlinear problems. Although they require high computation and memory resources, they can be performed in real-time simulation. Therefore, in this thesis, the optimization-based strategy will be used. Specifically, the mathematical optimization is used

due to its flexibility and its ability to model linear and nonlinear complex systems.

Table 1.1: Comparative analysis of EMS approaches [1]

EMS Approach	**Advantages**	**Disadvantages**
Rule-Based	Simple, and robust, low computation complexity, easy to implement	Not adaptive and poor parametric calibration, no guarantee of optimality.
Optimization-Based	Guarantee of optimal operation, robust, solve complex and nonlinear problems	High computational complexity

1.2 Thesis Structure and Contribution

The objective of this thesis is twofold: (1) to solve the parameter estimation problem of the PEM electrolyzer by using both optimization-based and analytical-based approaches, and (2) to optimize the production of hydrogen by using the development of a novel EMS.

Two approaches for estimating the parameters of PEM electrolyzer are proposed in chapters 2 and 3. Then, two EMSs are proposed in chapters 4 and 5 that aims to minimize the CoH production.

Chapter 2 proposes an optimization model that identifies the parameters of a detailed electrochemical model for a PEM electrolyzer. The estimation procedure is based on J-V measurements. The proposed model aims to estimate the values of seven modeling parameters of the electrolyzer electrochemical model. These parameters are change in Gibbs free energy, exchange current density for anode and cathode, charge transfer coefficient for both anode and cathode, conductivity of the membrane, and limiting current density. The parameter estimation problem is formulated based on a nonlinear least-squares objective function. Comparisons of results and analysis between experimental and estimated data for different operating conditions of temperature and pressure are presented. The results provide a root mean square error (RMSE) in the range of 10^{-6} which demonstrates the accuracy of the proposed model. To affirm the model's superiority, the

proposed model is compared with other electrolyzer parameter estimation models found in existing literature.

In chapter 3, a novel analytical approach based on the LSE method is proposed to estimate the model parameters and characterize the electrochemical behavior of the PEM electrolyzer under various operating conditions. The model has a non-linear J-V relationship with five model parameters that are subjected to change depending on the physical properties and chemical conditions of the PEM electrolyzer. The PEM electrolyzer modeling parameters are estimated, and the J-V characteristic is estimated in a non-iterative, fast, and low complexity process. The accuracy and validity of the proposed approach are tested under different case studies at various operating temperatures, output pressures, hydrogen production rates, and dataset sizes. Also, the relationship between the estimated parameters and the operating conditions of the PEM electrolyzer is explored. Finally, the superiority of the proposed approach is demonstrated by comparing it to numerical and heuristic optimization parameter estimation methods.

Chapter 4 proposes an optimal economic dispatch model for reliable scheduling operations of a clean hydrogen production system. The model aims to minimize CoH production through: i) minimizing total system costs, ii) maximizing hydrogen production efficiency, and iii) maximizing solar energy utilization. The model takes into consideration CoH production sensitivity to electrolyzer efficiency variation. Electrochemical hydrogen production mechanism and operational balance constraints are incorporated into the optimization model to guarantee accurate and stable system performance. The simulation results verified the economic feasibility of the proposed dispatch model in terms of meeting hydrogen demand, system stability, and storage capability. The optimization results reveal that the average CoH production for the proposed model is 2.67 \$/kg during the study period. The results of this study highlights the correlation between hydrogen production rate, electrolyzer efficiency, and CoH production. A comparative analysis with and without the consideration of the variability of the electrolyzer efficiency indicates the efficacy and feasibility of the proposed model in minimizing hydrogen production costs and maximizing solar power utilization.

Chapter 5 focuses on the design and implementation of an optimal scheduling EMS model of a hydrogen production system to optimize its operation in order to minimize the CoH while maintaining a reliable system operation. A Z-score statistical measure of historical electricity prices is incorporated into the proposed EMS in order to enable seasonal storage application. To demonstrate the validity of this model, it is tested for both

intraseasonal and seasonal storage. Four case studies are used to prove the techno-economic benefits of the proposed EMS model. Furthermore, the impact of the electrolyzer's capacity factor, the size of the hydrogen storage, and the PV share on the system's techno-economic benefits is investigated .

The conclusions and future work are given in Chapter 6.

Chapter 2

Electrochemical Optimization Model for Parameters Estimation of PEM Electrolyzer

The aim of this chapter is to estimate the parameters of the electrochemical model for a PEM electrolyzer using an optimization model. The estimation procedure relies on the J-V measurements. In the proposed model, seven modeling parameters of the electrolyzer electrochemical model have been estimated. The parameters that are estimated include the change in Gibbs free energy, exchange current density for the cathode and the anode, charge transfer coefficient for both the anode and cathode, and membrane conductivity. A nonlinear least-squares objective function is used to formulate the parameter estimation problem. For different operating temperatures and pressures, comparisons and analyses of experimental and estimate data are provided. As a way of demonstrating the model's superiority, it is compared with other electrolyzer parameter estimation models described in existing literature.

2.1 Introduction

Parameter estimation has long been a popular research area for several types of electrical and electrochemical systems such as motors [47], generators [48], fuel cells [49], and batteries [50]. The estimation of parameters for such systems is necessary in order to describe their characteristics and behavior under various operating conditions [8]. In the detailed electrochemical model of the PEM electrolyzer, there are modeling parameters that can be varied based on the physical and chemical characteristics of the electrolyzer. Estimation of these parameters at various operating conditions with a high degree of precision is necessary in order to have an accurate modeling and

visualization of the behavior of the PEM electrolyzer. This will ultimately make the most of PEM electrolyzers under various loading and operating conditions by ensuring efficient monitoring, control, and performance [8].

The parameter estimation problem of the PEM electrolyzer is commonly formulated as an optimization problem [8, 14, 22, 51]. The nonlinear and time-varying behavior of PEM electrolyzers under different operating and physical conditions, makes the analytical estimation of the parameters a challenging task [52]. In this regard, previous studies have used optimization algorithms to estimate three PEM electrolyzer parameters [14, 22, 51]. Another study done by Lebbal at el. [8] has estimated five model parameters. In [22], the cathode and anode exchange current density parameters as well as membrane conductivity are estimated. The work also estimated the operating temperature and partial pressures of the anode and cathode, along with membrane thickness. Reference[14] estimated three PEM electrolyzer parameters including anode charge transfer coefficient and its exchange current density, as well as the membrane conductivity. Harrison et al. [51], also estimated three parameters, namely, exchange current density for the anode and cathode parameters, along with the membrane conductivity. Lebbal [8] estimated five model parameters: charge transfer coefficient, exchange current density, diffusion coefficient, limiting current density, and membrane conductivity.

Based on the above literature survey, it is notable that previous works in the parameter estimation of PEM electrolyzers fall short in considering a detailed electrochemical model with seven parameters. Such a detailed model should take into consideration the operating conditions and physical properties' effect on the following parameters: change of Gibbs free energy (ΔG), exchange current density for anode ($J^{0,a}$) and cathode ($J^{0,c}$), charge transfer coefficient for anode (α^a) and cathode (α^c), conductivity of membrane (σ^m), and limiting current density (J^{Lim}). Therefore, the aim of this chapter is to introduce a new estimation model that takes into account all seven PEM electrolyzer parameters. This is achieved by formulating the model as a constrained nonlinear least-squares objective function. The model constraints are derived from electrochemical principles and previous PEM electrolyzer analysis in the literature. The proposed parameter estimation model is tested under various operating conditions. Furthermore, the proposed model estimated parameters are compared to three other models' parameters found in the literature.

2.2 Optimization-Based Parameter Estimation Model for PEM Electrolyzer

In this section, the parameter estimation of a PEM electrolyzer cell is formulated as an optimization problem. The optimization problem is formulated as a constrained least-squares based objective function. This formulation aims to estimate the seven unknown PEM electrolyzer parameters, which in turn enables the prediction of its electrical characteristics under various temperatures and pressures.

The parameter estimation model uses a set with N number of measured J-V data points of the PEM electrolyzer. These data points range from the minimum current required to start the electrolysis process to the maximum rating current of the PEM electrolyzer device at controlled operating temperature and pressure. The parameters that fit the collected measured data can be estimated by minimizing the following least-squares based objective function:

$$\underset{\Delta G, J^{0,c}, J^{0,a}, \alpha^a, \alpha^c, \sigma^m, J^{Lim}}{\text{Minimize}} : \sum_{i=1}^{N} (v_t^{Elz,c}(i) - v_t^{Elz,c,est}(i))^2. \tag{2.1}$$

The objective function stated by (2.1) aims to minimize the deviation between the actual ($v_t^{Elz,c}$) and estimated ($v_t^{Elz,c,est}$) values of the total voltage across the PEM electrolyzer cell.

The fact that the value of the open-circuit voltage expressed in equation (1.6) cannot exceed the rated voltage of the cell implies an upper bound constraint for the optimized parameter ΔG such that:

$$0 \leq \Delta G \leq V_{max}^{Elz,oc} \cdot 2F - RT^{Elz} \ln\left(\frac{\pi^{H_2}\sqrt{\pi^{O_2}}}{\pi^{H_2O}}\right). \tag{2.2}$$

The exchange current density at the cathode in equation (1.9) depends on the concentration of oxygen, while the exchange current density at the anode depends on the concentration of hydrogen [33]. These parameters range from nA/cm^2 to mA/cm^2 [53]. Consequently, the objective function in (2.1) is also subject to the anode and cathode exchange current density magnitude limits as follows:

$$J_{min}^{0,a} \leq J^{0,a} \leq J_{max}^{0,a}, \quad J_{min}^{0,c} \leq J^{0,c} \leq J_{max}^{0,c}, \tag{2.3}$$

Given that the cathode exchange current density is greater than the anode exchange current density [51], the objective function in (2.1) is imposed

by the following constraint as:

$$J^{0,a} \leq J^{0,c}. \tag{2.4}$$

The anode and cathode charge transfer coefficients are defined as being within a specified range given as follows [54]:

$$\alpha^a_{min} \leq \alpha^a \leq \alpha^a_{max}, \quad \alpha^c_{min} \leq \alpha^c \leq \alpha^c_{max}, \tag{2.5}$$

The objective function of the optimization problem in (2.1) is also subject to the fact that the sum of the anode and cathode charge transfer coefficients is equal to unity as described in (2.6). This is due to the assumption that the electrolysis of water is a single-step reaction [26]. Moreover, the fact that the anode charge transfer coefficient is higher than the cathode charge transfer coefficient, adds another constraint to the problem stated in (2.1), as follows [35]:

$$\alpha^c + \alpha^a = 1 \quad \forall\, \alpha^c \leq \alpha^a. \tag{2.6}$$

Equation (2.7) represents a constraint that forces the σ^m parameter in equation (1.8) to be within the device's capabilities, given as [55]:

$$\sigma^m_{min} \leq \sigma^m \leq \sigma^m_{max}, \tag{2.7}$$

The limiting current density parameters in equation (1.11) imposes an upper limit on the current density applied to the electrolyzer. Therefore, a lower bound constraint on the limiting current density is added to the objective function in (2.1) as:

$$J^{Lim}_{min} \leq J^{Lim}. \tag{2.8}$$

To that end, the proposed model in (2.1)-(2.8) can be extended to cover the PEM electrolyzer stack.

2.3 Performance Evaluation

The PEM electrolyzer cell is developed and modeled using MATLAB software to test the proposed parameter estimation model. The design of the PEM electrolyzer model is based on a comprehensive study of commercially available PEM electrolyzers and real-life J-V data [2, 8, 22, 33, 51]. The model is developed in order to operate within a temperature range of 50°C

Table 2.1: Modeling and simulation parameters

σ^m_{max}= 0.35 (S/cm)	σ^m_{min}= 0.1 (S/cm)	α^a_{max}= 1
$J^{0,a}_{max}$= $J^{0,c}$ (A/cm^2)	$J^{0,a}_{min}$= 1 (nA/cm^2)	α^a_{min}= α^c
$J^{0,c}_{max}$= 1 (A/cm^2)	$J^{0,c}_{min}$= $J^{0,a}$ (A/cm^2)	α^c_{max}= α^a
$V^{Elz,oc}_{max}$= 2.2 (V)	Cell Area = 160 (cm^2)	α^c_{min}= 0
t^m= 0.05 (cm)	J^{Lim}_{min}= $\max_{1\leq i\leq N}\{j^{Elz}_t(i)\}$	

Table 2.2: Estimated PEM electrolyzer cell parameters

Operating Condition	$T^{Elz} = 50^oC$	$T^{Elz} = 80^oC$
Parameter	π^{H_2}=20bar	π^{H_2}=1bar
ΔG (kJ/mol)	233.1	228.21
$J^{0,a}$ $(\mu A/cm^2)$	1.0723	11.853
$J^{0,c}$ (A/cm^2)	0.1143	0.131
α^c	0.2785	0.3044
α^a	0.7215	0.6956
σ^m (S/cm)	0.1359	0.1896
J^{Lim} (A/cm^2)	1.7025	2.135
RMSE	7.6053×10^{-6}	1.8336×10^{-6}
Convergence Time (sec)	0.720605	0.690956

to 80°C and a cell pressure range of 0bar to 30bar. The modeling and simulation parameters for the modeled PEM electrolyzer are listed in Table 5.1. In order to evaluate the proposed parameter estimation model, a current is applied to the PEM electrolyzer cell to have a current density ranging from zero to the rated value. A total of 54 J-V data points are collected at different operating points. The proposed parameter estimation model is coded and solved using the available optimization toolbox in MATLAB. The trust region reflective optimization algorithm is used to find the optimized seven parameters of the single PEM electrolyzer cell, and therefore, shows the effectiveness of the proposed model parameters. The algorithm is customized for a maximum iteration number of 600 and a function tolerance of 1×10^{-12}.

It is noteworthy that all the experiments are conducted on a Windows 10 Professional OS environment using Intel Core i7, 2.21 GHz, 16G RAM, and the codes are performed in Matlab 9.6.

The evaluation criteria in this work are based on the RMSE value and the computational time taken for the algorithm to converge. A good identifier

Table 2.3: Comparison between estimated parameters and different literature review parameters

Parameter	Proposed model	[14]	[8]	[51]
ΔG (kJ/mol)	228.21-233.1	-	-	-
$J^{0,a}$ $(\mu A/cm^2)$	1.0723-11.853	0.011-0.11	0.13×10^3(A)	0.0165
$J^{0,c}$ (A/cm^2)	0.1143-0.131	-	-	0.09
α^c	0.2785-0.3044	-	-	-
α^a	0.6956-0.7215	0.7353	0.452	-
σ^m (S/cm)	0.1359-0.1896	0.1031-0.1604	$3.2\times10^{-3}(\Omega)$	0.075
J^{Lim} (A/cm^2)	1.7025-2.135	-	120 (A)	-

is one that requires less computational effort with a small RMSE value.

Table 2.2 presents the results of the proposed PEM electrolyzer parameter estimation model under various operating conditions, as well as the values of the RMSE and convergence time. The results show that the estimated parameters vary under different operating temperatures and pressure levels. Table 2.2 reveals that the estimation of the parameters takes up to 0.72 seconds. Moreover, the parameter estimation model achieves a RMSE value of 1.83×10^{-6} and 7.6×10^{-6} in various operating conditions, resulting in an estimated J-V curve close to the real curve.

The estimated values of the change in the Gibbs free energy parameter reported in Table 2.2 correlate fairly well with the work in [52] and further support the idea that open-circuit voltage decreases with high temperature and low pressure, whereas it increases with low temperature and high pressure. It is worthwhile to note that with the increase in temperature comes an increase in the membrane conductivity, which is consistent with previous findings [22]. Additionally, there is a significant positive correlation between exchange current density and charge transfer coefficients with temperature as reported in literature [22] and [33].

The performance of the electrolyzer model using the estimated parameters in Table 2.2 confirms a very good reproduction of the PEM electrolyzer J-V characteristic curve. As shown in Fig.2.1, the estimated values using the estimated electrolyzer parameters and the experimental data are almost a perfect match under various temperatures and pressure levels. Fig.2.1 illustrates that the value of cell voltage increases at high pressure and low temperature requiring more power to split water, whereas at high temperature and low pressure, less power is required for water electrolysis.

To further show the superiority of the proposed model, data collected at

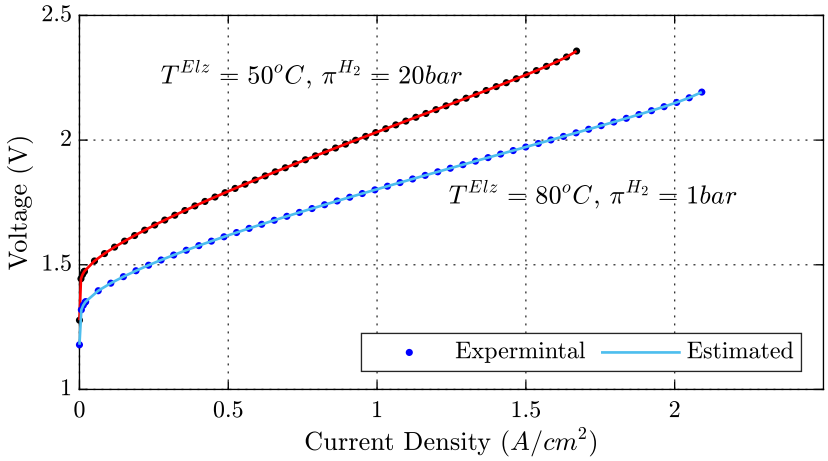

Figure 2.1: A comparison of J-V curves using the estimated parameter and the experimental data under various temperatures and cathode pressures.

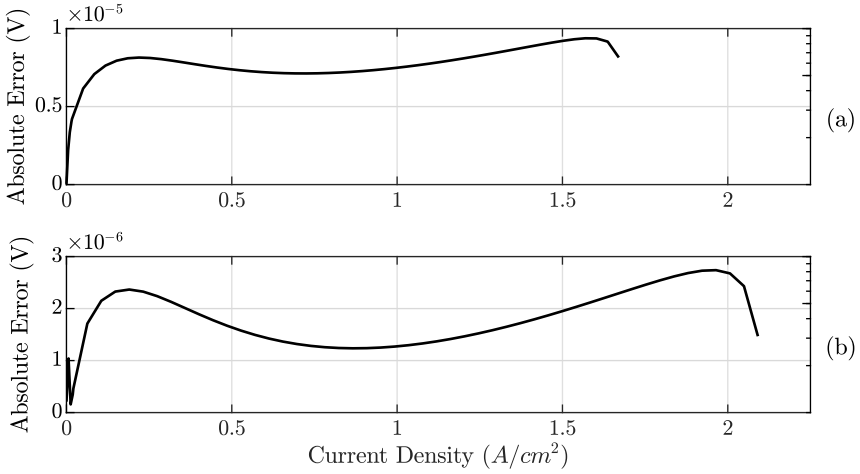

Figure 2.2: Absolute error at: (a) $T^{Elz} = 50\ ^oC$ and $\pi^{H_2} = 20\ bar$, and (b) $T^{Elz} = 80\ ^oC$ and $\pi^{H_2} = 1\ bar$.

two different operating temperatures and pressure levels are used to compute the absolute error as shown in Fig.2.2. It is worth noting that Fig.2.2 is given in a logarithmic scale for the absolute error, whereas the current density uses a linear scale. The figure concludes that the proposed model has high parameter estimation accuracy with an average absolute error of 10^{-6} over a wide range of operating points.

The performance of the proposed model is also verified across the proposed parameter estimation models in the literature as a part of the validation process. Table 2.3 compares the obtained parameters with literature review parameters to show effectiveness of the estimated parameters. The results obtained in this work are consistent with previous findings by [14, 51]. Moreover, the results enhance previous parameter estimation models by estimating additional parameters, which improve the overall accuracy of the electrolyzer behavior modeling. This will, in turn, ensure efficient control and monitoring, hence achieving better utilization of electrolyzers under various operating conditions.

2.4 Summary

An accurate electrochemical optimization model is proposed in this chapter to estimate the values of seven modeling parameters for the PEM electrolyzer. The parameter estimation of the PEM electrolyzer is modeled as an optimization problem with a least-squares objective function. The feasibility of the proposed model is tested and verified under different operating conditions of temperature and pressure levels. The estimated parameters can be achieved with high accuracy within a short computation time. The obtained results of the estimated J-V coincide with the experimental data. The results of comparisons with literature review models have also proved the superiority of the proposed model. Altogether, these findings add to a growing body of literature on PEM electrolyzer parameter estimation.

Chapter 3

Novel Analytical Approach for Parameters Estimation of PEM Electrolyzer

A novel analytical approach based on LSE is presented in this chapter. It is used to estimate the model parameters and characterize the electrochemical behavior of a PEM electrolyzer under a variety of operating conditions. In the model, the J-V relationship is non-linearly related, with five model parameters that are subject to change based on the physical properties and chemical conditions of the PEM electrolyzer. A non-iterative, fast, and low-complexity method for estimating the J-V characteristic of PEM electrolyzers is implemented. Different case studies are conducted to evaluate the accuracy and validity of the proposed approach at different operating temperatures, output pressures, hydrogen production rates, and data sizes. Further, the relationship between the estimated parameters and the performance of the PEM electrolyzer is discussed. A comparison of the proposed method to numerical and heuristic methods for parameter estimation of optimization is made to show the superiority of the proposed approach.

3.1 Introduction

The PEM electrolyzer's parameter estimation techniques require complex calculations due to the non-linear characteristics of the J-V relationship. In this regard, two common approaches have been adopted in the literature to estimate the unknown modeling parameters of the PEM electrolyzer model. One approach is to estimate unknown parameters using heuristic optimization algorithms, such as PSO [14, 49], and neural networks (NNs) [56]. In [14], the PSO algorithm is used to estimate three parameters of the PEM electrolyzer system. Reference [56] used NNs to estimate the PEM electrolyzer's parameters accurately. These parameters are

then used to estimate the electrolyzer's conversion efficiency and hydrogen production rate. Heuristic algorithms are effective in solving the problem of estimating the PEM electrolyzer parameters because they provide close to optimal solutions within a reasonable period of time. Nevertheless, they cannot always guarantee optimal results and are subject to tuning problems [57].

Numerical optimization approaches have also been used to estimate the unknown parameters of the PEM electrolyzer [7, 8, 22], [51]. The study in [22] used Taguchi optimization to estimate the operating parameters, including temperature and pressures of the anode and cathode. The study also estimated the membrane water content, membrane thickness, and cathode and anode exchange current density parameters. Guilbert et. al. [7] presented an estimation method based on the least squares regression algorithm. The method identifies the parameters of the static and dynamic electric circuit models for PEM electrolyzers. Labbal et. al. [8] used a Gauss-Newton optimization method based on a non-linear LSE objective function to estimate five model parameters, namely the charge transfer coefficient, the exchange current density, the diffusion coefficient, the limiting current density, and the series resistance. Harrison et. al. [51], estimated three parameters using Levenberg-Marquardt algorithm, namely anode and cathode exchange current densities and membrane conductivity. In contrast to heuristic optimization approaches, numerical optimization approaches guarantee optimal results to a given tolerance [58]. However, numerical optimization is prone to initialization and convergence problems, as well as computational complexity and cost.

Based on the aforementioned discussion, both heuristic and numerical optimization techniques present computational challenges when it comes to solve the problem of estimating the PEM electrolyzer parameters. Because of the iterative nature of the optimization algorithms, as well as its high complexity and dependency on the initial value. Analytical approaches, on the other hand, can estimate the PEM electrolyzer parameters in a non-iterative timely manner by solving a set of mathematical equations based on electrochemical characteristics. Solving the analytical model would then result in estimating the PEM electrolyzer unknown parameters without computational complexity, enabling an effective implementation of online parameter estimation. This implies that the model parameters can be estimated accurately during normal operation of the PEM electrolyzer. However, during the offline parameter estimation, the model parameters are estimated through a test bench and stored in look up tables. Therefore, offline parameter estimation does not accurately reflect the actual model parameters

during the PEM electrolyzer's operation. The application of the analytical approach allows the electrolyzer operators to perform accurate scheduling control of the hydrogen production along with several ancillary services to the power grid. As such, the proposed analytical approach will allow for the better integration of PtG into smart grids, thereby increasing grid stability, renewable energy penetration, and system efficiency [7].

For this reason, this chapter presents a novel analytical approach to estimate model parameters and characterize the electrochemical behavior and hydrogen production of the PEM electrolyzer under a variety of operating conditions. Based on the LSE method, a non-iterative approach is proposed that identifies five PEM electrolyzer modeling parameters namely: change in Gibbs free energy, charge transfer coefficient, exchange current density, series resistance, and limiting current density. The validity of the proposed approach is shown at various operating temperatures, hydrogen pressure levels, and hydrogen production rates. The proposed approach is described in terms of its sensitivity to different dataset sizes. Moreover, the relationship between the estimated parameters and the operating temperature is investigated. The effectiveness of the proposed approach is evaluated by comparing the median of absolute percentage error (APE) of the model with that of other parameter estimation approaches in literature.

3.2 Proposed Analytical Approach for Parameter Estimation of Electrolyzer

3.2.1 Formulation of PEM Electrolyzer Model

In this section, a new analytical estimation approach is proposed for estimating five unknown electrolyzer modeling parameters. As shown in section 1.1.2, the J-V characteristic equation can be rewritten by substituting equations (1.6), (1.7), (1.10), and (1.11) into (1.5) as follows:

$$V_n^{Elz,c} = \frac{\Delta G}{2F} + \frac{RT^{Elz}}{2F}\ln\Big(\frac{\pi^{H_2}\sqrt{\pi^{O_2}}}{\pi^{H_2O}}\Big) + \frac{RT^{Elz}}{2F\alpha}\operatorname{arcsinh}\big(\frac{J_n^{Elz}}{2J^0}\big) + J_n^{Elz}R^{Elz} + \frac{RT^{Elz}}{2F}\ln\Big(\frac{J^{Lim}}{J^{Lim}-J_n^{Elz}}\Big) \qquad \forall\, n \in \mathcal{N}, \tag{3.1}$$

In (3.1), F and R are constants, so their values are not affected by temperature and pressure. Meanwhile, the temperature T^{Elz} is considered to be controlled by a thermostat, and the values of π^{H_2}, π^{O_2}, and π^{H_2O} are

controlled and measured by a barometer. Therefore, under controlled operating conditions of temperature and pressure, only J_n^{Elz} and $V_n^{Elz,c}$ are variables in (3.1), and ΔG, α, J^0, R^{Elz}, and J^{Lim} can be regarded as constants as long as the operating conditions remain unchanged. Given that the operating temperature and pressure of the PEM electrolyzer are measured/controlled, the model of the PEM electrolyzer can be described by five unknown parameters, which are: change in Gibbs free energy, charge transfer coefficient, exchange current density, series resistance, and limiting current density.

It should be noted that the five parameters are subject to change according to the temperature and pressure. Therefore, their estimation under different operating conditions is paramount in order to reflect the accurate behavior of the system. Essentially, the parameters need to be estimated when a change in temperature and/or pressure is observed. Given that the parameters can only be considered constants under certain operating conditions and for a short period of time, the low computational complexity of the proposed approach enables the estimation of the parameters to be performed dynamically online to accommodate any changes in the model.

In order to simplify the representation of the $J_n^{Elz} - V_n^{Elz,c}$ characteristic described in (3.1), the inverse hyperbolic function in (3.1) can be expressed as a natural logarithmic function as:

$$\sinh^{-1}(c) = \ln(c + \sqrt{c^2 + 1}). \tag{3.2}$$

where c is an arbitrary number. Equation (1.10) can therefore be rewritten as follows:

$$V_n^{Elz,act} = \frac{RT^{Elz}}{2F\alpha} \ln\left(\frac{J_n^{Elz}}{2J^0} + \sqrt{\left(\frac{J_n^{Elz}}{2J^0}\right)^2 + 1}\right) \qquad \forall\, n \in \mathcal{N}. \tag{3.3}$$

The works in [3, 32] further indicate that $J^{Elz} >> J^0$, hence equation (3.3) is further approximated to:

$$V_n^{Elz,act} = \frac{RT^{Elz}}{2F\alpha} \ln\left(\frac{J_n^{Elz}}{J^0}\right) \qquad \forall\, n \in \mathcal{N}, \tag{3.4}$$

moreover, the natural logarithmic function in (1.11) can be written as a difference of logarithms as follows:

$$V_n^{Elz,con} = \frac{RT^{Elz}}{2F} \ln(J^{Lim}) - \frac{RT^{Elz}}{2F} \ln(J^{Lim} - J_n^{Elz}) \qquad \forall\, n \in \mathcal{N}. \tag{3.5}$$

Hence, equation (3.1) is represented as follows:

$$V_n^{Elz,c} = \frac{\Delta G}{2F} + \frac{RT^{Elz}}{2F}\ln\Big(\frac{\pi^{H_2}\sqrt{\pi^{O_2}}}{\pi^{H_2O}}\Big) + \frac{RT^{Elz}}{2F\alpha}\ln\big(\frac{J_n^{Elz}}{J^0}\big)$$
$$+J_n^{Elz}R^{Elz} + \frac{RT^{Elz}}{2F}\ln(J^{Lim}) - \frac{RT^{Elz}}{2F}\ln(J^{Lim} - J_n^{Elz}) \qquad \forall\, n \in \mathcal{N}. \quad (3.6)$$

3.2.2 Estimation of ΔG Parameter

By recognizing that the value of the voltage across the PEM electrolyzer cell at $J^{Elz} \approx 0$ equals the open-circuit voltage, one can algebraically estimate the value of ΔG parameter by solving equation (1.6) by using the data point at approximately zero current density, as follows:

$$\Delta G = 2F \cdot \left(V^{Elz,oc} - \frac{RT^{Elz}}{2F}\ln\Big(\frac{\pi^{H_2}\sqrt{\pi^{O_2}}}{\pi^{H_2O}}\Big)\right). \quad (3.7)$$

It is worth mentioning that the open-circuit voltage appears across the electrolyzer cell when a small amount of current is applied. The open-circuit voltage is accurately measured when the water humidifies at the anode or the cathode side. This occurs when the thermodynamics and electrochemical equilibrium for hydrogen gas formation is reached [59].

3.2.3 Estimation of α, R^{Elz}, and J^{Lim} parameters

The three parameters α, R^{Elz}, and J^{Lim} are estimated by transforming the J-V non-linear relationship in (3.6) into a linear one through linking the three model parameters to the linear differential equation (3.8). In other words, (3.6) can be represented as a relation to α, R^{Elz}, and J^{Lim} parameters, using the differential on both sides, which is represented as follows:

$$\frac{\partial V_n^{Elz,c}}{\partial J_n^{Elz}} = \frac{RT^{Elz}}{2F\alpha J_n^{Elz}} + R^{Elz} + \frac{RT^{Elz}}{2F(J^{Lim} - J_n^{Elz})} \qquad \forall\, n \in \mathcal{N}, \quad (3.8)$$

and then reformulating equation (3.8) to the standard regression form by first multiplying both sides by $(J^{Lim} - J_n^{Elz})$ and then using distributive property, as:

$$\frac{\partial V_n^{Elz,c}}{\partial J_n^{Elz}}J_n^{Elz} + \frac{RT^{Elz}}{2F} = \frac{\partial V_n^{Elz,c}}{\partial J_n^{Elz}}J^{Lim} - \frac{RT^{Elz}J^{Lim}}{2F\alpha J_n^{Elz}} + \frac{RT^{Elz}}{2F\alpha}$$
$$-R^{Elz}J^{Lim} + R^{Elz}J_n^{Elz} \quad \forall\, n \in \mathcal{N} \quad (3.9)$$

To that end, (3.9) is stated for the N data points as follows:

$$\frac{\partial V_1^{Elz,c}}{\partial J_1^{Elz}} J_1^{Elz} + \frac{RT^{Elz}}{2F} = \frac{\partial V_1^{Elz,c}}{\partial J_1^{Elz}} J^{Lim} - \frac{RT^{Elz} J^{Lim}}{2F\alpha J_1^{Elz}} + \frac{RT^{Elz}}{2F\alpha} - R^{Elz} J^{Lim} + R^{Elz} J_1^{Elz} \quad (3.10)$$

$$\frac{\partial V_2^{Elz,c}}{\partial J_2^{Elz}} J_2^{Elz} + \frac{RT^{Elz}}{2F} = \frac{\partial V_2^{Elz,c}}{\partial J_2^{Elz}} J^{Lim} - \frac{RT^{Elz} J^{Lim}}{2F\alpha J_2^{Elz}} + \frac{RT^{Elz}}{2F\alpha} - R^{Elz} J^{Lim} + R^{Elz} J_2^{Elz} \quad (3.11)$$

$$\vdots$$

$$\frac{\partial V_N^{Elz,c}}{\partial J_N^{Elz}} J_N^{Elz} + \frac{RT^{Elz}}{2F} = \frac{\partial V_N^{Elz,c}}{\partial J_N^{Elz}} J^{Lim} - \frac{RT^{Elz} J^{Lim}}{2F\alpha J_N^{Elz}} + \frac{RT^{Elz}}{2F\alpha} - R^{Elz} J^{Lim} + R^{Elz} J_N^{Elz} \quad (3.12)$$

The aforementioned set of equations is expressed in the matrix form as follows:

$$\underbrace{\begin{bmatrix} \frac{\partial V_1^{Elz,c}}{\partial J_1^{Elz}} & \frac{-RT^{Elz}}{2FJ_1^{Elz}} & \frac{RT^{Elz}}{2F} & -1 & J_1^{Elz} \\ \frac{\partial V_2^{Elz,c}}{\partial J_2^{Elz}} & \frac{-RT^{Elz}}{2FJ_2^{Elz}} & \frac{RT^{Elz}}{2F} & -1 & J_2^{Elz} \\ \vdots & \vdots & \vdots & \vdots & \vdots \\ \frac{\partial V_N^{Elz,c}}{\partial J_N^{Elz}} & \frac{-RT^{Elz}}{2FJ_N^{Elz}} & \frac{RT^{Elz}}{2F} & -1 & J_N^{Elz} \end{bmatrix}}_{C_x} \underbrace{\begin{bmatrix} J^{Lim} \\ \frac{J^{Lim}}{\alpha} \\ \frac{1}{\alpha} \\ R^{Elz} J^{Lim} \\ R^{Elz} \end{bmatrix}}_{\pi_x} = \underbrace{\begin{bmatrix} \frac{\partial V_1^{Elz,c}}{\partial J_1^{Elz}} J_1^{Elz} + \frac{RT^{Elz}}{2F} \\ \frac{\partial V_2^{Elz,c}}{\partial J_2^{Elz}} J_2^{Elz} + \frac{RT^{Elz}}{2F} \\ \vdots \\ \frac{\partial V_N^{Elz,c}}{\partial J_N^{Elz}} J_N^{Elz} + \frac{RT^{Elz}}{2F} \end{bmatrix}}_{D_x} \quad (3.13)$$

Equation (3.13) can be expressed in matrix form as:

$$D_x + E_x = C_x \pi_x \quad (3.14)$$

where, π_x is the model parameter and E_x indicates the error in the modeling that should be minimized to zero in an ideal case. Once the error is minimized, the values of the parameters α, R^{Elz}, and J^{Lim} are estimated which best fit the measured data points. Therefore, the modeling error represented by:

$$E_x = C_x \pi_x - D_x, \quad (3.15)$$

is minimized using the LSE method. The LSE minimizes the squared of the modeling error between the measured value and the estimated value as follows:

$$E_x E_x^{tr} = (C_x \pi_x - D_x)(C_x \pi_x - D_x)^{tr}, \quad (3.16)$$

where, tr indicates the transpose of the matrix. Equation (5.1) can be further simplified and expressed as (3.17)

$$E_x E_x^{tr} = (\pi_x^{tr} C_x^{tr} C_x \pi_x - 2\pi_x^{tr} C_x^{tr} D_x + D_x^{tr} D_x). \tag{3.17}$$

In (3.17), the estimation of the unknown parameters (π_x) can be accomplished when the modeling error is at its minimum, i.e., when $\partial E_x / \partial \pi_x = 0$. As such,

$$\frac{\partial}{\partial \pi_x}\Big(\pi_x^{tr} C_x^{tr} C_x \pi_x - 2\pi_x^{tr} C_x^{tr} D_x + D_x^{tr} D_x\Big) = \mathbf{0}, \tag{3.18}$$

which can then be simplified to:

$$2C_x^{tr} C_x \pi_x - 2C_x^{tr} D_x = \mathbf{0}. \tag{3.19}$$

To that end, the model parameter π_x includes the values of the parameters α, R^{Elz}, and J^{Lim} is obtained as follows:

$$\pi_x = \Big[[C_x^{tr} C_x]^{-1} C_x^{tr}\Big] D_x = [\pi_{x_1}, \pi_{x_2}, \pi_{x_3}, \pi_{x_4}, \pi_{x_5}]^{tr}. \tag{3.20}$$

Once π_x is obtained from (3.20), the values of α, R^{Elz}, and J^{Lim} parameters can be given as:

$$\alpha = \frac{\pi_{x_1}}{\pi_{x_2}} = \frac{1}{\pi_{x_3}}, \quad R^{Elz} = \pi_{x_5} = \frac{\pi_{x_4}}{\pi_{x_1}}, \quad J^{Lim} = \pi_{x_1} = \frac{\pi_{x_4}}{\pi_{x_5}}. \tag{3.21}$$

In order for the LSE's solution in (3.20) to be valid, the following assumptions should be met [60]:

- Matrix C_x with $n \times k$ dimension is assumed to have $n \geq k$ with rank k.
- The expected value of all elements in the error matrix (E_x) is equal to zero.
- The parameters are linearly related to the data collected as shown in equation (3.9).
- The diagonal elements of the covariance matrix for all elements in the error matrix (E_x) are equal.
- The off-diagonal elements of the covariance matrix for all elements in the error matrix (E_x) are zero.
- The obtained parameters in the model parameter matrix (π_x) are scalar and constant with a standard deviation greater than zero.
- The elements of the error matrix (E_x) are normally distributed.

3.2.4 Estimation of J^0 Parameter

The value of the parameter J^0 can be determined by first considering (3.6) with an expanded form of a natural logarithmic function as:

$$V_n^{Elz,c} = \frac{\Delta G}{2F} + \frac{RT^{Elz}}{2F}\ln\left(\frac{\pi^{H_2}\sqrt{\pi^{O_2}}}{\pi^{H_2O}}\right) + \frac{RT^{Elz}}{2F\alpha}\ln(J_n^{Elz}) - \frac{RT^{Elz}}{2F\alpha}\ln(J^0) + J_n^{Elz}R^{Elz} + \frac{RT^{Elz}}{2F}\ln\left(\frac{J^{Lim}}{J^{Lim}-J_n^{Elz}}\right) \quad n \in \mathcal{N}. \quad (3.22)$$

Equation (3.22) can be written in a standard regression matrix form as follows:

$$\underbrace{\begin{bmatrix} V_1^{Elz,c} - \frac{\Delta G}{2F} - \frac{RT^{Elz}}{2F}\ln(\frac{\pi_{H_2}\sqrt{\pi_{O_2}}}{\pi_{H_2O}}) - \frac{RT^{Elz}}{2F\alpha}\ln(J_1^{Elz}) - J_1^{Elz}R^{Elz} - \frac{RT^{Elz}}{2F}\ln(\frac{J^{Lim}}{J^{Lim}-J_1^{Elz}}) \\ V_2^{Elz,c} - \frac{\Delta G}{2F} - \frac{RT^{Elz}}{2F}\ln(\frac{\pi^{H_2}\sqrt{\pi^{O_2}}}{\pi^{H_2O}}) - \frac{RT^{Elz}}{2F\alpha}\ln(J_2^{Elz}) - J_2^{Elz}R^{Elz} - \frac{RT^{Elz}}{2F}\ln(\frac{J^{Lim}}{J^{Lim}-J_2^{Elz}}) \\ \vdots \\ V_N^{Elz,c} - \frac{\Delta G}{2F} - \frac{RT^{Elz}}{2F}\ln(\frac{\pi_{H_2}\sqrt{\pi^{O_2}}}{\pi^{H_2O}}) - \frac{RT^{Elz}}{2F\alpha}\ln(J_N^{Elz}) - J_N^{Elz}R^{Elz} - \frac{RT^{Elz}}{2F}\ln(\frac{J^{Lim}}{J^{Lim}-J_N^{Elz}}) \end{bmatrix}}_{D_y}$$

$$= \underbrace{\begin{bmatrix} -\frac{RT^{Elz}}{2F\alpha} & -\frac{RT^{Elz}}{2F\alpha} & \cdots & -\frac{RT^{Elz}}{2F\alpha} \end{bmatrix}^{tr}}_{C_y} \underbrace{\begin{bmatrix} \ln(J^0) \end{bmatrix}}_{\pi_y} \quad (3.23)$$

The regression model in (3.23) can be represented with E_y error:

$$D_y + E_y = C_y \ln(J^0) \quad (3.24)$$

Using the LSE method discussed in (3.15) to (3.19), one can derive the solution of the regression model as follows:

$$\ln(J^0) = \left[[C_y^{tr}C_y]^{-1}C_y^{tr}\right]D_y \quad (3.25)$$

The exchange current density parameter (J^0) is thus set to:

$$J^0 = \exp\left(\left[[C_y^{tr}C_y]^{-1}C_y^{tr}\right]D_y\right), \quad (3.26)$$

where "exp" denotes an exponential function. It should be noted that the existence of the LSE solution for equations (3.20) and (3.26) relies on the nonsingularity of $C_x^{tr}C_x$ and $C_y^{tr}C_y$ matrices. That is when the $C_x^{tr}C_x$ and $C_y^{tr}C_y$ matrices are invertible with a zero determinant. Following the approach proposed in this section, all the five modeling parameter of a PEM electrolyzer cell can be analytically estimated.

It is noteworthy that the proposed approach could be extended to electrolyzer stacks consisting of a number of identical cells by considering the relationship described in equation (1.12) between the voltage of the electrolyzer stack and the voltage of the single cell.

3.3 Performance Evaluation

In this section, the proposed parameter estimation approach for modeling the electrochemical behavior of the PEM electrolyzer is tested and evaluated. Validation analysis are conducted for the PEM electrolyzer developed in MATLAB/Simulink software based on a broad survey of commercially available PEM electrolyzer systems [2, 3]. The PEM electrolyzer modeling and simulation parameters are reported in Table 3.1. The PEM electrolyzer cell is designed to operate between 50°C and 80°C with a maximum output pressure of 35 bar. In this work, the values of the hydrogen, oxygen, and water partial pressures are evaluated using Dalton's law [3, 14]. The single PEM electrolyzer cell has an active surface area of 160 cm^2 and can produce 0.15 cubic meters of hydrogen per hour. Fig. 3.1 shows a schematic diagram of the experimental setup. As depicted in the figure, the electrolyzer is powered by a DC power supply. Utilizing a voltmeter and an ammeter, the voltage across the electrolyzer and the current flowing through it are measured, respectively. During operation, the electrolyzer's temperature is measured using a thermostat. In addition, the pressure of the water supplied to the electrolyzer, hydrogen gas, and oxygen gas produced are measured using a barometer. The measurements data are collected and filtered on the computer side before being used for the proposed parameter estimation approach.

Different datasets of measured J-V over a broad range of operating conditions are considered to ensure an accurate modeling of the PEM electrolyzer system. The data points are collected by applying an increasing current starting at zero ampere up to the maximum rated current value. Here, it is worth noting that a sufficiently informative data points (rich data) that give insights into both linear and nonlinear characteristics of the

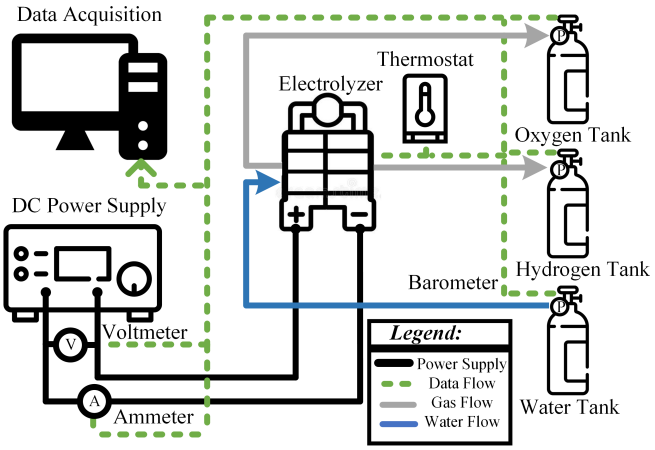

Figure 3.1: Schematic diagram of the experiment setup for the estimation of the PEM electrolyzer parameters.

PEM electrolyzer are measured, in order to have a well-defined solution. Therefore, the J-V dataset used in the proposed parameter estimation approach is generated using MATLAB software based on the model equations presented in Section 1.1.2. In practice, voltage and current measurements are subject to noise as a result of many factors. Hence without loss of practicality, the measured data will need to be cleaned and filtered in a former process before being utilized in the proposed parameter estimation approach. As data filtering may not eliminate all measurement noise, the LSE attempts to minimize the error between measured and estimated values while taking into account measurement noise [61]. It is worth noting that the J-V characteristics results have been verified by several experimental results that are reported in the literature [8, 14, 22]. It is also important to note that numerical differentiation is used to calculate the partial derivative of the cell voltage in relation to the current density at different operating conditions.

In Section 3.3.1, the model parameter estimation is first tested at constant temperature and pressure, and then in Section 3.3.2 the results of the cell operation analysis are examined at different temperatures, pressures, production rates, and dataset sizes. In Section 3.3.7, the performance of the proposed parameter estimation approach is statistically analyzed. Lastly, Section 3.3.8 provides evidence of the superiority of the proposed parameter estimation approach by comparing it with other parameter estimation approaches.

Table 3.1: Modeling and simulation parameters [2, 3]

Cell Area = 160 cm^2	I_{max}^{Elz} = 320 A	T^{Elz} = 50 - 80 ^oC
M_{max}^{Elz} = 0.15 m^3/hr	$N^{Elz,c}$ = 1 cell	π^{H_2} = 0 - 35 bar
R = 0.0821 atm/(K·mol)	F = 96485.33 C/mol	$V_{max}^{Elz,c}$= 3 V

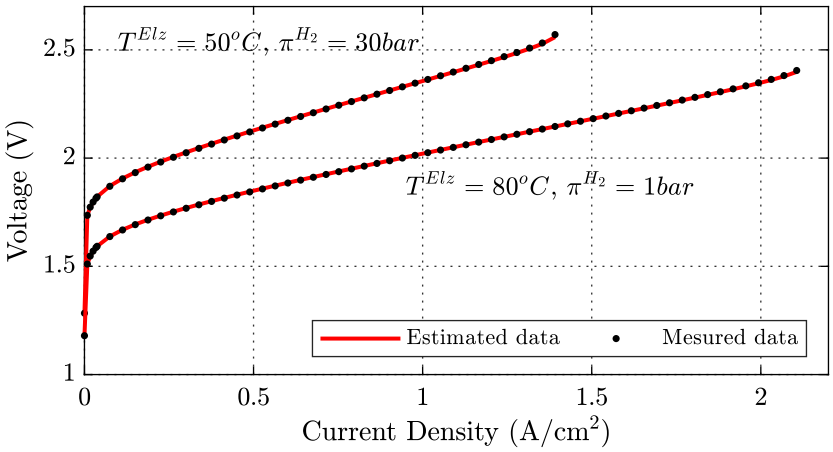

Figure 3.2: Measured and estimated J-V curve obtained by the proposed approach for PEM electrolyzer cell.

Table 3.2: Estimated PEM electrolyzer cell parameters

Operating Condition Parameter	T^{Elz}=50^oC π^{H_2} = 30bar	T^{Elz}=80^o π^{H_2} = 1bar
ΔG (kJ/mol)	233.1020	228.2060
J^0 (μA/cm^2)	1.3533	13.4576
α	0.2719	0.2993
R^{Elz} (Ω)	0.3631	0.2614
J^{Lim} (A/cm^2)	1.4092	2.1469

3.3.1 Estimating PEM Electrolyzer Cell Parameters

The proposed parameter estimation approach is validated by comparing the estimated results with the measured results. In this section, two operating conditions are considered for the validation of the proposed model. The first condition considers an operating temperature of 50^{o}C with an output

hydrogen pressure of 30 bar, while the second condition realizes an operating temperature of 80°C with an output hydrogen pressure of 1 bar. The modeling parameters estimated using the proposed approach for the two conditions are listed in Table 3.2. The difference between the modeling parameters for the two conditions is due to their dependence on the operating temperature and pressure. Fig. 3.2 shows the measured data and the results of the estimated proposed model obtained for the two operating conditions. The figure indicates the validity of the proposed parameter estimation approach. The graph also shows a perfect match between the estimated and measured data for the proposed PEM electrolyzer model. Fig. 3.2 shows to what extent the different operation conditions can change the operating current density range of a PEM electrolyzer. This can be observed in Fig. 3.2 when the temperature is 50°C, the maximum allowed current density is about 1.4 A/cm^2, as reported in Table 3.2. On the other hand, when the temperature is 80°C, the maximum allowed current is about 2.14 A/cm^2, as reported in Table 3.2.

Fig. 3.3 shows the absolute voltage errors of the proposed parameter estimation approach for the two considered operating conditions. The figure shows the absolute error in a logarithmical scale, and the current density in a linear scale. Fig. 3.3 shows that the absolute errors are within a range of 10^{-4} to 10^{-2} for a wide range of operating points, thus demonstrating the accuracy of the proposed approach compared to previous works [7, 8, 14].

3.3.2 Operation of the Proposed PEM Electrolyzer Model under Different Operation Conditions

Based on four different case studies, the validity of the estimated model parameters is explored on the basis for different temperatures, pressures, hydrogen production rates, and dataset sizes. Table 3.3 presents the operational conditions and the size of the dataset for the four case studies. Where, T^{Elz} indicates the operating temperature, and π^{H_2} represents the output hydrogen pressure. In Table 3.3, the value of J^{Elz} represents the applied current to the PEM electrolyzer cell which is proportional to the hydrogen production rate, and N represents the total number of data points for the estimation approach.

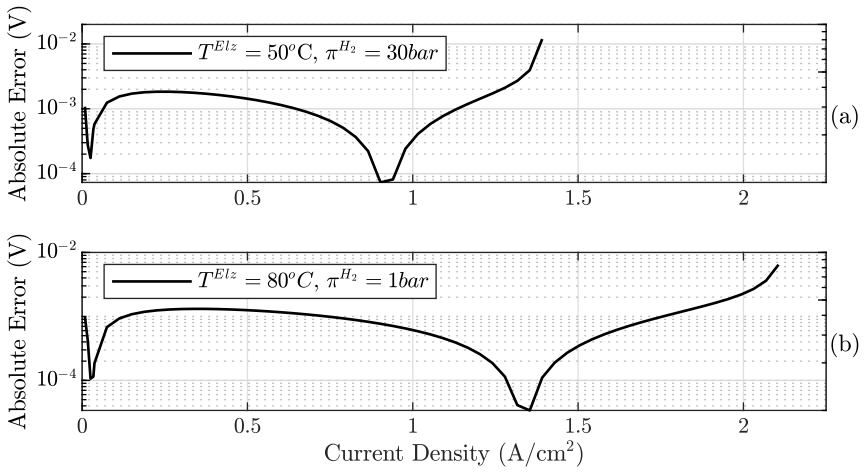

Figure 3.3: Absolute error values of estimated and measured voltage data for PEM electrolyzer cell at: (a) T^{Elz}=50°C and π^{H_2}=30 bar, and (b) T^{Elz}=80°C and π^{H_2}=1 bar.

Table 3.3: Operating conditions and dataset size for the four case studies

Cases	$T^{Elz}(^oC)$	$\pi^{H_2}(bar)$	$J^{Elz}(A/cm^2)$	N
1	50 - 80	19	1	57
2	60	0 - 30	1	57
3	60	30	0 - 2	57
4.A	60	30	0 - 2	60
4.B	60	30	0 - 2	120
4.C	60	30	0 - 2	230

3.3.3 Case 1: Relation between the operating temperature and estimated voltage

For a better understanding of the accuracy of the proposed approach under different operating conditions, this case discusses the relationship between operating temperature and estimated voltage. Further, the dependence of the modeling parameters on the PEM electrolyzer temperature is examined. The relationships between the five parameters and temperature have been modeled by using the expressions given in [14, 22, 34, 62]. The temperature of the PEM electrolyzer is simulated to rise from 50°C to 80°C, as reported in Table 3.3 [2]. The parameters are therefore estimated by collecting multiple datasets at various temperatures. Fig. 3.4 shows the model estimated voltage across the PEM electrolyzer over the simulated range of temper-

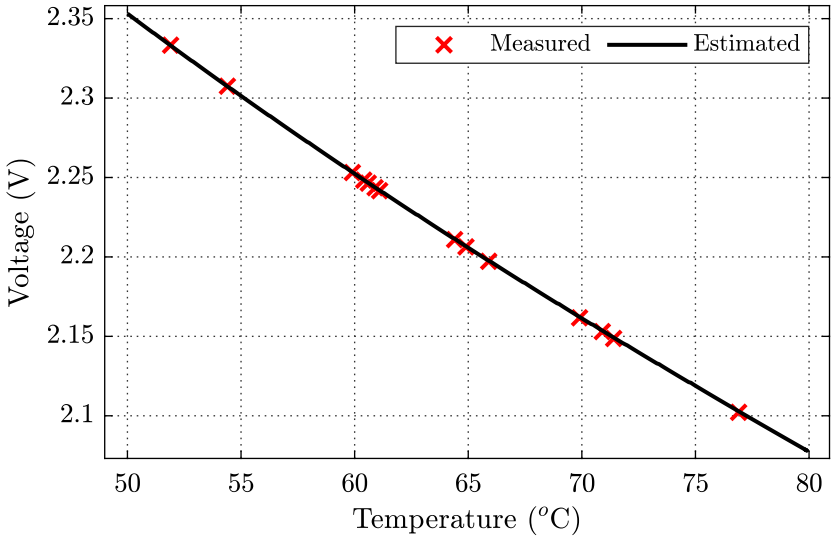

Figure 3.4: PEM electrolyzer voltage under different operating temperature.

atures. The estimated voltage results are decreasing as the temperature increases, showing an inverse relationship between temperature and voltage measurement across the PEM electrolyzer. These findings are consistent with those in the literature [63]. The figure depicts 14 measured data points at various operating temperatures as cross points. It is shown that the estimated curve superimposes the measured points, demonstrating the high accuracy and effectiveness of the proposed parameter estimation approach under various operating temperatures.

Fig. 3.5(a) shows the relationship between the change in the Gibbs free energy parameter and operating temperature for the PEM electrolyzer cell. It can be observed that the ΔG decreases linearly with increasing temperature. Therefore, there is a significant linear negative correlation between the change in Gibbs free energy and the PEM electrolyzer's operating temperature. The results in Fig. 3.5(a) confirms previous findings in [52].

Fig. 3.5(b) illustrates the relationship between the limiting current density parameter and the operating temperature of the PEM electrolyzer cell under study. The value of J^{Lim} increases linearly with increasing temperature. This implies that when operating at low temperatures, the PEM electrolyzer operates within a narrow current density operating window.

The dependence of exchange current density parameter on the operating

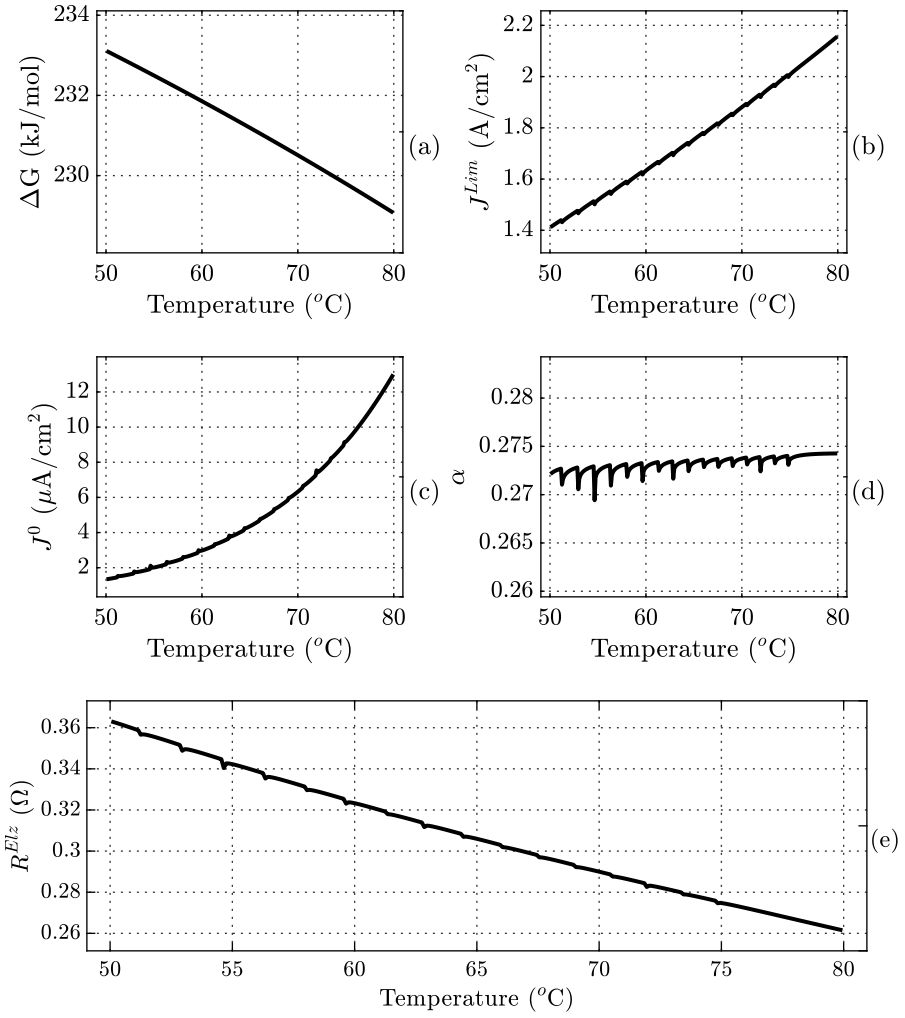

Figure 3.5: PEM electrolyzer operating temperature relationship with: (a) Change in Gibbs free energy (ΔG), (b) Limiting current density (J^{Lim}), (c) Exchange current density (J^0), (d) Charge transfer coefficient (α), and (e) Series resistance (R^{Elz}).

temperature is shown in Fig. 3.5(c). The results show that the exchange current density increases exponentially as the operating temperature increases. Such results are in a complete agreement with the previous results reported

in [22].

Fig. 3.5(d) reveals the dependency of the charge transfer coefficient parameter on the operating temperature. The results illustrate that α parameter marginally increases with temperature, which correlates well with the work reported in [22].

The relationship between the resistance parameter of PEM electrolyzers and the operating temperature is represented in Fig. 3.5(e). The figure illustrates an inverse linear relationship between R^{Elz} and the temperature i.e., the higher the operating temperature, the more efficient electron transfer will be, and thereby more hydrogen will be produced for the same applied current [64]. The reason for this is that at high temperatures, the ionic bonds between electrolytes weaken and the conductivity of electrodes increases.

3.3.4 Case 2: Relation between the output pressure and estimated voltage

In this case, the output pressure of the hydrogen produced by the PEM electrolyzer is simulated to increase from 0 to 30 bar, as reported in Table 3.3 [3]. The operating temperature of the PEM electrolyzer is set at 60°C, with a constant current supply of 1 A/cm^2. It is worth mentioning that the estimated electrolyzer voltage is computed based on the five parameters estimated at different pressure levels between 0 and 30 bar. Therefore, multiple datasets are used to estimate the parameters for estimating the voltage at different pressure levels. Fig. 3.6 shows the estimated voltage results for the different hydrogen pressure levels. The estimated voltage has a logarithmic growth curve, which increases rapidly with a large gain when the pressure is between 0 and 5 bar, and then with a small gain as the pressure increases. The results are consistent with equation (1.6) which indicates a logarithmic relationship between the hydrogen pressure and the open-circuit voltage of the PEM electrolyzer. Fig. 3.6 also presents 16 measured data points plotted as cross points at different output pressures. It is evident that the measured data points and the estimated curve agree well, showing the applicability of the parameter estimation approach under different output pressures.

3.3.5 Case 3: Relation between the hydrogen production rates and estimated voltage

In this case, the hydrogen production rate of the PEM electrolyzer is assumed to be continuously changing within a range of 0 to 0.1 m^3/hr, as

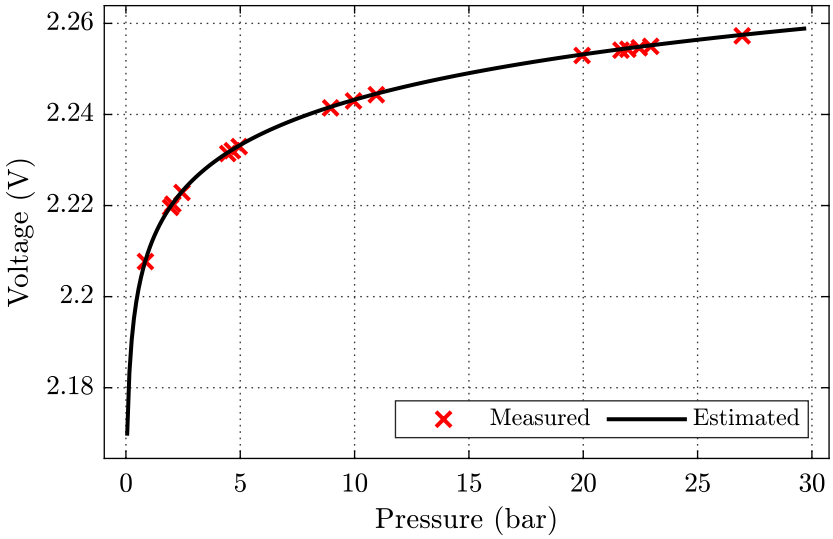

Figure 3.6: PEM electrolyzer voltage under different hydrogen pressures.

reported in Table 3.3. In other words, the supplied current density to the electrolyzer is continuously varying between 0 and 2 A/cm^2 to produce a hydrogen production between 0 and 0.1 m^3/hr. Unlike cases 1 and 2, case 3 analysis collects only one dataset in order to estimate the parameters due to the fixed temperature and pressure conditions. The hydrogen output pressure is set at 30 bar and the operating temperature is set to 60^{o}C. As shown in Fig. 3.7, the voltage has almost the same profile as the hydrogen production rate. Hence, the voltage across the PEM electrolyzer correlates with the production rate of hydrogen.

In order to further validate the accuracy of the proposed parameter estimation approach, the electrolyzer system conversion efficiency is calculated based on the estimated and measured voltage of the electrolyzer system using equation (1.3). According to Fig. 3.7(c), the estimated efficiency is in good agreement with the measured efficiency over a wide range of operating conditions.

Moreover, Fig. 3.7(c) shows a good agreement between the measured and estimated voltage results under different hydrogen production rates. The absolute error of the voltage is presented in Fig. 3.7(d) to clearly show the difference between the measured and estimated voltages. As shown in the figure, a greater level of accuracy is evident when the electrolyzer is

running at a high production rate in the linear region of the J-V curve. This figure also shows a lower accuracy at low hydrogen production rates, which is in the exponential region of the electrolyzer J-V curve. Under this case, the average absolute error was found to be around 0.01.

The proposed parameter estimation can therefore estimate the PEM electrolyzer parameters at different hydrogen production rates with high precision. It is worth mentioning that the voltage measurements were taken under a controlled temperature and pressure environment. The electrolyzer cooling controller was set to adapt any significant changes in the operating temperature in order to maintain a constant temperature.

3.3.6 Case 4: Impact of different dataset size on the proposed approach

In order to investigate the impact of the dataset size on the accuracy of the proposed parameter estimation approach, three different dataset sizes are examined, namely N= 60, 120, and 239 are considered in this case at a controlled temperature of 60°C and pressure of 30 bar, as reported in Table 3.3. The dataset is collected by supplying a current density that ranges from 0 to 2 A/cm^2. Fig. 3.8 shows that the parameter estimation approach remains highly accurate over a wide range of operating points for the three different dataset sizes. Therefore, the proposed approach can be applied to both small and large datasets without sacrificing accuracy as long as the dataset includes a wide range of operating points over the J-V curve. As shown in Fig. 3.8, a larger dataset results in progressively better accuracy at the J-V curve's edge.

3.3.7 Error Estimation

In order to determine the accuracy of the estimated model, mean absolute percentage error (MAPE) and standard deviation absolute percentage error (SAPE) are calculated between the estimated and measured voltage values in the J-V curves, where MAPE and SAPE are defined as follows:

$$MAPE = \frac{1}{N}\sum_{n=1}^{N}\frac{V_n^{Elz,c} - V_n^{Elz,c,est}}{V_n^{Elz,c}} \times 100\%, \tag{3.27}$$

$$SAPE = \sqrt{\frac{1}{N}\sum_{n=1}^{N}(V_n^{Elz,c} - V_n^{Elz,c,est})^2} \times 100\%, \tag{3.28}$$

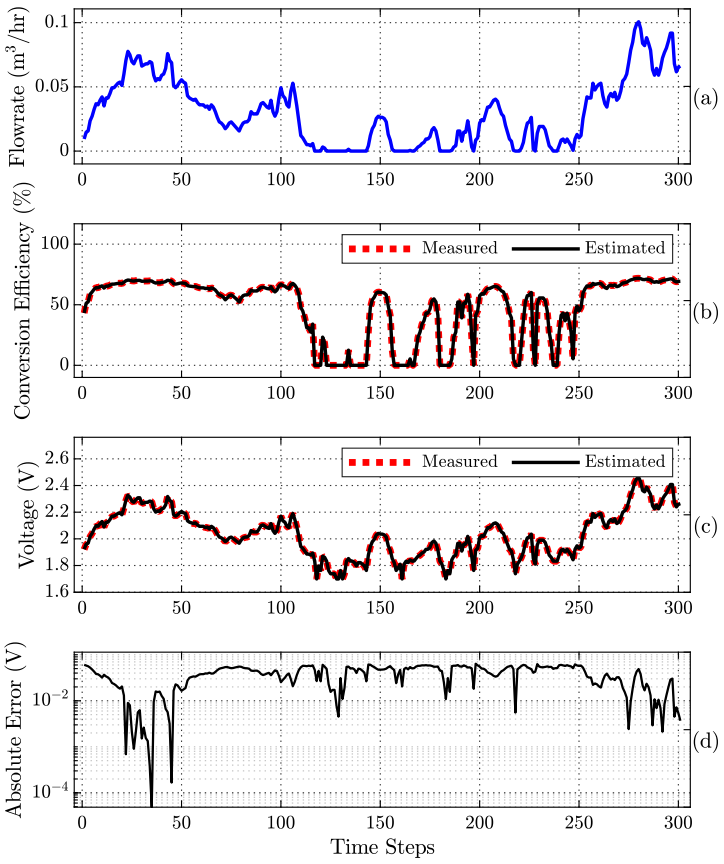

Figure 3.7: PEM electrolyzer: (a) Hydrogen production rate, (b) Efficiency, (c) voltage, and (d) Absolute error values under case 3.

Table 3.4 gives the values of MAPE and SAPE of the estimated J-V PEM electrolyzer characteristic curve under the four cases in sections 3.3.3 to 3.3.6. As depicted in Table 3.4, the MAPE and SAPE values are close to zero, indicating that the proposed approach is superior and adequate. In case 4, both SAPE and MAPE values decrease as the dataset size increases.

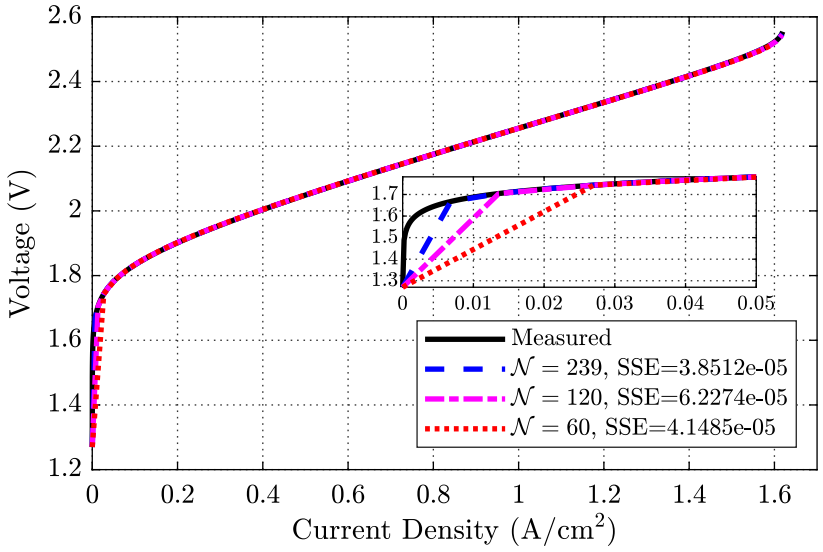

Figure 3.8: A comparison of$J$-V curves using the proposed estimated parameter model and the measured data under different dataset sizes.

Table 3.4: Proposed approach MAPE and SAPE for different studied cases

Cases	MAPE (%)	SAPE (%)
1	0.0181	0.0455
2	0.0098	0.0234
3	0.0553	0.1210
4.A	0.0271	0.0832
4.B	0.0185	0.0720
4.C	0.0124	0.0401

3.3.8 Comparative Analysis of PEM Electrolyzer's Parameter Estimation Approaches

Prior work has mostly used numerical techniques and heuristic algorithms to estimate the PEM electrolyzer parameters [14]-[56], [51]. Therefore, the parameters estimated using the proposed approach are compared to that of prior work using trust region numerical method, NNs, and PSO algorithms to verify the effectiveness of the proposed approach. The selected PSO tuning parameters include; number of particles in the swarm 100, maximum number of iterations 1000, lower and upper bounds of the adaptive inertia 0.1 and 1.1, respectively. The selected NN training parameters are; learning

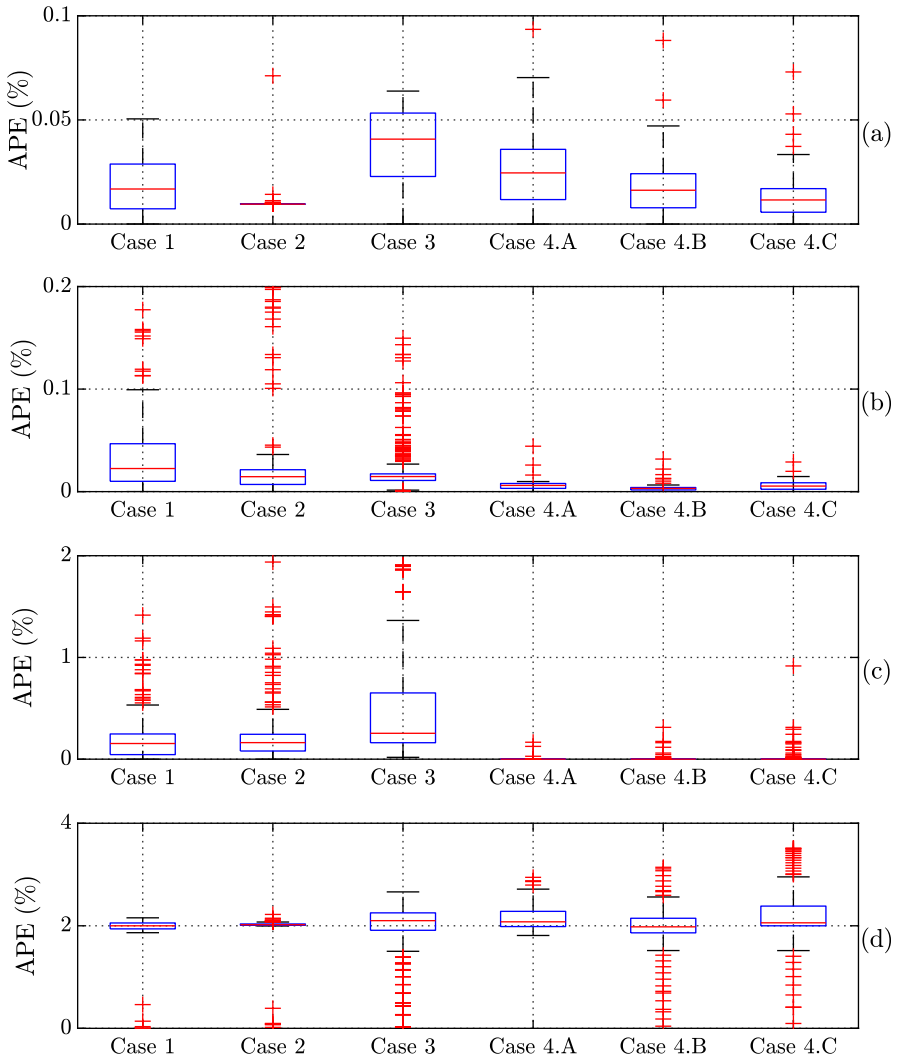

Figure 3.9: APEs distribution of estimated data under: (a) Proposed approach (b) Trust region method (c) NNs (d) PSO algorithm.

rate 0.01, maximum number of training epochs is 1000, maximum validation failures are 6, and ratios to increase and to decrease the learning rate are 1.05 and 0.7, respectively. It is worth noting that all algorithms were conducted using MATLAB 2020b software on an Intel®core™i7-8750H CPU, 2.20 GHz, and 16 GB RAM. The absolute percentage error (APE) is used to evaluate

Table 3.5: APE median for the four cases under different techniques

Case	Proposed Approach	Numerical Optimization	NN	PSO Algorithm
1	0.017	0.023	0.15	2.00
2	0.0096	0.015	0.16	2.02
3	0.041	0.015	0.25	2.10
4.A	0.025	0.0060	2.42E-4	2.08
4.B	0.016	0.0031	2.80E-4	1.98
4.C	0.012	0.0054	2.76E-4	2.06
Computational Time (sec)	0.0026	0.58	1.56	0.68

the performance of the different techniques for the four cases presented in sections 3.3.3 to 3.3.6. The APE is defined as follows:

$$APE = \sum_{n=1}^{N} \frac{V_n^{Elz,c} - V_n^{Elz,c,est}}{V_n^{Elz,c,est}} \times 100\%. \tag{3.29}$$

Fig. 3.9 shows the box plots of the APE distribution pattern for the comparative analysis, where the central mark represents the median, the bottom and top edges of each box indicate the 25th and 75th percentiles of the APE data, respectively. The plus sign indicates an outlier. The median values of the APEs for the four cases studied under the various techniques are listed in Table 3.5. It is evident from the table that the APE median of the proposed approach for all cases is lower by 4.8% and 102% than that of NNs and PSO algorithms, respectively. However, the average APE median of the trust region method is slightly lower than the proposed approach by 1.8%. According to Table 3.5, the proposed approach is faster than NNs, the trust region method, and the PSO algorithm by 222, 600, and 260 times, respectively. Despite the fact that the trust region method is slightly more accurate than the proposed approach, the proposed approach is much faster in terms of computational time. This makes it useful for online parameter estimation of PEM electrolyzer systems. Thus, the proposed approach provides highly accurate model parameters with less computational time than those developed using the aforementioned methods.

3.4 Summary

In this chapter, a novel analytical approach based on the LSE is proposed to estimate the PEM electrolyzer modeling parameters and characterize its

electrochemical behavior under various operating conditions. Five unknown modeling parameters are estimated in a non-iterative manner to model the PEM electrolyzer, including the change in Gibbs free energy, charge transfer coefficient, exchange current density, series resistance, and limiting current density. The dependence of the parameters on the operating conditions is observed. Tests have been conducted at various temperatures, pressures, and hydrogen production rates to determine the accuracy of the model. The sensitivity analysis shows the validity of the proposed approach under different dataset sizes. The simulation results show that the estimated model has an average APE median of 0.12% under all cases, showing the superiority of the proposed methodology. The superiority of the proposed approach is evidenced by comparison with other PEM electrolyzer parameter estimation approaches.

Chapter 4

Energy Management System for Minimizing Hydrogen Production Cost Using Integrated Battery Energy Storage and Photovoltaic Systems

This chapter presents an optimal economic dispatch model for a clean hydrogen production system. To minimize the CoH production, the model aims to: i) minimize total system costs, ii) improve hydrogen production efficiency, and iii) improve solar energy utilization. This model accounts for the variation in electrolyzer efficiency as it relates to CoH production. In order to ensure accurate and stable system performance, electrochemical hydrogen production mechanisms and operational balance constraints are incorporated into the optimization model. Based on simulation results, it have proven that the proposed dispatch model is economically viable in terms of meeting hydrogen demand, maintaining system stability, and storing hydrogen. According to the optimization results, the average CoH production for the studied period was 2.67 $/kg. This study reveals a correlation between hydrogen production rate, electrolyzer efficiency, and CoH production. Analyzing the proposed model with and without consideration of the variability in electrolyzer efficiency indicates its effectiveness and feasibility in minimizing hydrogen production costs and maximizing the utilization of PV energy.

4.1 Introduction

With concerns being raised about the affordability of producing hydrogen, there have been steadily increase in research efforts to alleviate these

concerns. The CoH is influenced by the capital costs, operation and maintenance costs, feedstock costs, electricity costs, and other variable costs [16]. The price of electricity used is usually responsible for over 70% of the CoH [65]. It can be argued from an economic point of view that the contribution of electricity costs to the CoH can be reduced by using cheap renewable electricity [66]. In a recent study by the International Renewable Energy Agency, it is highlighted that renewable power generation has led to lower electricity prices compared to coal-fired power plants [66]. Therefore, incorporating renewable electricity, in particular from solar PV and wind turbines, can help to alleviate concerns of high electricity costs associated with hydrogen production. Several techno-economical models have been studied that utilize renewable energy resources to estimate the CoH production [28, 29, 67, 68]. In [67], the authors studied the development of a hydrogen system using grid electricity and wind power. The results obtained imply that the CoH produced by grid electricity is 17.65 $/kg, while the CoH produced by wind power is 3.82 $/kg. Another study reported in [68] on the use of wind power for hydrogen production showed that the CoH using wind power is about 6.46 $/kg. Hydrogen production through wind and solar power is also assessed in [28] by developing a cost-effective model to estimate the CoH. The results highlight the following CoH ranges: i) 1.72-3.81 $/kg using wind power, ii) 2.32-2.5 $/kg using solar power, and iii) 2.08-3.14 $/kg using both solar and wind power. Touili et al.[29] conducted a comparison of solar power hydrogen production between Morocco and Spain. The comparison shows that Morocco can achieve a hydrogen cost of 5.78 $/kg, whereas Spain can achieve a cost of 5.96 $/kg. The aforementioned research studies demonstrated that the CoH production from renewable energy sources varies significantly due to various factors. These factors include geographic considerations, such as location, technological considerations, such as renewable energy type, and economic considerations, such as system costs.

Technically, the CoH can be reduced by utilizing a high conversion efficiency electrolysis technology [12]. Electrolyzer efficiency improvements have been studied previously in the literature [69–74]. In [69], a comprehensive analysis study is conducted to investigate the impact of different electrolyzer sizes and system efficiencies on the CoH. The study indicates that CoH is significantly affected by system efficiency in large electrolyzers systems. In [70], a comparison between an electrolyzer system supplied with a stable grid power and surplus renewable power is conducted. The study showed that, although surplus renewable power is cheap, an electrolyzer system with a stable grid power is the most economically viable option for

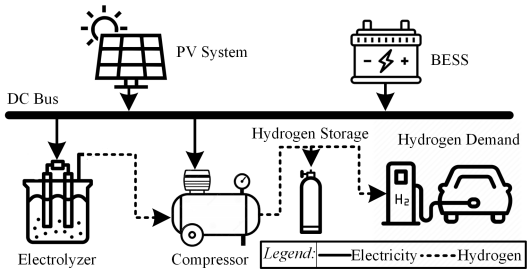

Figure 4.1: Proposed hydrogen system architecture using PV and BESS.

hydrogen production. Reference [71] reported that electrolyzer efficiency varies with load level. Reference [72] proposed an optimal dispatch model for power-to-hydrogen-and-heat systems to increase system conversion efficiency by 15%. Another study [73] shows the impact of device structure on electrolyzer efficiency. Reference [74] studied the improvement of electrolyzer efficiency through minimizing reaction resistances associated with electrolysis process.

The integration of the hydrogen system, including the electrolyzer, compressor, and hydrogen storage with a PV system and a BESS shown in Fig. 4.1 enables clean and efficient hydrogen production. Such integration also mitigates the impact of the uncertain nature of solar power. The use of a BESS in the hydrogen production system is essential for two main reasons: first to manage the power injection into the electrolyzer in order to achieve a high production efficiency, and second to mitigate the impact of the uncertain nature of wind and solar power. However, the integration of the hydrogen production system, including the electrolyzer, compressor, and hydrogen storage with the PV system and BESS, increases system operation complexity and costs. Therefore, system optimization is needed to find an optimum operation strategy that compromises between the costs and system performance. Many efforts have been made on the economical and reliable operation of renewable hydrogen production [75–80].

The economic operation of renewable hydrogen production requires the use of an EMS to address the uncertainties associated with load and renewable energy generation and to find an optimal operation strategy that compromises between system costs and performance. In [75], an EMS of grid-connected hybrid power system that combines hydrogen-based energy storage system with a power plant consisting of wind and solar energy sources, and BESS is presented. The authors concluded that the battery and hybrid system efficiency can be increased by using adaptive neuro-fuzzy inference

systems instead of classical EMS, which uses state-based supervisory control systems. Zhang et al. [76] proposed an optimal operation method for a regional multi-energy system considering electrolyzer, fuel cell, BESS, hydrogen storage (HS), and PV reliability constraints. The authors improved system economics through using intraseasonal complementary energy based on HS. Yang et al. [77] also presented a hierarchical control scheme for hybrid microgrids with hydrogen and BESS. The control objective is to minimize system costs while ensuring system stability. In [78], an energy management strategy is presented for an integrated PV, wind turbine, fuel cell, and hydrogen system. The results show that the proposed method can reduce the system costs with full coverage of load demand. In [79] the authors proposed a supervisory-based model for the optimal scheduling of distributed hydrogen production stations. The model optimizes hydrogen generation setpoints with the aim of maximizing system profitability. In [80], a model for the central scheduling of distributed electrolyzer–based hydrogen fueling stations is proposed. The model optimizes electrolyzer operation in order to increase system profitability and optimize the hydrogen selling price.

However, previous studies failed to investigate the impact of electrolyzer efficiency variation on the CoH production, assuming an electrolyzer operating at a constant efficiency [28, 68, 78–80]. Based on the aforementioned factors that affect CoH production, further studies need to consider the importance of electrolyzer efficiency variation on the CoH production under various operating conditions. Therefore, the need for an optimal EMS for an economical and reliable hydrogen production with the consideration of electrolyzer efficiency variation is clearly recognized.

4.2 Proposed Hydrogen Production Energy Management System

In order to complement previous work, this chapter proposes an economical dispatch model for the hydrogen production system shown in Fig. 4.1. Unlike the previous studies that considered constant electrolyzer conversion efficiency, this study develops an EMS for the combined hydrogen system-PV-BESS with consideration of the dynamic variability of the electrolyzer efficiency. The objectives of the proposed model are to i) minimize CoH production, ii) maximize hydrogen system efficiency, and iii) maximize solar energy usage and thereby achieve the optimal economic efficiency. The model also aims to maintain reliable and stable operation of the hydrogen

system by satisfying system operational and physical capacity constraints. Two cases are considered to evaluate the proposed model: the first case considers the operation of the electrolyzer at a variable conversion efficiency, and the second case considers that the electrolyzer operates at a constant conversion efficiency. The proposed model is designed for the system structure shown in Fig. 4.1. The proposed optimal operation model of the system is formulated below.

4.2.1 Objective Function

The objective function of the optimization problem is defined as follows:

$$\text{Minimize:} \quad \sum_{t=1}^{T} \Big(TC_t^{H_2} + TC_t^{BESS} + TC_t^{PV} \Big) \cdot \Delta t. \tag{4.1}$$

Equation (4.1) expresses the total system costs as the summation of the initial investment, degradation, and operation and maintenance costs of each individual component in the system with Δt as the time step resolution. The first term in (4.1) represents hydrogen system costs, $TC_t^{H_2}$. This includes the capital, operational, and degradation costs of both electrolyzer and compressor, along with the CoH system balance of plant components. Therefore, the total hydrogen cost is given as follows:

$$\begin{aligned} TC_t^{H_2} = &\Big(C^{Elz} + O^{Elz} + D^{Elz} + C^{BoP} \Big) \cdot p_t^{Elz} \\ &+ \Big(C^{Cmp} + O^{Cmp} \Big) \cdot p_t^{Cmp} \quad \forall\ t \in T, \end{aligned} \tag{4.2}$$

The second term in (4.1) states the total cost of the BESS (TC_t^{BESS}) which can be described as follows:

$$\begin{aligned} TC_t^{BESS} = &\big(C^{BESS} + O^{BESS} + D_t^{BESS} \big) \\ &\cdot \big(p_t^{BESS,Chg} + p_t^{BESS,Dhg} \big) \ \ \forall\, t \in T \end{aligned} \tag{4.3}$$

The third term in (4.1) includes the total cost of the PV system (TC_t^{PV}) as:

$$TC_t^{PV} = \big(C^{PV} + O^{PV} \big) \cdot P_{max}^{PV} + \lambda^{PV} \cdot p_t^{PV,Crt}\ \forall\, t \in T, \tag{4.4}$$

The added penalty term in equation (4.4) ensures minimal PV power curtailment while optimizing the system's operation. This will in turn encourage the BESS to be in a charging mode utilizing solar energy as long as its maximum capacity limit is not reached.

4.2.2 Optimization Constraints

The objective function in (4.1) is subject to a set of operational and physical constraints of each individual unit, along with system balance constraints.

4.2.2.1 Electrolyzer Constraints

The adopted modeling of the hydrogen production in this work is based on the electrochemical characteristic of the electrolyzer system. Therefore, the power consumed by the electrolyzer stack system at time t depends on the operating and physical characteristics of the electrolyzer stack system. It can be described using equation 1.13 The adopted electrochemical model for the electrolyzer system can be found in 1.1.2.

The operation of the electrolyzer is constrained by its minimum and maximum operational power limits, given as follows:

$$P_{min}^{Elz} \leq p_t^{Elz} \leq P_{max}^{Elz} \;\; \forall t \in T\,. \tag{4.5}$$

Also, the maximum and minimum supply current and voltage of the electrolyzer are given in (4.6) and (4.7), respectively.

$$0 \leq i_t^{Elz} \leq I_{max}^{Elz} \quad \forall t \in \mathcal{T}, \tag{4.6}$$

$$V_{min}^{Elz,s} \leq v_t^{Elz} \leq V_{max}^{Elz,s} \quad \forall\, t \in \mathcal{T}. \tag{4.7}$$

The hydrogen production rate is also constrained by its maximum rate as:

$$0 \leq M_t^{Elz} \leq M_{max}^{Elz} \quad \forall t \in T. \tag{4.8}$$

4.2.2.2 Compressor Constraints

The power consumed by the compressor at time t is calculated based on the polytropic model formulated as [27]:

$$p_t^{Cmp} = M_t^{Elz} \cdot \frac{2 \cdot R \cdot T^{Elz} \cdot k}{(k-1) \cdot \eta^{Cmp}} \cdot \left[\left(\frac{\pi_t^{HS}}{\sqrt{\pi_t^{H_2} \cdot \pi_t^{HS}}} \right)^{\frac{k-1}{k}} - 1 \right] \forall t \in T, \tag{4.9}$$

The compressor's minimum and maximum power operational limits are given as:

$$P_{min}^{Cmp} \leq p_t^{Cmp} \leq P_{max}^{Cmp} \;\; \forall t \in T. \tag{4.10}$$

4.2.2.3 Hydrogen Storage Constraints

The objective function in (4.1) is also subjected to the State-of-Hydrogen (SoH) balance equation of the hydrogen storage as follows:

$$SoH_t = SoH_{t-1} + \frac{M_t^{Elz}}{Q^{HS}} \cdot \Delta t - \frac{M_t^{Ld}}{Q^{HS}} \cdot \Delta t - \gamma^{HS,Dsp} \cdot SoH_{t-1} \quad \forall t \in T, \tag{4.11}$$

While the hydrogen storage pressure balance is ensured as [81]:

$$\pi_t^{HS} = \pi_{t-1}^{HS} + z \cdot \left(\frac{R \cdot T^{HS}}{Q^{HS}}\right) \cdot \left(M_t^{Elz} - M_t^{Ld}\right) \quad \forall\, t \in T, \tag{4.12}$$

Hydrogen storage is also subject to the maximum and minimum physical capabilities of pressure and SoH as expressed in (4.13) and (4.14), respectively.

$$\Pi_{min}^{HS} \leq \pi_t^{HS} \leq \Pi_{max}^{HS} \quad \forall t \in T, \tag{4.13}$$

$$SoH_{min} \leq SoH_t \leq SoH_{max} \quad \forall t \in T, \tag{4.14}$$

4.2.2.4 BESS Constraints

The BESS operation is subject to the State-of-Charge (SoC) balance equation as follows:

$$SoC_t = SoC_{t-1} + \frac{\eta^{BESS,Chg} \cdot p_t^{BESS,Chg} \cdot \Delta t}{Q^{BESS}} - \frac{p_t^{BESS,Dhg} \cdot \Delta t}{\eta^{BESS,Dhg} \cdot Q^{BESS}} - \gamma^{BESS,Dsp} \cdot SoC_{t-1} \quad \forall t \in T \tag{4.15}$$

Constraint (4.16) specifies the minimum and maximum boundaries of the SoC.

$$SoC_{min} \leq SoC_t \leq SoC_{max} \quad \forall t \in T. \tag{4.16}$$

Furthermore, the maximum and minimum BESS charging and discharging operational limits are shown in (4.17) and (4.18).

$$P_{min}^{BESS,Chg} \leq p_t^{BESS,Chg} \leq P_{max}^{BESS,Chg} \quad \forall t \in T, \tag{4.17}$$

$$P_{min}^{BESS,Dhg} \leq p_t^{BESS,Dhg} \leq P_{max}^{BESS,Dhg} \quad \forall t \in T, \tag{4.18}$$

In order to minimize power loss during charging and discharging due to processes efficiencies, the constraint (4.19) is included to prevent simultaneous charging and discharging, and it is stated as:

$$p_t^{BESS,Chg} \cdot p_t^{BESS,Dhg} = 0 \tag{4.19}$$

4.2.2.5 System Balance Constraints

The system power balance equality constraint of the hydrogen production system shown in Fig. 4.1 is defined as follows:

$$P_{max}^{PV} - p_t^{PV,Crt} = p_t^{Elz} + p_t^{Cmp} - p_t^{BESS,Dhg} + p_t^{BESS,Chg} \quad \forall\, t \in T \tag{4.20}$$

4.3 Performance Evaluation

The performance of the proposed model for the hydrogen system integrated with the PV system and BESS shown in Fig. 4.1 has been investigated and analyzed. Simulations have been conducted for a period of one week. The optimization problem is formulated as a nonlinear programming model and is coded and solved using MATLAB Optimization toolbox. In this work, the optimization horizon is defined as 4 hours with a 1-hour time interval, which is a typical real-time scheduling resolution [82]. It is noteworthy that all of the experiments were conducted on a Windows 10 Professional OS environment using an Intel Core i7, 2.21 GHz, 16G RAM, and the codes are performed in Matlab 9.6. The convergence and the constraint tolerances are each set to 10^{-6}. The modeling and simulation parameters of the system under the study are listed in Table 5.1. The listed system cost coefficients per year are converted into hourly costs, due to 1-hour being the schedule resolution of the proposed optimization model. The solar irradiance and hydrogen demand profiles were obtained within a 1-hour time resolution from [83].

The determination of the degradation cost of the BESS in this work is based on its SoC, number of charge-discharge cycles, battery price and capacity, and round-trip efficiency as given in [84].

The simulation results of the proposed economical dispatch model are presented in Fig. 4.2. The hydrogen demand and production from the electrolyzer during the week are shown in Fig. 4.2(a). It can be observed that hydrogen demand is at its peak values with an average of 50 kg/hr, while it drops to 30 kg/hr during the night hours. Fig. 4.2(a) also shows that hydrogen production flow rate tends to follow PV power profile by increasing during midday periods and decreasing during nighttime. As a result, the electrolyzer runs at almost maximum rating during midday time, sacrificing system conversion efficiency in order to minimize PV power curtailments (i.e., maximize solar power utilization).

Fig. 4.2(b) highlights both solar power generated and curtailed during the week under study. It can be observed that PV power curtailments are

Table 4.1: Modeling and simulation parameters [4, 5]

P^{Elz}_{min}=P^{Cmp}_{min}=0MW	k=1.4	O^{Cmp}=1.5% $\cdot$ C^{Cmp} \$/kW-yr
Q^{BESS}=6 MWh	SoH_{min}=10%	$P^{B,Chg}_{min}$ =$P^{B,Dhg}_{min}$ =0 MW
η^{F}=85%	Q^{HS}=1600 kg	$\eta^{BESS,Chg}$=$\eta^{BESS,Dhg}$=88.3%
C^{BoP} =50 \$/kW-yr	SoH_{max}=95%	O^{BESS}=1.5% $\cdot$ C^{BESS} \$/kW-yr
η^{Cmp}=63%	T^{HS}=333.15K	D^{Elz}=50% $\cdot$C^{Elz} \$/kW-yr
λ^{PV}=1000 \$/kWh	SoC_{max}=90%	C^{Cmp}=7.52\$/kW-yr
C^{BESS}=124\$/kW-yr	Π^{HS}_{max}=700 bar	O^{Elz}=1.5% $\cdot$ C^{Elz} \$/kW-yr
π^{H_2}=20 bar	P^{Cmp}_{max}=177kW	$P^{BESS,Chg}_{max}$=$P^{BESS,Dhg}_{max}$=1.5MW
Π^{HS}_{min}=350 bar	SoC_{min}=20%	C^{Elz}=1466 \$/kW-yr
M^{Elz}_{max}=65 kg/hr	z=1.02	$\gamma^{BESS,Dsp}$=$\gamma^{HS,Dsp}$=0.006%/hr
P^{Elz}_{max}=3.8 MW	T^{Elz}=323.15K	C^{PV} =1000 \$/kW-yr

minimized during peak PV power generation. Therefore, PV power is nearly fully utilized during the study period.

Fig. 4.2(c) shows the SoH profile, which is an indirect measure of the amount of hydrogen fuel in the hydrogen storage. The SoH tends to increase during excessive PV power generation, as shown during the first two days of the week, and hence maintaining the system sustainability in the long run. On the fifth day and during the day, both hydrogen demand and PV are at their peak values, however, rated hydrogen production cannot meet the demand. As a result, the hydrogen storage starts to discharge while the electrolyzer keeps operating at its maximum rating to satisfy the demand. It can also be observed that the operation of the hydrogen storage is within the SoH's limits.

The BESS charging and discharging power are plotted in Fig. 4.2(d). It can be observed that the charging power follows a constant behavior during the week according to the PV power generation profile. However, the discharging power has varying rates based on electrolyzer demand. This can be clearly recognized during no PV power generation periods.

Fig. 4.2(e) shows the SoC profile of the BESS which tends to increase smoothly during midday, when there is excess PV output power after satisfying electrolyzer demand. On the other hand, the SoC starts to decrease during the night as BESS power is consumed by the electrolyzer to meet the mid-peak hydrogen demand. In addition, the figure shows how the BESS accounts for variations in the PV power while maintaining the SoC within operational limits.

The electrolzyer's efficiency during the simulation period is shown in

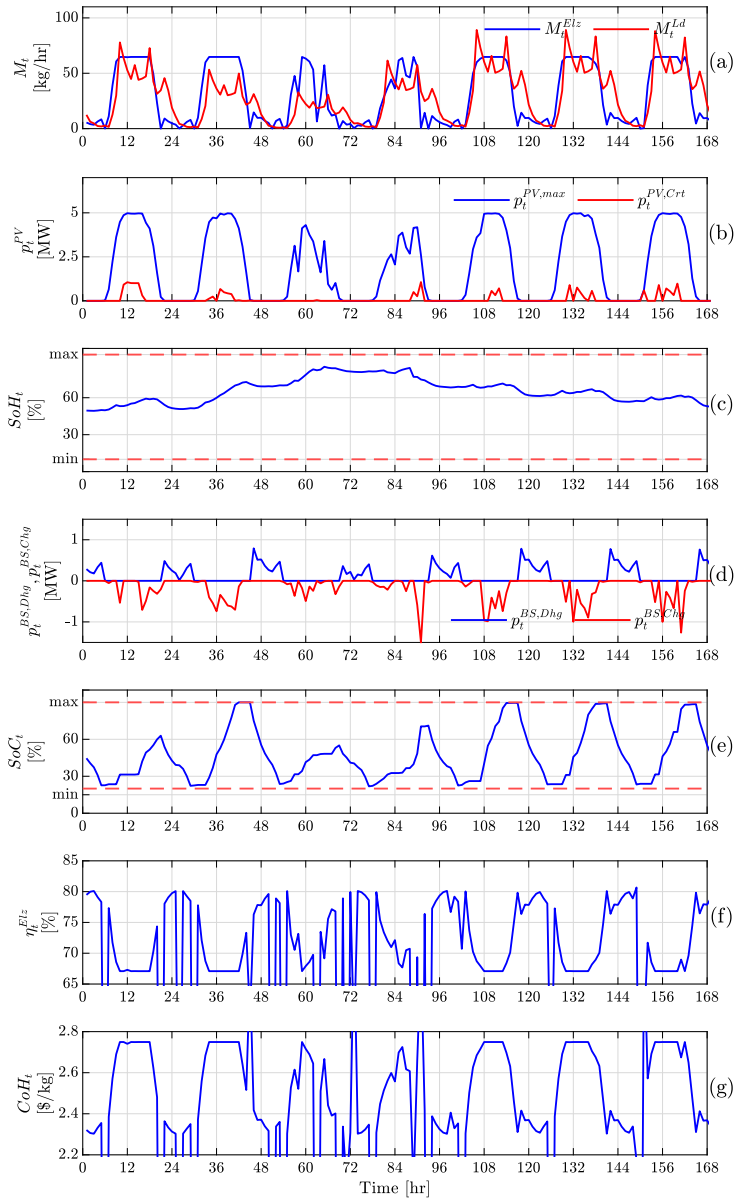

Figure 4.2: Optimization results for: (a) Hydrogen production and hydrogen demand, (b) PV generated and curtailment power, (c) SoH, (d) BESS Power, (e) SoC, (f) Electrolyzer conversion efficiency, and (g) Hourly CoH production.

Fig. 4.2(f). During on-peak hydrogen demand and/or on-peak PV power generation, the electrolyzer tends to run at a high production rate, resulting in a low conversion efficiency while meeting hydrogen demand and ensuring maximum PV power utilization. Conversely, high electrolyzer efficiencies are recognized during mid-peak and off-peak hours of hydrogen demand and off-peak hours of solar power.

The hourly CoH production through the week can be depicted in Fig. 4.2(g). With increasing the electrolyzer efficiency from 70% to 80%, CoH production decreases to around 20%, showing the impact of electrolyzer efficiency variation on CoH production. The increase in CoH during daytime is attributed to the high hydrogen production rate that leads to low system efficiency, resulting from high hydrogen demand and PV utilization.

These results offer considerable insights into the relationships between the hydrogen production rate, electrolyzer efficiency, and CoH production. There is a positive correlation between the hydrogen production rate and CoH production, and a negative correlation between the electrolyzer conversion efficiency and both hydrogen production rate and CoH production.

In order to verify the economic benefits of the proposed model, the optimal look-ahead dispatch operation obtained by the proposed model is compared to the conventional model where electrolyzer is assumed to be running at a constant efficiency. The constant electrolyzer conversion efficiency adopted for this comparison is 60% based on the models proposed by [79, 80]. The following indicators are used for comparison analysis: total utilized and unutilized solar energy, total hydrogen produced, total system cost, and average of CoH production. The detailed comparison results are listed in Table 4.2. As specified in Table 4.2, the proposed model produced 854.88 kg of hydrogen more than the conventional model over the study period. The proposed model meets hydrogen demand with excess hydrogen production of 266.15 kg, while the conventional model fails to meet the hydrogen demand without the help of the initial value of the hydrogen storage. As a result, the proposed model has a lower average of CoH production, with 2.67 $/kg over the week. Compared to the conventional model that has an average CoH of 3.15$/kg, the proposed model achieves a decrease of 16.5% in CoH. It is worth mentioning that the average electrolyzer efficiency of the proposed model was found to be about 73.26%. This finding indicates that the proposed model succeeded in maximizing the electrolyzer efficiency, compared to the conventional model. Hence, the proposed model shows superiority in meeting hydrogen demand with low CoH production and high efficiency.

Table 4.2: Comparison results

Parameter	Proposed Model	Conventional Model
Hydrogen Demand	4,979.69 kg	
PV energy generated	333.32 MWh	
Utilized PV energy	316.63 MWh	303.77 MWh
PV energy curtailment	16.68 MWh	29.55 MWh
Hydrogen Produced	5,245.84 kg	4,390.96 kg
Total system costs	$27,751.17	$26,172.66
CoH	2.67 $/kg	3.15 $/kg

4.4 Summary

This chapter introduces an economical dispatch scheduling model for an optimal operation of hydrogen system connected with PV system and BESS. The use of BESS increases hydrogen production efficiency and PV power utilization, leading to a reliable and sustainable hydrogen production. The proposed model does not only aim to minimize CoH production by maximizing hydrogen production efficiency, but also maximize the benefits of PV power by minimizing its curtailments. The model takes into account the capital, operation, and degradation costs of each system, electrolyzer efficiency variations under various operating conditions, and operational and physical constraints. The simulation results reveal significant relationships between the hydrogen production rate, electrolyzer conversion efficiency, and CoH production. A comparison has been carried out between the dispatch of the proposed model and conventional model to demonstrate the economic feasibility and benefits of the proposed model. Comparison results show a decrease of 16.5 % in CoH production as a result of implementing the proposed economic dispatch model.

Chapter 5

Optimal Energy Management of Grid Connected Hydrogen Energy Facility Integrated with Battery Energy Storage and Solar Photovoltaic Systems

This chapter is an extension work of chapter 4 and focuses on designing and implementing an optimal scheduling EMS model for a hydrogen production system to maximize the system's performance while minimizing the CoH. Unlike the work in chapter 4, 5 proposes an EMS that is designed to enable seasonal storage applications by incorporating a Z-score statistical measure of historical electricity prices. Furthermore, the EMS designed in 5 is applied to a grid-connected microgrid that has an electrical and hydrogen demand. For the purpose of demonstrating the validity of this model, it is tested for both intraseasonal and seasonal storage. Using four case studies, the proposed EMS model is demonstrated to have significant techno-economic benefits. Additionally, the contribution of the electrolyzer's capacity factor, the size of the hydrogen storage, and the share of PV power to the system are evaluated in the context of their techno-economic benefits.

The key contributions of the proposed hydrogen production EMS in this chapter are listed as follows:

- An optimal scheduling EMS model is presented for a hydrogen energy system that would (i) minimize the CoH production, (ii) consider a detailed electrolyzer energy conversion efficiency model, and (iii) maintain reliable operation of the hydrogen production facility system by considering system operational and physical constraints.

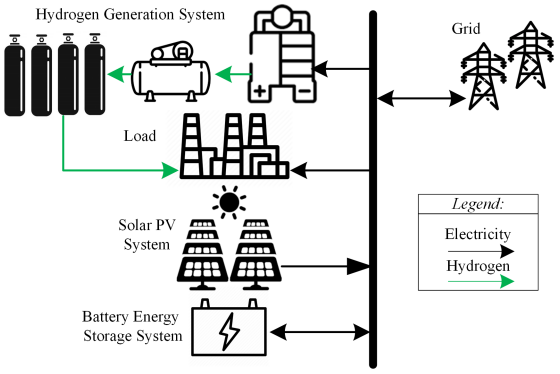

Figure 5.1: Schematic diagram for the industrial electricity and hydrogen energy system.

- A new objective function is developed to motivate seasonal storage of hydrogen energy. The proposed objective function uses the Z-score statistical measure of historical electricity prices to whether reward or penalize the operation of electrolyzer under different electricity prices.
- The impact of different sizes for the electrolyzer, HS, and share of PV energy on the CoH and system efficiency is investigated considering electrolyzer efficiency variation.

5.1 Problem Hypothesis

Fig. 5.1 illustrates the grid-connected renewable hydrogen production facility that is considered for the proposed EMS model. This facility includes PV system, BESS, electrolyzer, compressor, and HS. In order to schedule and optimize the operation of the hydrogen production facility's units based on the availability of PV power, hydrogen and electricity demand, as well as real-time electricity prices, an EMS model must be developed for the hydrogen production facility. The electrolyzer converts electrical energy into chemical energy using water electrolysis technology. The detailed electrochemical characteristics of the electrolyzer cell are obtained from the model presented in section 1.1.2.

Understanding the electrolyzer conversion efficiency behavior is crucial for an economic and technical analysis of hydrogen production. By improving electrolyzer efficiency, hydrogen production costs can be minimized. The conversion efficiency of the electrolyzer system represents the ratio of the

output energy content of the produced hydrogen at the electrolyzer stack to the input DC power energy into the electrolyzer stack as described in equation (1.3).

Equation (1.3) describes the dependency of the electrolyzer efficiency on system power consumption. As a result, the efficiency of the electrolyzer depends on the voltage across the electrolyzer described in equations (1.5) to (1.12), which are functions of the operating temperature, pressure, and loading point. The electrolyzer operating temperature has a significant positive correlation with electrolyzer conversion efficiency [85]. This is attributed to the dependence of the electrolysis reaction and electrolyzer resistance on the operating temperature of the electrolyzer [85]. This dependence can be recognized directly from the open-circuit, activation, concentration, and ohmic voltage equations described in equations (1.6) to (1.11). However, operating an electrolyzer at a high temperature negatively impacts its lifetime [85]. Furthermore, the electrolyzer efficiency is inversely related to the hydrogen output pressure [85]. As a result, a high hydrogen output pressure will decrease the electrolyzer's conversion efficiency [85].

Fig. 5.2 shows the relationships between the conversion efficiency, hydrogen production rate, and CoH production of a 1 MW electrolyzer system with a fixed electricity cost of 100 $/MWh.

The figure illustrates that the electrolyzer's efficiency increases with increasing input power up to a certain operating point, which occurs at light loading conditions, before the electrolyzer begins consuming more electric energy that cannot be converted entirely to chemical energy, and at this point, the efficiency of the electrolyzer begins to decrease. The figure also illustrates the trade-off between system efficiency and the CoH production. Where, high hydrogen production rates lead to low system efficiency, resulting in high power losses, which eventually increase the CoH. It is noteworthy that the minimum CoH is obtained at the maximum electrolyzer conversion efficiency. However, at a minimum CoH, the electrolyzer would operate at a very low hydrogen production rate. Additionally, operating an electrolyzer at maximum efficiency mandates oversizing of the electrolyzer, and hence increases its capital cost significantly [85]. Therefore, the production of hydrogen typically involves high operating expenditure with poor system efficiency, which necessitates the optimization of the system to find the optimum operating point that balances system cost and efficiency [85].

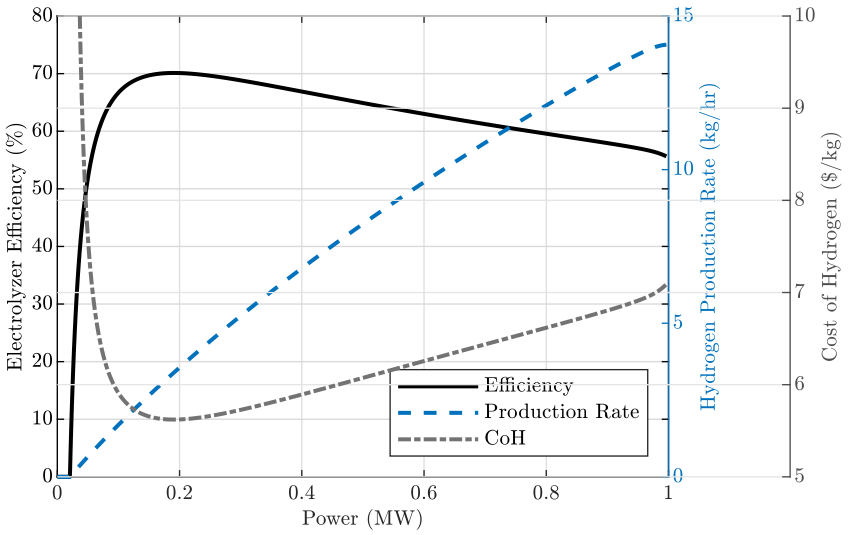

Figure 5.2: The relationship between electrolyzer power, conversion efficiency, hydrogen production rate, and CoH

5.2 Optimization Model of the Energy Management System

The optimal operation of the hydrogen production system must be able to guarantee an optimal balance between the demand for hydrogen and the CoH production by managing the flow of energy between the integrated facility units. A new objective function that motivates the seasonal hydrogen energy storage is proposed in this work. The net costs of the hydrogen system, PV system, BESS, and grid power are considered to define the objective function of the optimization problem that is to be minimized.

$$\text{Minimize:} \quad \sum_{t \in \mathcal{T}} TC + TO_t + TD_t + E_t^{Grd} + A_t^{PV} \;\forall\; t \in \mathcal{T}. \tag{5.1}$$

The objective function in (5.1) represents five system costs components which describes the system net cost of the hydrogen energy facility shown in Fig. 5.1, given as: (i) total CapEx given in (5.2), (ii) total OpEx given in (5.3), (iii) degradation costs of the BESS and electrolyzer system as in

(5.4), (iv) electricity purchasing cost from the main grid as in (5.5), and (v) penalty cost due to PV power curtailment as in (5.6). The grid cost in (5.5) is multiplied by the Z-score of the historical set of electricity prices, $\mathcal{T}^H = \{1, 2, ..., t^h, ..., t\}$, that serve as a reward or a penalty for seasonal storage application purposes. The Z-score statistical measure acts as a reward or a penalty factor for the hydrogen production in order to motivate the seasonal hydrogen energy storage. It shows how far the current electricity price at time t is from the average of the electricity prices during the time period T^H, which represents the time period of the historical electricity prices. The sign of Z-score determines whether the grid power purchased should be penalized or rewarded. In other words, it defines whether to maximize the use of electricity (i.e, hydrogen production and BESS charging) during low electricity prices or to minimize the power consumption during high electricity prices.

$$\begin{aligned} TC = (i, y^{PV}) \cdot C^{PV} \cdot P_{max}^{PV,m} + R(i, y^{BESS}) \cdot P_{max}^{BESS} \cdot C^{BESS} \\ + R(i, y^{Cmp}) \cdot C^{Cmp} \cdot P_{max}^{Cmp} + R(i, y^{HS}) \cdot Q^{HS} \cdot C^{HS} \\ + R(i, y^{Elz}) \cdot \left(C^{Elz} + C^{BoP}\right) \cdot P_{max}^{Elz}, \end{aligned} \tag{5.2}$$

$$\begin{aligned} TO_t = \left(O^w + O^{HS}\right) \cdot M_t^{Elz} + O^{Elz} \cdot p_t^{Elz} \\ + O^{Cmp} \cdot p_t^{Cmp} + O^{PV} \cdot p_t^{PV,m} \; \forall t \in \mathcal{T}, \end{aligned} \tag{5.3}$$

$$TD_t = D_t^{BESS} \cdot \left(p_t^{BESS,Chg} + p_t^{BESS,Dhg}\right) + D^{Elz} \cdot p_t^{Elz} \, \forall t \in \mathcal{T}, \tag{5.4}$$

$$E_t^{Grd} = \frac{e_{t^h}^{Pr} - \sum_{t^h \in \mathcal{T}^H} \frac{e_{t^h}^{Pr}}{T^H}}{\sqrt{\frac{\sum \left(e_{t^h}^{Pr} - \frac{e_{t^h}^{Pr}}{T^H}\right)^2}{T^H}}} \cdot e_t^{Pr} \cdot p_t^{Grd} \, \forall \, t \in \mathcal{T}, t^h \in \mathcal{T}^H, \tag{5.5}$$

$$A_t^{PV} = \lambda^{PV} \cdot p_t^{PV,Crt} \quad \forall \, t \in \mathcal{T}. \tag{5.6}$$

Here it is worth noting that the CapEx of each system unit in (5.2) captures the time value of money by using the annuity factor formula with a i interest rate for a period of y years, given as [86]:

$$R(i, y) = \frac{r(1+r)^y}{(1+r)^y - 1} \cdot \frac{1}{8760} \tag{5.7}$$

The objective function is subjected to the operational and capacity constraints as discussed hereunder.

5.2.1 Hydrogen Production System Constraints

Given the detailed model of electrolyzer voltage described in Section 1.1.2 that consider the conversion efficiency curve discussed in Section 5.1, the power consumed by an electrolyzer stack can be calculated by using the following equation (1.13). The active power capacity of the electrolyzer system is constrained by its minimum and maximum power capacities, as described in equation (4.5). Also, the maximum and minimum supply current and voltage of the electrolyzer are given in (4.6) and (4.7), respectively. The hydrogen generation rate given in (1.2) is constrained by the electrolyzer maximum outflow rate as described in equation (4.8). The hydrogen gas produced by the electrolyzer is compressed to increase its storage density. The compressor power is determined based on the polytrophic model presented in equation (4.9). The compressor power is imposed by the maximum and minimum power limits as given in equation (4.10). Compressed hydrogen gas is then stored in high-pressure HS for later use. Therefore, the objective function is also subjected to the HS state-of-hydrogen (SoH) balance equation (4.11). The HS pressure balance equation is modeled as given in equation (4.12). HS is also subject to the maximum and minimum physical capabilities of pressure and SoH as expressed in (4.13) and (4.14), respectively.

5.2.2 BESS Constraints

Similar to the HS, the BESS also has operational constraints that ensure its safe operation. The BESS operation is subject to maximum and minimum limits, as shown in (4.17)-(4.18) to avoid excessive charging and discharging that can damage the BESS. The BESS is also constrained by the state-of-charge (SoC) balance equation (4.15). In order to minimize power lost during charging and discharging due to processes efficiencies, a constraint (4.19) is included to prevent simultaneous charging and discharging. Constraint (4.16) specifies the SoC range.

Degradation of the BESS has a significant impact on its cycle life which translates into operation costs. The degradation cost of the BESS is calculated in (5.8) by taking into consideration: depth of discharge (DoD), state of charge (SoC), charging and discharging frequencies, BESS capital expenditure (CapEx) and residual value, as well as its capacity and round-trip

efficiency [87, 88].

$$D_t^{BESS} = \frac{C^{BESS} - RS^{BESS}}{2DoD_t \cdot Q^{BESS} \cdot ACC_t \sqrt{\eta^{BESS,Chg} \cdot \eta^{BESS,Dhg}}} \; \forall\, t \in \mathcal{T}, \quad (5.8)$$

$$DoD_t = 1 - SoC_t \quad \forall\, t \in \mathcal{T}, \quad (5.9)$$

$$ACC_t = \frac{a}{DoD_t^b} \quad \forall\, t \in \mathcal{T}. \quad (5.10)$$

5.2.3 PV System Constraints

Even though the output PV power changes according to solar irradiation, ambient temperature, and operating point, there is an operating point that extracts the maximum amount of PV power under the subjected conditions. Therefore, PV arrays are operated with maximum power point tracking (MPPT) controllers to ensure optimal power generation under a variety of environmental conditions. The maximum power generated by a PV array is calculated as [89]:

$$p_t^{PV,M} = N^{PV} \cdot \eta_t^{PV} \cdot A^{PV} \qquad \forall\, t \in \mathcal{T}, \quad (5.11)$$

where the PV system efficiency is calculated as follows [89]:

$$\eta_t^{PV} = \eta_r^{PV} \cdot \eta^{PV,M} \cdot \Big(1 - \beta_t^{PV} \cdot \big(T_t^{PV} - T_r^{PV}\big)\Big) \forall t \in \mathcal{T}, \quad (5.12)$$

and the PV's temperature is determined using [89]:

$$T_t^{PV} = T_t^{PV,a} + \left(\frac{T^N - T^{PV,a,N}}{S^N}\right) \cdot S_t \;\forall\; t \in \mathcal{T}. \quad (5.13)$$

The PV power curtailment is constrained by the following minimum and maximum operational limits as follows:

$$0 \leq p_t^{PV,Crt} \leq P_t^{PV,M} \quad (5.14)$$

5.2.4 System Power Balance

The system power balance equality constraint ensures a balance operation of the system. It is defined as:

$$p_t^{PV,M} - p_t^{PV,Crt} + p^{BESS,Dhg} - p_t^{BESS,Chg} - p_t^{Elz} - p_t^{Cmp} + p_t^{Grd} - p_t^{Ld} = 0 \;\; \forall\, t \in \mathcal{T} \quad (5.15)$$

The amount of power purchased from the power grid is limited by the maximum and minimum grid operational capabilities as follows:

$$P_{min}^{Grd} \leq p_t^{Grd} \leq P_{max}^{Grd} \quad (5.16)$$

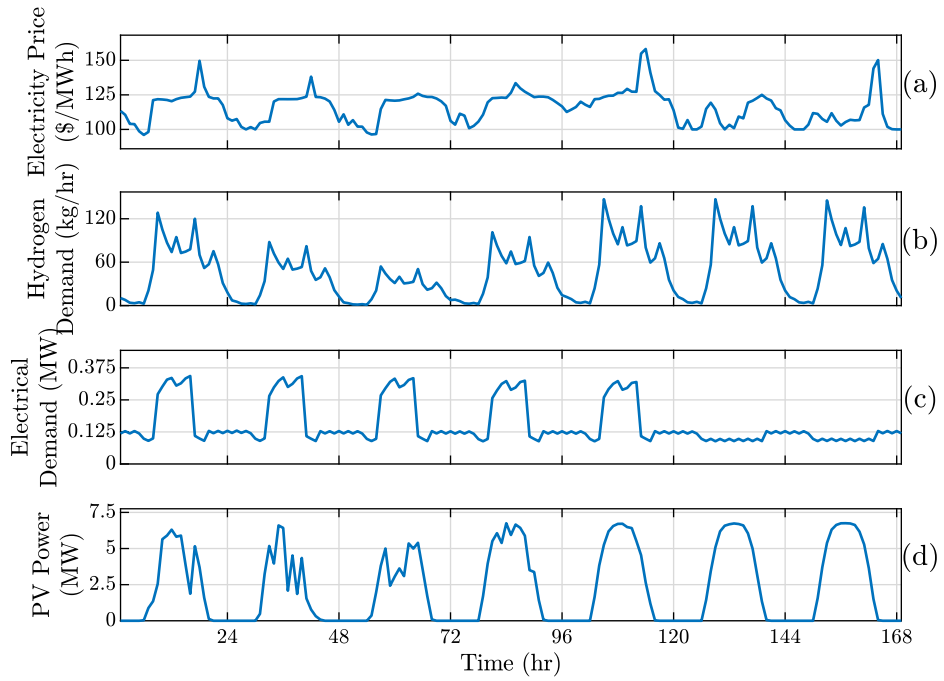

Figure 5.3: System input data: (a) Electricity price , (b) Hydrogen demand, (c) Electrical demand, and (d) PV power generation.

5.3 Performance Evaluation

Simulations were conducted for the grid-tied hydrogen production facility shown in Fig. 5.1 with and without a PV system and a BESS to show and verify the performance of the proposed EMS model to minimize the CoH and obtain seasonal hydrogen storage functionality. The analysis is carried out over a time window of one week, which is divided into 168 periods of 1-hour each. Further analysis is conducted over a one-year period to analyze the implementation of seasonal hydrogen storage.

The hydrogen facility shown in Fig. 5.1 contains a hydrogen generation unit, PV, and BESS to meet its electrical and hydrogen demands. Based on historical practical data, Fig. 5.3 shows data fed into the proposed EMS for several inputs. Fig. 5.3(a) shows the hourly electricity prices in Ontario, Canada, during the study period [90]. Fig. 5.3(b) and Fig. 5.3(c) depicts the hourly historical hydrogen and electrical consumption data for an industrial load profile, respectively [83, 91, 92]. The figures show that the hydrogen facility has been selected to have a hydrogen peak demand of

Table 5.1: Modeling and simulation parameters

C^{BESS}=100 k$/MW	C^{PV}= 818 k$/MW	C^{Cmp}=7.52 k$/MW
C^{HS}=124 $/kg	C^{Elz}=784 k$/MW	C^{BoP}=50 k$/MW
D^{Elz}= 40% $\cdot$ C^{Elz} k$/MWh	O^{HS}=2% $\cdot$ C^{HS} $/kg	O^{Elz}= 17 k$/MWh
O^{Cmp}=1.5% $\cdot$ C^{Cmp} k$/MWh	O^{PV}=9.85 k$/MWh	O^{w}= 0.08 $/kg
y^{Elz}=y^{HS}=y^{PV}=y^{Cmp}= 20 yr	y^{BESS}= 15 yr	i= 5.75%
π^{H_2}=20bar,π^{O_2}=1bar,π^{H_2O}=0.2bar	R= 8.31 J/mol$\cdot$ K,	T^{Elz}= 323 K
$J^{0,a}$=1$\times10^{-7}$A/cm^2,$J^{0,c}$=0.1A/cm^2	α^a= 0.8, α^c= 0.25	N^{PV}= 880
P^{Elz}_{min}= 0 MW, P^{Elz}_{max}= 5 MW	J^{Lim}= 2 A/cm^2	η^{PV}_r= 16 %
M^{Elz}_{max}= 0 kg/hr, M^{Elz}_{max}= 77 kg/hr	ΔG= 2.33$\times10^5$ J	R^{Elz}= 200 Ω
P^{Cmp}_{min}= 0 MW, P^{Cmp}_{max}= 0.2 MW	$N^{Elz,c}$= 1500	λ^{PV}= 1000 $/MWh
P^{PV}_{min}= 0 MW, P^{PV}_{max}= 7 MW	A^{PV}= 29.97 m^2	Q^{HS}= 1500 kg
$\eta^{BESS,Chg}$=$\eta^{BESS,Dhg}$= 97.5%	Q^{BESS}= 7 MWh	T^{HS}=333.15K
$P^{BESS,Chg}_{min}$=$P^{BESS,Dhg}_{min}$= 0 MW	HHV= 141.9 MJ/kg	T^{N}= 45^{o}C
$P^{BESS,Chg}_{max}$=$P^{BESS,Dhg}_{max}$= 1.75 MW	F= 96.49 kC/mol	$\eta^{PV,M}$= 100%
P^{Grd}_{max} = 6 MW, P^{Grd}_{min}= 0 MW	S^N= 800 W/m^2	T^{PV}_r= 25^{o}C
$\gamma^{HS,Dsp}$= $\gamma^{BESS,Dsp}$= 0.006%	$T^{PV,a,N}$= 20^{o}C	η^{Cmp}= 63%
a= 2744, b= 1.665, z= 1.02, k= 1.4	c_1=-0.0034, c_2=-0.001711	d=-1, f=1

147 kg and an electrical peak demand of 0.34 MW, excluding the electrical power consumption of the hydrogen production system. The local electrical demand profile is adopted from an industrial load [92]. Furthermore, the profile of hydrogen demand considered in this study is based on [83].

The hourly solar irradiation for Toronto, Ontario, Canada is also used to predict the maximum PV power as shown in Fig. 5.3(d) [83]. Furthermore, the related system modeling and simulation parameters used of each system component in this work are listed in Table 5.1 [3, 5, 30, 80, 83, 89, 93–95].

The performance of the proposed EMS model is investigated through a techno-economics analysis of two system configurations: hydrogen-grid, and hydrogen-BESS-PV-grid. The hydrogen-grid configuration utilizes grid power to meet electricity demand while supplying the hydrogen system, which consists of an electrolyzer, compressor, and hydrogen storage. The hydrogen-BESS-PV-grid system, on the other hand, relies on PV power for the majority of the system's electrical demand. The addition of the BESS aims to maximize the output of the PV system while balancing the system load and generation of the hydrogen facility system. The hydrogen facility system is further connected to the power grid in order to meet electrical demand when PV power is unavailable. Different system conditions are studied for the two hydrogen-grid and hydrogen-BESS-PV-grid configurations to demonstrate the validity of the proposed model. Each configuration is simulated and studied with and without the use of Z-score of historical electricity prices. Therefore, four case studies are implemented to analyze the performance of the hydrogen production system in minimizing the CoH

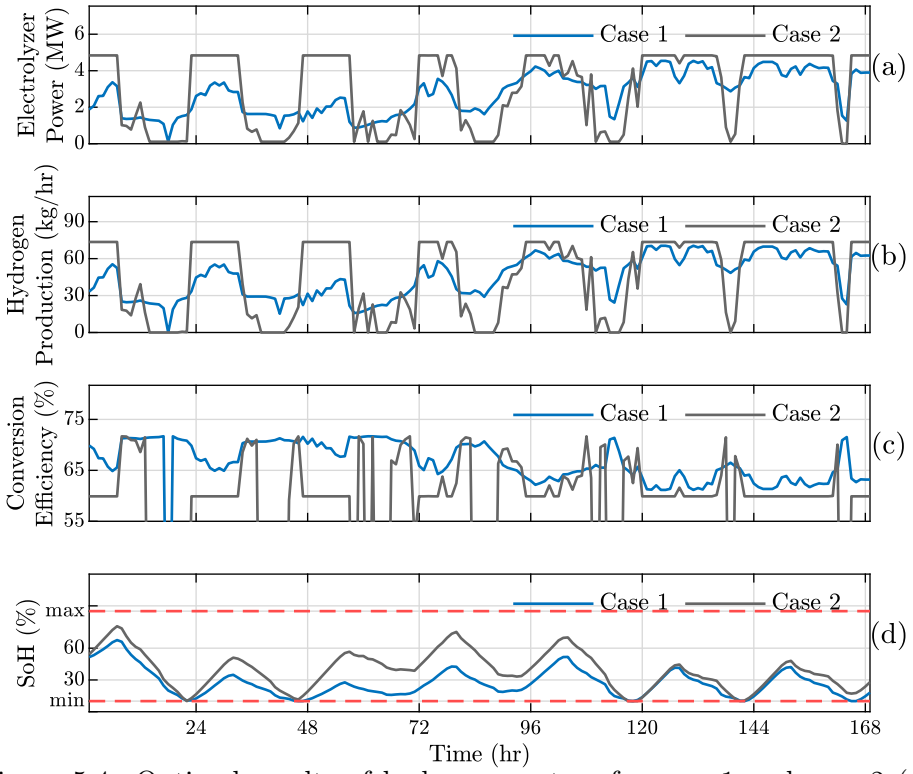

Figure 5.4: Optimal results of hydrogen system for case 1 and case 2 (a) Electrolyzer power consumption, (b) Hydrogen production rate, (c) Conversion efficiency, and (d) SoH level of HS in the two cases

and achieving seasonal hydrogen storage. Section 5.3.1 discusses the results of hydrogen-grid system configuration under case 1 and case 2. Unlike case 1, case 2 considers the use of Z-score for intraseasonal hydrogen storage from grid power. Section 5.3.2 discusses the results of hydrogen-BESS-PV-grid system configuration under Case 3 and case 4. In contrast to case 3, case 4 considers the use of Z-score for intraseasonal hydrogen storage from PV and grid power.

5.3.1 Hydrogen-Grid System Configuration

Figs. 5.4-5.5 show the performance of the proposed EMS model on a sunny summer week for the hydrogen-grid system configuration. Figs. 5.4(a) and (b) show the hourly optimal scheduling for power consumption and hydrogen production by the electrolyzer system, respectively. The figures show

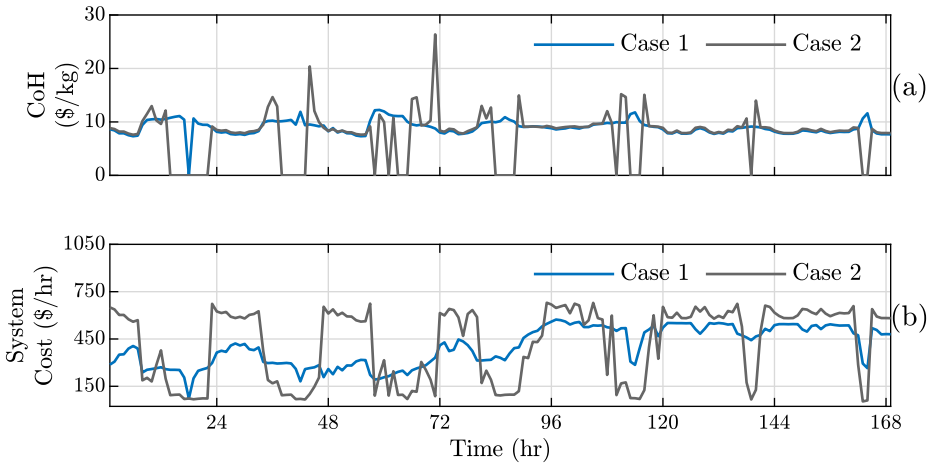

Figure 5.5: Economical results for case 1 and case 2 (a) CoH and (b) Total system cost

that the operation of the electrolyzer in case 1 is positively correlated with hydrogen demand shown in Fig. 5.3(b). On the other hand, through comparison with Fig. 5.3(a), it can be seen that the electrolyzer operation under case 2 is mainly affected by the electricity price. As a result, the maximum operation of electrolyzer occurs during nighttime when low electricity prices are observed, resulting in an excess production of 150 kg of hydrogen compared to case 1. The operation behavior of the electrolyzer during the night under case 2 is mainly due to the use of Z-score of historical electricity prices that motivates the use of low-cost power to fill the HS.

Fig. 5.4(c) shows the conversion efficiency of the electrolyzer system under cases 1 and 2. It can be observed that the electrolyzer conversion efficiency under case 1 is negatively correlated with hydrogen production rates. Therefore, efficient conversion of hydrogen energy is observed at low hydrogen production rates during the first four days of the week under study. On the other hand, low conversion efficiency of hydrogen energy is observed on the last three days of the studied week, when high hydrogen production rates occur to meet the corresponding high hydrogen demand levels. As a result, a high conversion efficiency of 66.80% is observed. Unlike case 1, case 2 conversion efficiency of the electrolyzer system in Fig. 5.4(c) is maintaining a constant low conversion average value at 62.86% most of its operation time with a relatively slight changes during mid electricity prices.

Fig. 5.4(d) shows the SoH level of the HS under case 1 and case 2. The figure shows that the SoH level under both cases is influenced by the

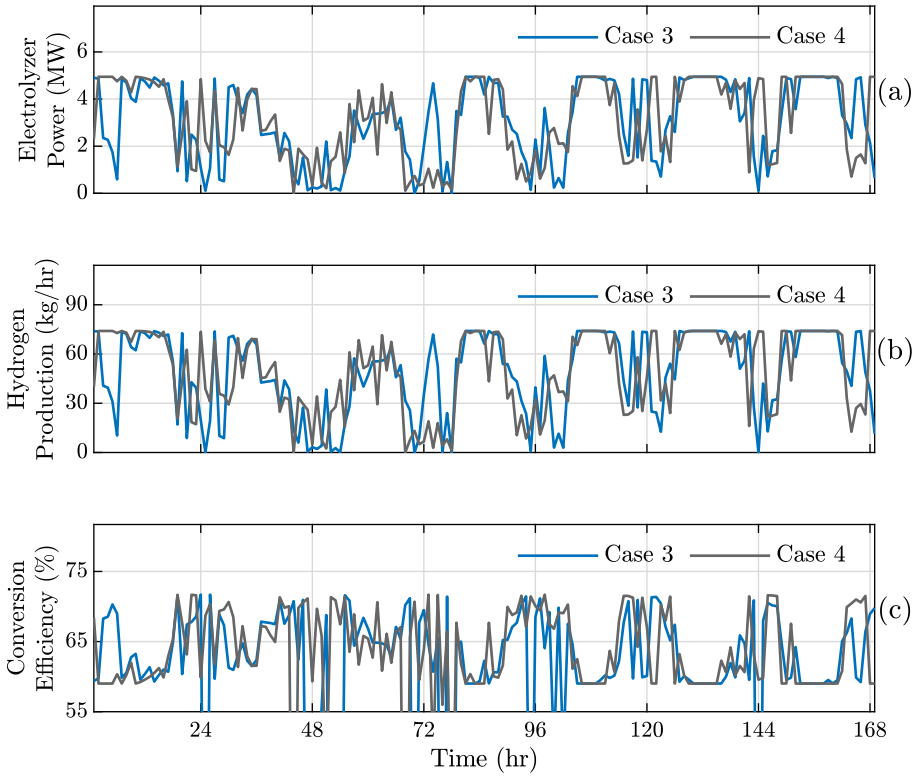

Figure 5.6: Optimal results of hydrogen system for case 3 and case 4 (a) Electrolyzer power consumption, (b) Hydrogen production rate, and (c) Conversion efficiency.

hydrogen demand. It also demonstrates that the SoH level under case 2 is influenced by the electricity price, which validates the efficacy of the proposed model for intraseasonal hydrogen storage.

The CoH and total system cost under case 1 and case 2 are depicted in Figs. 5.5(a) and (b). Fig. 5.5(a) shows that the CoH production under case 1 is consistent throughout the studied week, indicating that the CoH production in this case is not affected by the changes in hydrogen demand. Similarly, the CoH production under case 2 is constant when the electrolyzer is on, but it is unpredictable when the electrolyzer is off. Fig. 5.5(b) shows the net system cost over the week. The system cost under case 1 and 2 follows the same behavior of electrolyzer power and hydrogen production, which are highly affected by the hydrogen demand levels in case 1, and by the electricity prices in case 2.

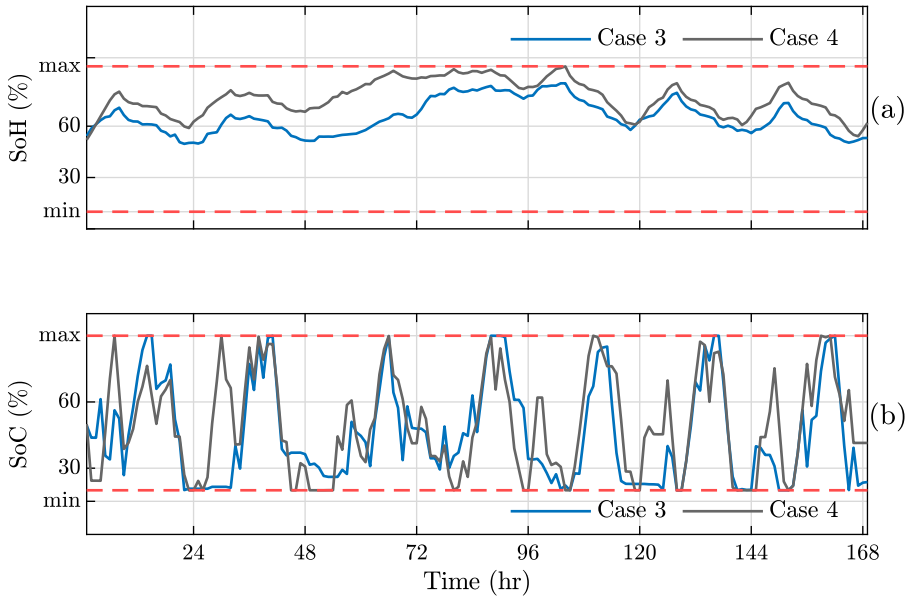

Figure 5.7: Optimal results of hydrogen system for case 3 and case 4 (a) SoH level of HS, (b) SoC level of BESS

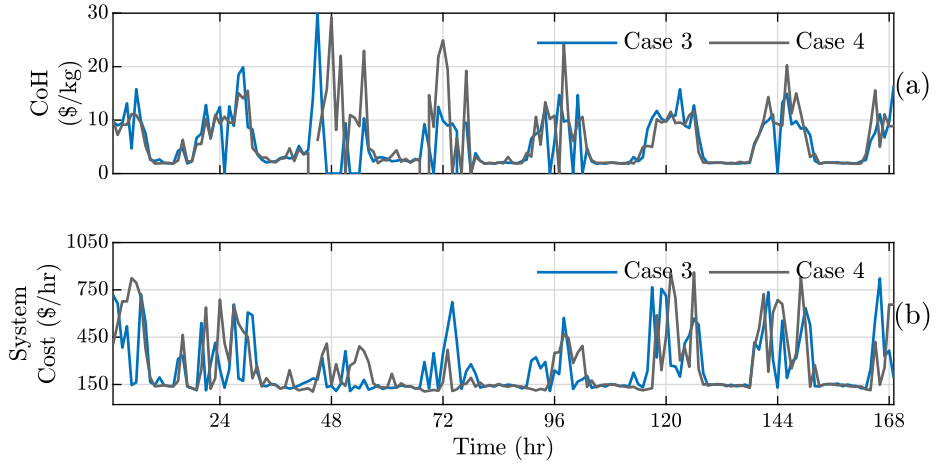

Figure 5.8: Economical results for case 3 and case 4 (a) CoH and (b) Total system cost

5.3.2 Hydrogen-BESS-PV-Grid System Configuration

Figs. 5.6-5.8 show the performance of the hydrogen-BESS-PV-grid system configuration. The operation of the electrolyzer system under cases 3 and 4 is mainly impacted by the PV power generation shown in Fig. 5.3(d). It can be observed from Fig. 5.6(a) and Fig. 5.6(b) that during daytime, the electrolyzer runs at its maximum hydrogen production rate to maximize the utilization of PV power. Therefore, the majority of around 68% of the hydrogen demand in the two cases is met by PV power, while the grid power is responsible for 32% of the hydrogen demand.

Furthermore, the average conversion efficiency in Fig. 5.6(c) under the two cases is 64.16% and 64.43, respectively. The low value of conversion efficiency can be attributed to the high production rates that utilize the PV available power. The figure shows that the conversion efficiency under the two cases goes to minimum values during excessive PV power generation during the daytime while it increases at night when no PV power is available, and power is being consumed from the grid to satisfy necessary hydrogen demand.

The SoH of the HS for cases 3 and 4 is illustrated in Fig. 5.7(a), while the SoC of the BESS under the two cases is shown in Fig. 5.7(b). The results in Fig. 5.7(a) shows that the SoH level under both cases is influenced by the changes of both hydrogen demand level and the PV power generation. Furthermore, the SoH under case 4 is influenced by electricity prices. This is due to the use of Z-score which motivates the hydrogen production during low grid power costs, proving the validity of the proposed EMS model to achieve intraseasonal storage. Fig. 5.7(b) shows that the BESS charges during the day with high PV generation, and the discharging operation is observed at night. Moreover, the SoC level under case 4 shows that there are some charging operations conducted at night due to low electricity prices at that time.

The CoH and total system cost of cases 3 and 4 are depicted in Figs. 5.8(a) and (b). Fig. 5.8(a) shows that the CoH production under the two cases is almost the same during daytime, that is when PV power is available. However, the CoH production during nighttime relies mainly on the electricity price. Fig. 5.8(b) shows the net system cost under case 3 and 4. Considering the figure, the net system cost is closely correlates with the electrolyzer power and hydrogen production, which are strongly influenced by PV power generation, hydrogen demand levels, and electricity prices.

Table 5.2: Optimal scheduling results of four cases

System Configuration		Case 1	Case 2	Case 3	Case 4
Electrical Energy Consumed (MW)	Grid	513	559	190	209
	PV	-	-	395	395
Hydrogen Produced (kg)	Grid	7,730	7,880	3,042	3,083
	PV	-	-	5,219	5,312
Conversion Efficiency (%)		66.80	62.86	64.16	64.43
System CapEx Cost (10k$)		6.92		17.47	
System OpEx Cost (10k$)		1.02	1.12	1.58	1.59
System Degradation Cost (10k$)		1.43	1.56	2.53	3.74
System Grid Power Cost (10k$)		58.17	61.49	21.03	22.41
System Net Cost (10k$)		67.54	71.09	42.61	45.21
CoH ($/kg)		8.74	9.02	5.16	5.39

5.3.3 Comparative Analysis

The comparative analysis of the techno-economic benefits under four cases is given in Table 5.2. The table lists the energy production and consumption details along with the different system costs including CapEx, OpEX, degradation, and grid power costs for the two configurations. It can be observed that the CoH is low and in the range of 5$/kg for hydrogen-BESS-PV-grid configuration, which results in saving about 3.5$/kg compared to the hydrogen-grid system configuration. Furthermore, one can see that the power cost from the grid represent 87% of the CoH in the hydrogen-grid configuration, which, in turn, indicates that the electricity price is the control variable that determine the CoH. On the other hand, the CoH in the hydrogen-BESS-PV-grid configuration is impacted mainly by; the CapEx of the PV system, which takes up to 40% of the overall CoH, and the cost of electricity purchased from grid, which represents about 50% of the total CoH. Given that the price of electricity purchased from the grid is higher than the investment cost of PV system, the PV based system configuration is the most economical compared to grid-based system configuration. Therefore, the results show the economic benefits of using PV and BESS for hydrogen production.

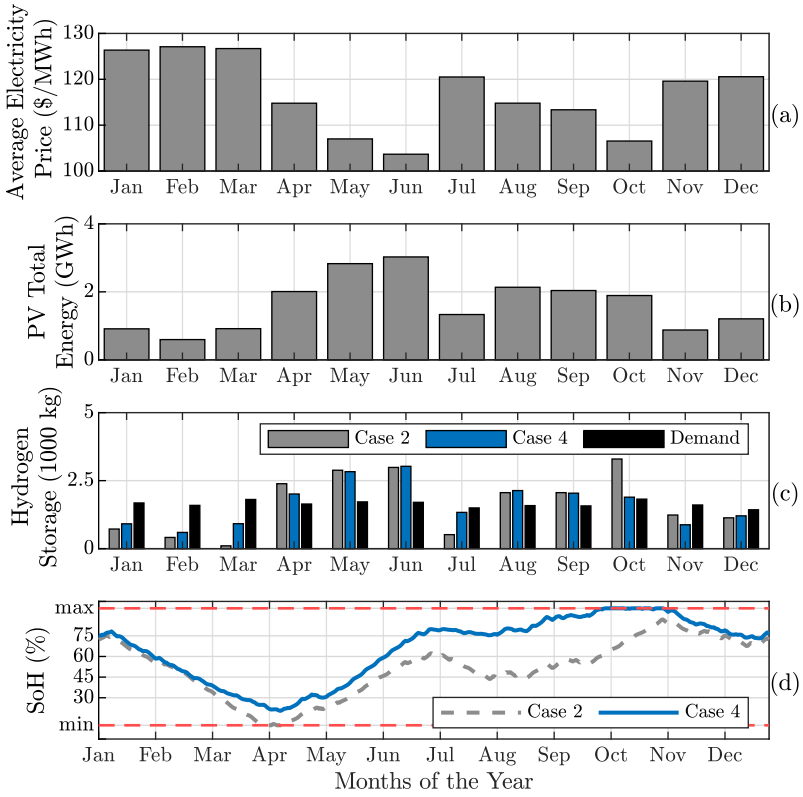

Figure 5.9: Monthly average of: (a) Electricity price, (b) HS generation and demand, and (c) HS SoH

5.3.4 Seasonal Storage of Hydrogen Energy

Fig. 5.9 shows the results yielded from the optimal operation of the electrolyzer and hydrogen seasonal storage. The figure represents the monthly average of (a) electricity prices, (b) PV total energy generation, (c) hydrogen production and demand, and (d) the SoH level under cases 2 and 4. As shown in the figure, the electrolyzer under case 2 shows higher operation during the months with low electricity prices. Fig. 5.9 (c) shows that the hydrogen demand is fairly consistent in various months over the year, while hydrogen production varies depending on the electricity price in each month as shown in Fig. 5.9(a). Fig. 5.9(c) shows that the SoH under case 2 decreases when the demand exceeds the generation and vice versa as depicted in Fig. 5.9(d). The PV total energy generation shown in Fig. 5.9(b) shows that during April to September, there is an excess PV energy when the SoH

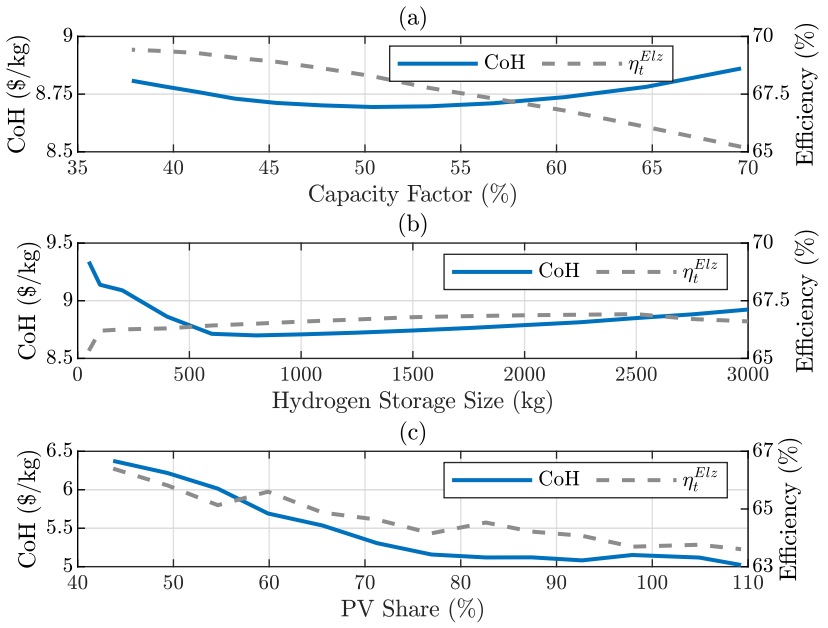

Figure 5.10: Case 1: a) Impact of electrolyzer capacity factor on CoH, b) Impact of HS size on CoH, c) Impact of BESS size on CoH, d) Impact of PV size on CoH, e) Impact of PV size on PV power curtailments

level of HS under case 4 increases as shown in Fig. 5.9(d). In October and July, the amount of hydrogen produced by the electrolyzer is just able to satisfy the hydrogen demand for those months. As a result, the proposed EMS model works to store the hydrogen during the months of April to June and August to September, in order to supply the hydrogen demand between November and March. Therefore, the SoH of the HS follows both the intraseasonal and seasonal trends as depicted in Figs. 5.9(c), Fig. 5.4(d) and Fig. 5.7(a) to minimize intraseasonal and seasonal CoH. Based on the above analysis, the total CoH for the entire simulated year is calculated as 9.41$/kg and 6.27$/kg for cases 2 and 4, respectively.

5.3.5 Impact of Electrolyzer, HS, and PV Capacities on Optimal Scheduling

The proposed EMS has several of important parameters that can change the results of the optimization process, which presents a real-world challenge. In order to illustrate the effects of the important parameters in the optimization process, further analysis is conducted to study the impact of electrolyzer size, HS size, and share of PV generation on the CoH and energy conversion efficiency. Given that the use of Z-score of historical electricity prices forced the electrolyzer to run at maximum rating during low electricity prices resulting in a minimum conversion efficiency. The following analysis is only conducted for cases 1 and 3 at which the value Z-score is set to 1. The corresponding CoH and conversion efficiency under the two cases are shown in Fig. 5.10.

Fig. 5.10(a) shows the impact of different electrolyzer capacity factors on the CoH and conversion efficiency for case 1. The electrolyzer size is considered to vary to give a capacity factor range of 40% to 70%. With capacity factor decreasing from 70% to 50%, the electrolyzer is able to run at a low production rate with a high conversion efficiency and still meet hydrogen demand, as a result the CoH decreases. However, when the capacity factor goes below 50%, the CoH starts to increase gradually due to the over-sizing of the electrolyzer system.

Several HS sizes are considered to show their impact on CoH and conversion efficiency, which is shown in Fig. 5.10(b). The figure shows that with an increase in the size of HS from 50 kg to 500 kg, a considerable decrease in the CoH is observed. Further increase in the HS size has a slight impact on the CoH.

It is of an interest to show the variation of CoH and electrolyzer conversion efficiency as functions of the PV energy share. Fig. 5.10(c) shows the CoH and system conversion efficiency under several PV capacities to provide a PV energy share between 40% and 110% under case 3. As depicted, when PV energy share increases, the CoH decreases. However, once PV share goes up 70%, the CoH starts to be steady at around 5 $/kg due to the oversized of PV system and the low system conversion efficiency as shown in Fig. 5.10(c). It is also worth noting that the conversion efficiency follows the same behavior as the CoH, which decreases as the PV share increases. This decline is a result of running the electrolzyer at high production rates to utilize as much PV energy as possible. Therefore, an economical hydrogen production can be achieved at a PV energy share of around 70%.

5.4 Summary

In this chapter, an optimal scheduling EMS model of hydrogen production systems has been proposed. The proposed model aims to minimize the CoH while considering the intraseasonal and seasonal hydrogen energy storage for both renewable and non-renewable grid-connected hydrogen facilities. The historical information of electricity prices is considered to motivate the the charging and discharging of hydrogen storage. The optimization is performed under four case studies using real solar irradiation, electricity price, and hydrogen and electrical demand profile data as input. Case studies revealed that the proposed model is able to achieve both intraseasonal and seasonal hydrogen energy storage. Furthermore, the results show that the PV based system configuration can lead to a reduction of 3.5$/kg compared to grid-based system configuration. The results also show the effects of different electrolyzer's capacity factor, HS size, and PV share on the optimal operation of the hydrogen production system using the proposed EMS model.

Chapter 6

Conclusions and Future Works

6.1 Conclusions

Hydrogen is produced through the integration of an electrolyzer system with renewable energy sources. The integration of electrolyzer and renewable energy resources presents significant operational and economic challenges for maintaining system balance and producing hydrogen at a cost-effective level due to the intermittency and variability of renewable energy resources as well as the nonlinearities associated with electrolyzer models. In this thesis, the modeling problem of the PEM electrolyzer is solved by proposing two distinct approaches to estimate the model parameters accurately through the use of an optimization-based and an analytical-based approaches. The accurate PEM electrolyzer is then used to propose two optimization-based energy management schemes that will enable the seasonal storage of hydrogen energy and ensure a low-cost hydrogen production process by taking into account the nonlinearity of the efficiency curve of the electrolyzer.

In Chapter 2, the problem of parameter estimation of a detailed electrochemical PEM electrolyzer model is studied, considering seven parameters as well as their technical constraints. The parameter estimation is formulated an optimization problem that is based on a least-squares objective function. By using different operating conditions of temperature and pressure levels, the model parameters can be estimated with high accuracy within a short computation time.

In Chapter 3, the problem of parameter estimation of the PEM electrolyzer is addressed where analytical-based approach is used. The majority of existing parameter estimation approaches use a simplified PEM electrolyzer model and ignore some important parameters. Consequently, these approaches may not produce a fully accurate model and are therefore not feasible in practice. As a result, a novel analytical approach based on

the LSE is proposed to estimate the PEM electrolyzer modeling parameters and to estimate its electrochemical behavior under different operating conditions. Specifically, five unknown modeling parameters are estimated in a non-iterative manner to model the PEM electrolyzer, including the change in Gibbs free energy, charge transfer coefficient, exchange current density, series resistance, and limiting current density. Furthermore, the parameters were observed to depend on the different levels of temperature and pressure. The accuracy of the model has been tested at various temperatures, pressures, and hydrogen production rates. Sensitivity analysis confirms the validity of the proposed approach for different dataset sizes. The superiority of the proposed approach is demonstrated by comparison to other methods of electrolyzer parameters estimation.

In Chapter 4, the EMS problem that uses PV system and BESS to produce hydrogen economically using water electrolysis is studied. Compared with the existing literature, the proposed EMS incorporates the electrolyzer efficiency variations under various operating conditions. Particularly, the proposed model aims to minimize CoH production by maximizing hydrogen production efficiency, as well as to optimize the benefits of PV energy by minimizing its energy curtailment. Simulation results indicate significant correlations between hydrogen production rate, electrolyzer conversion efficiency, and COH production. To demonstrate the economic feasibility and benefits of the proposed model, a comparison of the dispatch of the proposed model with a conventional model has been made. As a result of the proposed economic dispatch model being implemented, the CoH production decreased by 16.5%.

In Chapter 5, the design and implementation of an optimal scheduling EMS model of hydrogen production systems has been studied. An EMS model that aims to minimize the CoH while considering the intraseasonal and seasonal hydrogen energy storage is proposed for both renewable and non-renewable grid-connected hydrogen facilities. The charging and discharging of hydrogen storage is motivated by historical information of electricity prices. Using real-world data of solar irradiation, electricity prices as well as hydrogen and electrical demand profiles, the optimization is carried out using four case studies. Several case studies have demonstrated that the proposed model is capable of storing hydrogen energy both intraseasonally and seasonally. Additionally, the PV-based system configuration has the potential to lower system costs by an average of 3.5$/kg when compared to grid-based system configurations. Based on the proposed hydrogen production system EMS model, it is also shown that the capacity factor, size, and PV share of the electrolyzers affect the optimal operation of the system.

6.2 Future Works

Future studies focus on the development a model-based controller using the proposed parameter estimation approach to control hydrogen production, maximize system efficiency, and detect system faults, which may lead to more detailed investigation into the integration of electrolyzer system in order to optimize system reliability and stability.

Further work will aim to design an EMS for economical hydrogen production with short time intervals and considering dynamic system models along with more system constraints in order to study the impact of hydrogen production dynamics and transients on the power system and use that to provide grid ancillary services. Furthermore, the sizing problem of renewable hydrogen production system that aims to maximize energy conversion efficiency will be considered for future work.

Bibliography

[1] J. C. Alberizzi, M. Rossi, and M. Renzi, "A milp algorithm for the optimal sizing of an off-grid hybrid renewable energy system in south tyrol," *Energy Reports*, vol. 6, pp. 21–26, 2020, the 6th International Conference on Energy and Environment Research - Energy and environment: challenges towards circular economy.

[2] X. Xing, J. Lin, Y. Song, Y. Zhou, S. Mu, and Q. Hu, "Modeling and operation of the power-to-gas system for renewables integration: a review," *CSEE Journal of Power and Energy System*, vol. 4, no. 2, p. 168–178, 2018.

[3] M. Koundi and H. E. Fadil, "Mathematical modeling of pem electrolyzer and design of a voltage controller by the smpwm approach," *International Conference Power Generation System and Renewable Energy Technologies*, 2019.

[4] R. Singh and R. C. Bansal, "Optimization of an autonomous hybrid renewable energy system using reformed electric system cascade analysis," *IEEE Transactions on Industrial Informatics*, vol. 15, no. 1, pp. 399–409, 2019.

[5] T. Zhou and B. Francois, "Modeling and control design of hydrogen production process for an active hydrogen/wind hybrid power system," *International Journal of Hydrogen Energy*, vol. 34, no. 1, pp. 21 – 30, 2009.

[6] O. Atlam and M. Kolhe, "Equivalent electrical model for a proton exchange membrane (pem) electrolyser," *Energy Conversion and Management*, vol. 52, no. 8-9, p. 2952–2957, 2011.

[7] D. Guilbert and G. Vitale, "Experimental validation of an equivalent dynamic electrical model for a proton exchange membrane electrolyzer," in *2018 IEEE International Conference on Environment and Electrical Engineering and 2018 IEEE Industrial and Commercial Power Systems Europe (EEEIC / I CPS Europe)*, 2018, pp. 1–6.

[8] M. Lebbal and S. Lecœuche, "Identification and monitoring of a pem electrolyser based on dynamical modelling," *International Journal of Hydrogen Energy*, vol. 34, pp. 5992–5999, 07 2009.

[9] G. Pan, W. Gu, Y. Lu, H. Qiu, S. Lu, and S. Yao, "Optimal planning for electricity-hydrogen integrated energy system considering power to hydrogen and heat and seasonal storage," *IEEE Transactions on Sustainable Energy*, vol. 11, no. 4, pp. 2662–2676, 2020.

[10] A. Sawas, H. Khani, N. El-Taweel, and H. E. Farag, "Comparative time-of-use and wholesale electricity price-based scheduling in embedded power and natural gas distribution grids penetrated with large renewable generation," *Electric Power Systems Research*, vol. 177, p. 105975, 2019.

[11] U.S. Energy Information Administration - EIA - Independent Statistics and Analysis, "Production of hydrogen," 2020. [Online]. Available: https://www.eia.gov/energyexplained/hydrogen/production-of-hydrogen.php

[12] IEA, "The future of hydrogen – analysis." [Online]. Available: https://www.iea.org/reports/the-future-of-hydrogen

[13] X. Wu, H. Li, X. Wang, and W. Zhao, "Cooperative operation for wind turbines and hydrogen fueling stations with on-site hydrogen production," *IEEE Transactions on Sustainable Energy*, vol. 11, no. 4, pp. 2775–2789, 2020.

[14] M. Espinosa-López, C. Darras, P. Poggi, R. Glises, P. Baucour, A. Rakotondrainibe, S. Besse, and P. Serre-Combe, "Modelling and experimental validation of a 46 kW pem high pressure water electrolyzer," *Renewable Energy*, vol. 119, pp. 160 – 173, 2018.

[15] P. García, C. A. García, L. M. Fernández, F. Llorens, and F. Jurado, "Anfis-based control of a grid-connected hybrid system integrating renewable energies, hydrogen and batteries," *IEEE Transactions Industrial Informatics*, vol. 10, no. 2, pp. 1107–1117, 2014.

[16] J. Li, J. Lin, H. Zhang, Y. Song, G. Chen, L. Ding, and D. Liang, "Optimal investment of electrolyzers and seasonal storages in hydrogen supply chains incorporated with renewable electric networks," *IEEE Transactions on Sustainable Energy*, vol. 11, no. 3, pp. 1773–1784, 2020.

[17] Iea, "The future of hydrogen – analysis." [Online]. Available: https://www.iea.org/reports/the-future-of-hydrogen

[18] Hydrogeit, "Electrolyzer target: 100 megawatts ' h2-international," Sep 2017. [Online]. Available: https://www.h2-international.com/2017/09/01/electrolyzer-target-100-megawatts/

[19] D. Klotz, "Characterization and modeling of electrochemical energy conversion systems by impedance techniques," Ph.D. dissertation, 2012.

[20] B. Yodwong, D. Guilbert, M. Phattanasak, W. Kaewmanee, M. Hinaje, and G. Vitale, "Proton Exchange Membrane Electrolyzer Modeling for Power Electronics Control: A Short Review," *Journal of Carbon Research*, May 2020.

[21] H. Gorgun, "Dynamic modelling of a proton exchange membrane (pem) electrolyzer," *International Journal of Hydrogen Energy*, vol. 31, no. 1, p. 29–38, 2006.

[22] S. Toghyani, S. Sheikh Fakhradini, E. Afshari, E. Baniasadi, M. Jamalabadi, and M. S. Shadloo, "Optimization of operating parameters of a polymer exchange membrane electrolyzer," *International Journal of Hydrogen Energy*, vol. 44, no. 13, pp. 6403 – 6414, 2019.

[23] Øystein Ulleberg, "Modeling of advanced alkaline electrolyzers: a system simulation approach," *International Journal of Hydrogen Energy*, vol. 28, no. 1, pp. 21 – 33, 2003.

[24] D. Martinez and R. Zamora, "Electrical implementations of an empirical electrolyser model for improved matlab/simulink simulations," *International Journal of Renewable Energy Research*, vol. 9, pp. 1060–1070, 06 2019.

[25] M. Sánchez, E. Amores, L. Rodríguez, and C. Clemente-Jul, "Semi-empirical model and experimental validation for the performance evaluation of a 15kw alkaline water electrolyzer," *International Journal of Hydrogen Energy*, vol. 43, no. 45, pp. 20 332–20 345, 2018.

[26] Y. Naimi and A. Antar, "Hydrogen generation by water electrolysis," in *Advances In Hydrogen Generation Technologies*, M. Eyvaz, Ed. Rijeka: IntechOpen, 2018, ch. 1.

[27] M. Trifkovic, M. Sheikhzadeh, K. Nigim, and P. Daoutidis, "Modeling and control of a renewable hybrid energy system with hydrogen storage," *IEEE Transactions on Control Systems Technology*, vol. 22, no. 1, pp. 169–179, 2014.

[28] Y. Ennassiri, I. Belhaj, and H. Bouzekri, "Techno-economic assessment of hydrogen production from vre in morocco case study: Laayoune, ouarzazate, midelt," in *2019 7th International Renewable and Sustainable Energy Conference (IRSEC)*, 2019, pp. 1–6.

[29] S. Touili, A. A. Merrouni, Y. El Hassouani, A. Amrani, and A. Azouzoute, "A techno-economic comparison of solar hydrogen production between morocco and southern europe," in *2019 International Conference on Wireless Technologies, Embedded and Intelligent Systems (WITS)*, 2019, pp. 1–6.

[30] B. Yodwong, D. Guilbert, M. Phattanasak, W. Kaewmanee, M. Hinaje, and G. Vitale, "Faraday's efficiency modeling of a proton exchange membrane electrolyzer based on experimental data," *Energies*, vol. 13, no. 18, p. 4792, 2020.

[31] P. Flowers, K. Theopold, R. Langley, and W. R. Robinson, *Chemistry*. OpenStax, Rice University, 2018.

[32] A. H. A. Rahim, A. S. Tijani, F. H. Shukri, S. Hanapi, and K. I. Sainan, "Mathematical modelling and simulation analysis of pem electrolyzer system for hydrogen production," in *3rd IET International Conference on Clean Energy and Technology (CEAT) 2014*, 2014, pp. 1–7.

[33] C. Biaku, N. Dale, M. Mann, H. Salehfar, A. Peters, and T. Han, "A semiempirical study of the temperature dependence of the anode charge transfer coefficient of a 6kw pem electrolyzer," *International Journal of Hydrogen Energy*, vol. 33, no. 16, pp. 4247 – 4254, 2008.

[34] R. Guidelli, R. G. Compton, J. M. Feliu, E. Gileadi, J. Lipkowski, W. Schmickler, and S. Trasatti, "Defining the transfer coefficient in electrochemistry: An assessment (iupac technical report)," *Pure and Applied Chemistry*, vol. 86, no. 2, pp. 245 – 258, 2014.

[35] A. S. Tijani, N. A. B. Kamarudin], and F. A. B. Mazlan], "Investigation of the effect of charge transfer coefficient (ctc) on the operating voltage of polymer electrolyte membrane (pem) electrolyzer," *International Journal of Hydrogen Energy*, vol. 43, no. 19, pp. 9119 – 9132, 2018.

[36] P. M. V. Raja and A. R. Barron, "Book: Physical methods in chemistry and nano science (barron)," Jun 2019.

[37] F. Yang, X. Feng, and Z. Li, "Advanced microgrid energy management system for future sustainable and resilient power grid," *IEEE Transactions on Industry Applications*, vol. 55, no. 6, pp. 7251–7260, 2019.

[38] J. Xiao, P. Wang, L. Setyawan, and Q. Xu, "Multi-level energy management system for real-time scheduling of dc microgrids with multiple slack terminals," *IEEE Transactions on Energy Conversion*, vol. 31, no. 1, pp. 392–400, 2016.

[39] J. S. Giraldo, J. A. Castrillon, J. C. López, M. J. Rider, and C. A. Castro, "Microgrids energy management using robust convex programming," *IEEE Transactions on Smart Grid*, vol. 10, no. 4, pp. 4520–4530, 2019.

[40] D. Arcos-Aviles, J. Pascual, F. Guinjoan, L. Marroyo, G. García-Gutiérrez, R. Gordillo-Orquera, J. Llanos-Proaño, P. Sanchis, and T. E. Motoasca, "An energy management system design using fuzzy logic control: Smoothing the grid power profile of a residential electro-thermal microgrid," *IEEE Access*, vol. 9, pp. 25 172–25 188, 2021.

[41] T. Pippia, J. Sijs, and B. De Schutter, "A single-level rule-based model predictive control approach for energy management of grid-connected microgrids," *IEEE Transactions on Control Systems Technology*, vol. 28, no. 6, pp. 2364–2376, 2020.

[42] C. Sun, G. Joos, S. Q. Ali, J. N. Paquin, C. M. Rangel, F. A. Jajeh, I. Novickij, and F. Bouffard, "Design and real-time implementation of a centralized microgrid control system with rule-based dispatch and seamless transition function," *IEEE Transactions on Industry Applications*, vol. 56, no. 3, pp. 3168–3177, 2020.

[43] G. K. Venayagamoorthy, R. K. Sharma, P. K. Gautam, and A. Ahmadi, "Dynamic energy management system for a smart microgrid," *IEEE Transactions on Neural Networks and Learning Systems*, vol. 27, no. 8, pp. 1643–1656, 2016.

[44] S. M. Hosseini, R. Carli, and M. Dotoli, "Robust optimal energy management of a residential microgrid under uncertainties on demand and renewable power generation," *IEEE Transactions on Automation Science and Engineering*, vol. 18, no. 2, pp. 618–637, 2021.

[45] F. Delfino, G. Ferro, M. Robba, and M. Rossi, "An energy management platform for the optimal control of active and reactive powers in sustainable microgrids," *IEEE Transactions on Industry Applications*, vol. 55, no. 6, pp. 7146–7156, 2019.

[46] Y. Xu and X. Shen, "Optimal control based energy management of multiple energy storage systems in a microgrid," *IEEE Access*, vol. 6, pp. 32 925–32 934, 2018.

[47] Z.-H. Liu, X.-H. Li, L.-H. Wu, S.-W. Zhou, and K. Liu, "Gpu-accelerated parallel coevolutionary algorithm for parameters identification and temperature monitoring in permanent magnet synchronous machines," *IEEE Transactions on Industrial Informatics*, vol. 11, no. 5, pp. 1220–1230, 2015.

[48] J. Su, Y. Chen, D. Zhang, and Y. Kang, "Stand-alone brushless doubly fed generation control system with feedforward parameters identification," *IEEE Transactions on Industrial Informatics*, vol. 15, no. 11, pp. 6011–6022, 2019.

[49] C. Restrepo, T. Konjedic, A. Garces, J. Calvente, and R. Giral, "Identification of a proton-exchange membrane fuel cell's model parameters by means of an evolution strategy," *IEEE Transactions on Industrial Informatics*, vol. 11, no. 2, pp. 548–559, 2015.

[50] Y. Zhou, B.-C. Wang, H.-X. Li, H.-D. Yang, and Z. Liu, "A surrogate-assisted teaching-learning-based optimization for parameter identification of the battery model," *IEEE Transactions on Industrial Informatics*, vol. 17, no. 9, pp. 5909–5918, 2021.

[51] K. W. Harrison, E. Hernández-Pacheco, M. Mann, and H. Salehfar, "Semiempirical model for determining pem electrolyzer stack characteristics," *Journal of Fuel Cell Science and Technology*, vol. 3, no. 2, p. 220–223, 2005.

[52] F. Marangio, M. Santarelli, and M. Calì, "Theoretical model and experimental analysis of a high pressure pem water electrolyser for hydrogen production," *International Journal of Hydrogen Energy*, vol. 34, no. 3, pp. 1143 – 1158, 2009.

[53] F. Barbir, *PEM fuel cells: theory and practice*, 2nd ed. Burlington: Elsevier Acadademic Press, 2013.

[54] Z. Abdin, C. Webb, and E. Gray, "Modelling and simulation of a proton exchange membrane (pem) electrolyser cell," *International Journal of Hydrogen Energy*, vol. 40, no. 39, pp. 13 243 – 13 257, 2015.

[55] V. der Merwe and J. Petrus, "Characterisation of a proton exchange membrane electrolyser using electrochemical impedance spectroscopy," Master's thesis, North-West University, potchefstroom campus, 2012.

[56] S. Becker and V. Karri, "Implementation of neural network models for parameter estimation of a pem-electrolyzer," *Journal of Advanced Computational Intelligence and Intelligent Informatics*, vol. 14, no. 6, pp. 735–745, 2010.

[57] H. A. Eiselt, C.-L. Sandblom, and K. Spielberg, *Integer programming and network models*. Springer, 2011.

[58] A. Miró, C. Pozo, G. Guillen-Gosalbez, J. A. Egea, and L. Jiménez Esteller, "Deterministic global optimization algorithm based on outer approximation for the parameter estimation of nonlinear dynamic biological systems," *BMC bioinformatics*, vol. 13, p. 90, 05 2012.

[59] G. Chiodelli and L. Malavasi, "Electrochemical open circuit voltage (ocv) characterization of sofc materials," *Ionics*, vol. 19, pp. 1135–1144, 2013.

[60] C. Heij, P. de Boer, P. H. Franses, T. Kloek, and H. van Dijk, *Econometric Methods with Applications in Business and Economics*. Oxford University Press, 2004.

[61] J.-H. Zhou, C. K. Pang, F. L. Lewis, and Z.-W. Zhong, "Intelligent diagnosis and prognosis of tool wear using dominant feature identification," *IEEE Transactions on Industrial Informatics*, vol. 5, no. 4, pp. 454–464, 2009.

[62] M. Carmo, D. L. Fritz, J. Mergel, and D. Stolten, "A comprehensive review on pem water electrolysis," *International Journal of Hydrogen Energy*, vol. 38, no. 12, pp. 4901 – 4934, 2013.

[63] J. Kai, R. Saito, K. Terabaru, H. Li, H. Nakajima, and K. Ito, "Effect of temperature on the performance of polymer electrolyte membrane water electrolysis: Numerical analysis of electrolysis voltage considering gas/liquid two-phase flow," *Journal of The Electrochemical Society*, vol. 166, no. 4, pp. F246–F254, 2019.

[64] S. Toghyani, E. Afshari, E. Baniasadi, S. Atyabi, and G. Naterer, "Thermal and electrochemical performance assessment of a high temperature pem electrolyzer," *Energy*, vol. 152, pp. 237–246, 2018.

[65] "DOE technical targets for hydrogen production from electrolysis." [Online]. Available: https://www.energy.gov/eere/fuelcells/doe-technical-targets-hydrogen-production-electrolysis

[66] I. (2020), "Renewable power generation costs in 2019," International Renewable Energy Agency, Abu Dhabi, September 2019.

[67] E. Haghi, M. Fwoler, and K. Raahemifar, "Economic analysis of hydrogen production in context of a microgrid," in *2017 IEEE International Conference on Smart Energy Grid Engineering (SEGE)*, 2017, pp. 79–84.

[68] A. M. Ferrario, C. Amoruso, R. V. Robles, L. Del Zotto, E. Bocci, and G. Comodi, "Power-to-gas from curtailed res electricity in spain: potential and applications," in *2020 IEEE International Conference on Environment and Electrical Engineering and 2020 IEEE Industrial and Commercial Power Systems Europe (EEEIC / I CPS Europe)*, 2020, pp. 1–6.

[69] G. Saur, "Wind-to-hydrogen project: Electrolyzer capital cost study. technical report," National Renewable Energy Laboratory, Colorado, U.S., Tech. Rep., 2008.

[70] Y. Shibata, "Economic Analysis of Hydrogen Production from Variable Renewables," *IEEJ Energy Journal*, vol. 10, no. 2, pp. 26–46, 2015.

[71] A. Belderbos, "Storage via power-to-gas in future energy systems: The need for synthetic fuel storage in systems with high shares of intermittent renewables," 2019.

[72] J. Li, J. Lin, Y. Song, X. Xing, and C. Fu, "Operation optimization of power to hydrogen and heat (p2hh) in adn coordinated with the district heating network," *IEEE Transactions on Sustainable Energy*, vol. 10, no. 4, pp. 1672–1683, 2019.

[73] J. T. Davis, "Membraneless Electrolyzers for Solar Fuels Production," 2019.

[74] D. M. Santos, C. A. Sequeira, and J. L. Figueiredo, "Hydrogen production by alkaline water electrolysis," *Quimica Nova*, vol. 36, no. 8, pp. 1176–1193, 2013.

[75] P. García, C. A. García, L. M. Fernández, F. Llorens, and F. Jurado, "Anfis-based control of a grid-connected hybrid system integrating renewable energies, hydrogen and batteries," *IEEE Transactions on Industrial Informatics*, vol. 10, no. 2, pp. 1107–1117, 2014.

[76] M. Zhang, N. Zhang, D. Guan, P. Ye, K. Song, X. Pan, H. Wang, and M. Cheng, "Optimal design and operation of regional multi-energy systems with high renewable penetration considering reliability constraints," *IEEE Access*, vol. 8, pp. 205 307–205 315, 2020.

[77] H. Yang, Q. Li, S. Zhao, W. Chen, and H. Liu, "A hierarchical self-regulation control for economic operation of ac/dc hybrid microgrid with hydrogen energy storage system," *IEEE Access*, vol. 7, pp. 89 330–89 341, 2019.

[78] H. Shahinzadeh, M. Moazzami, M. Abbasi, H. Masoudi, and V. Sheigani, "Smart design and management of hybrid energy structures for isolated systems using biogeography- based optimization algorithm," in *2016 Smart Grids Conference (SGC)*, 2016, pp. 1–7.

[79] H. Khani, N. A. El-Taweel, and H. E. Z. Farag, "Supervisory scheduling of storage-based hydrogen fueling stations for transportation sector and distributed operating reserve in electricity markets," *IEEE Transactions on Industrial Informatics*, vol. 16, no. 3, pp. 1529–1538, 2020.

[80] N. A. El-Taweel, H. Khani, and H. E. Z. Farag, "Hydrogen storage optimal scheduling for fuel supply and capacity-based demand response program under dynamic hydrogen pricing," *IEEE Transactions on Smart Grid*, vol. 10, no. 4, pp. 4531–4542, 2019.

[81] N. Naseri, S. El Hani, A. Aghmadi, H. Mediouni, I. Aboudrar, and M. Benbouzid, "Solar photovoltaic energy storage as hydrogen via pem fuel cell for later conversion back to electricity," in *IECON 2019 - 45th Annual Conference of the IEEE Industrial Electronics Society*, vol. 1, 2019, pp. 4549–4554.

[82] Z. Li, W. Wu, B. Zhang, and B. Wang, "Adjustable robust real-time power dispatch with large-scale wind power integration," *IEEE Transactions on Sustainable Energy*, vol. 6, no. 2, pp. 357–368, 2015.

[83] N. A. El-Taweel, H. Khani, and H. E. Z. Farag, "Analytical size estimation methodologies for electrified transportation fueling infrastructures using public–domain market data," *IEEE Transactions on Transportation Electrification*, vol. 5, no. 3, pp. 840–851, 2019.

[84] M. O. Badawy and Y. Sozer, "Power flow management of a grid tied pv-battery system for electric vehicles charging," *IEEE Transactions on Industry Applications*, vol. 53, no. 2, pp. 1347–1357, 2017.

[85] P. Lettenmeier, "Efficiency – electrolysis," Siemens Energy Global GmbH Co. KG, München, Germany, White Paper, 2021.

[86] M. Mehrtash, F. Capitanescu, P. K. Heiselberg, T. Gibon, and A. Bertrand, "An enhanced optimal pv and battery sizing model for zero energy buildings considering environmental impacts," *IEEE Transactions on Industry Applications*, vol. 56, no. 6, pp. 6846–6856, 2020.

[87] J. Kim, J. Lee, S. Park, and J. K. Choi, "Battery-wear-model-based energy trading in electric vehicles: A naive auction model and a market analysis," *IEEE Transactions on Industrial Informatics*, vol. 15, no. 7, pp. 4140–4151, 2019.

[88] Yohwan Choi and Hongseok Kim, "Optimal scheduling of energy storage system for self-sustainable base station operation considering battery wear-out cost," in *2016 Eighth International Conference on Ubiquitous and Future Networks (ICUFN)*, 2016, pp. 170–172.

[89] A. Abuelrub, M. Khamees, J. Ababneh, and H. Al-Masri, "Hybrid energy system design using greedy particle swarm and biogeography-based optimisation," *IET Renewable Power Generation*, vol. 14, no. 10, pp. 1657–1667, 2020.

[90] IESO, "Hourly Ontario Energy Prices (HOEP)," *IESO Data Directory-Ontario Power Data*, Accessed: Apr. 06, 2021. [Online]. Available: http://www.ieso.ca/power-data/data-directory

[91] N. A. El-Taweel, H. Khani, and H. E. Z. Farag, "Optimal sizing and scheduling of lohc-based generation and storage plants for concurrent services to transportation sector and ancillary services market," *IEEE Transactions on Sustainable Energy*, vol. 11, no. 3, pp. 1381–1393, 2020.

[92] F. Angizeh, A. GHOFRANI, and M. Jafari, "Dataset on hourly load profiles for a set of 24 facilities from industrial, commercial, and residential end-use sectors," *Mendeley Data*, 2020.

[93] J. Yates, R. Daiyan, R. Patterson, R. Egan, R. Amal, A. Ho-Baille, and N. L. Chang, "Techno-economic analysis of hydrogen electrolysis from off-grid stand-alone photovoltaics incorporating uncertainty analysis," *Cell Reports Physical Science*, vol. 1, no. 10, p. 100209, 2020.

[94] S. You, J. Hu, Y. Zong, and J. Lin, "Value assessment of hydrogen-based electrical energy storage in view of electricity spot market," *Journal of Modern Power Systems and Clean Energy*, vol. 4, no. 4, pp. 626–635, 2016.

[95] A. Christensen, "Assessment of hydrogen production costs from electrolysis: United states and europe," International Council on Clean Transportation, Washington DC, US, 2020.